



**BRNO UNIVERSITY OF TECHNOLOGY**

VYSOKÉ UČENÍ TECHNICKÉ V BRNĚ

**FACULTY OF MECHANICAL ENGINEERING**

FAKULTA STROJNÍHO INŽENÝRSTVÍ

**INSTITUTE OF SOLID MECHANICS, MECHATRONICS AND BIOMECHANICS**

ÚSTAV MECHANIKY TĚLES, MECHATRONIKY A BIOMECHANIKY

**COMPUTATIONAL SIMULATION OF MECHANICAL BEHAVIOUR OF  
ENDOTHELIAL CELLS**

VÝPOČTOVÁ SIMULACE MECHANICKÉHO CHOVÁNÍ ENDOTELIÁLNÍCH BUNĚK

**DOCTORAL THESIS**

DIZERTAČNÍ PRÁCE

**AUTHOR**

**Veera Venkata Satya Varaprasad Jakka, M.Sc.**

AUTOR PRÁCE

**SUPERVISOR**

**Prof. Ing. Jiří Burša, Ph.D.**

ŠKOLITEL

**BRNO 2022**

## Abstrakt

Ateroskleróza je v rozvinutém světě hlavní příčinou úmrtí a finančně zatěžuje zdravotnické systémy po celém světě. Převládající hemodynamické působení spolu s lokální koncentrací mechanického napětí hrají důležitou roli v lokální povaze aterosklerózy a jejím rozvoji ve specifických oblastech lidských cév.

Endotel v krevních cévách je tvořen tenkou vrstvou buněk, ležící na rozhraní mezi krevním řečištěm a cévní stěnou. Dysfunkce endoteliálních buněk se podílí na hlavních patologiích. Například ateroskleróza se rozvíjí, když jsou narušeny bariérové a protizánětlivé funkce endotelu, což umožňuje akumulaci cholesterolu a dalších materiálů v arteriální stěně. U rakoviny je klíčovým krokem v růstu nádoru jeho vaskularizace a proces migrace endoteliálních buněk. Mechanické zatížení endoteliálních buněk hraje klíčovou roli v jejich funkci a dysfunkci.

Počítačové modelování může zlepšit porozumění buněčné mechanice a tím přispět k poznání vztahů mezi strukturou a funkcí různých typů buněk v různých stavech. K dosažení tohoto cíle jsou v této práci navrženy konečnoprvkové modely endoteliálních buněk, tj. model buněk plovoucích v roztoku a model buněk přilnutých k podložce, které objasňují reakci buňky na globální mechanické zatížení, jako je tah a tlak, jakož i model buňky s jeho přirozeným tvarem uvnitř endoteliální vrstvy. Zachovávají hlavní principy tensegritních struktur, jako je předpětí a spolupůsobení jednotlivých součástí, ale prvky se mohou organizovat vzájemně nezávisle. Při implementaci nedávno navržené bendo-tensegritní koncepce uvažují tyto modely namáhání mikrotubulů nejen v tahu/tlaku, ale i ohybu a také zohledňují vlnitost intermediálních filament. Modely umožňují, že jednotlivé komponenty cytoskeletu mohou změnit svůj tvar a uspořádání bez zhroutení celé buněčné struktury, dokonce i když jsou odstraněny, a umožňují nám tak vyhodnotit mechanický přínos jednotlivých cytoskeletálních složek k buněčné mechanice.

Navržené modely jsou validovány porovnáním jejich křivek síla-posunutí s experimentálními výsledky. Model plovoucí buňky realisticky popisuje silově-deformační odezvu buňky při tahu a tlaku a obě reakce ilustrují nelineární zvýšení tuhosti s mechanickým zatížením.

Je simulována také tlaková zkouška ploché endoteliální buňky a porovnána s testem přilnuté buňky a jeho simulací. Poté se simuluje smykový test ploché buňky, aby se vyhodnotilo její chování při smykovém zatížení vyskytujícím se v cévní stěně v důsledku proudění krve.

Poté byla zkoumána mechanická odezva ploché buňky ve vrstvě endotelu za fyziologických podmínek v arteriální stěně. Později byla zkoumána buněčná odezva při odtrhování od položky během cyklických úseků pomocí 3D simulací metodou konečných prvků.

Navrhované modely poskytují cenné poznatky o vzájemných souvislostech mechanických vlastností buněk, o mechanické roli jednotlivých cytoskeletálních složek i jejich synergii a o deformaci jádra za různých podmínek mechanického zatížení. Proto by práce měla přispět k lepšímu pochopení cytoskeletální mechaniky, zodpovědné za chování buněk, což může zase pomoci při zkoumání různých patologických stavů souvisejících s buněčnou mechanikou, jako je rakovina a vaskulární onemocnění.

**Klíčováslova:** Cytoskelet, Bendo-tensegrita, Endoteliální buňky, Metoda konečných prvků, Buněčná biomechanika, Mechanotransdukce, Tahová a tlaková zkouška, Zkouška adheze.

# Abstract

Atherogenesis is the leading cause of death in the developed world, and is putting considerable monetary pressure on health systems the world over. The prevailing haemodynamic environment together with the local concentration of mechanical load play an important role in the focal nature of atherosclerosis to very specific regions of the human vasculature.

In blood vessels, the endothelium, a thin monolayer of cells, lies at the interface between the bloodstream and the vascular wall. Dysfunction of endothelial cells is involved in major pathologies. For instance, atherosclerosis develops when the barrier and anti-inflammatory functions of the endothelium are impaired, allowing accumulation of cholesterol and other materials in the arterial wall. In cancer, a key step in the growth of a tumour is its vascularization, a process driven by endothelial cell migration. The mechanical environment of endothelial cells plays a key role in their function and dysfunction.

Computational modelling can enhance the understanding of cell mechanics, which may contribute to establishing structure-function relationships of different cell types in different states. To achieve this, finite element (FE) models of endothelium cell are proposed in this thesis, i.e. a suspended cell model and adherent model elucidating the cell's response to global mechanical loads, such as tension and compression, as well as a model of the cell with its natural shape inside the endothelial layer. They keep the central principles of tensegrity such as prestress and interplay between components, but the elements are free to rearrange independently of each other. Implementing the recently proposed bendo-tensegrity concept, these models consider flexural (buckling) as well as tensional/compressional behaviour of microtubules (MTs) and also incorporate the waviness of intermediate filaments (IFs). The models assume that the individual cytoskeletal components can change their form and organization without collapsing the entire cell structure when they are removed and thus, they enable us to evaluate the mechanical contribution of individual cytoskeletal components to the cell mechanics.

The proposed models are validated with experimental results by comparison of their force-displacement curves. The suspended cell model mimics realistically the force-deformation responses during cell stretching and compression, and both responses illustrate a non-linear increase in stiffness with mechanical loads.

The compression test of flat endothelial cell is simulated and compared with adherent cell test and its simulation. Then, the shear test of flat cell is simulated to assess its shear behaviour

occurring in vascular wall due to blood flow. Then investigated the mechanical response of the flat cell within the endothelium layer under physiological conditions in arterial wall. Later, investigated the cell response in debonding during cyclic stretches using 3-D finite element simulations.

The proposed models provide valuable insights into the interdependence of cellular mechanical properties, the mechanical role of cytoskeletal components in endothelial cells individually and synergistically, and the nucleus deformation under different mechanical loading conditions. Therefore, the thesis should contribute to the better understanding of the cytoskeletal mechanics, responsible for endothelial cell behaviour, which in turn may aid in investigation of various pathological conditions related to cell mechanics like cancer and vascular diseases.

**Keywords:** Cytoskeleton, Bendo-tensegrity, Endothelial cells, Finite element modelling, Cell biomechanics, Mechanotransduction, Tensile test, Compression test, Adhesion.

## **Declaration**

Prohlašuji, že tuto disertační práci jsem vypracoval samostatně s použitím odborné literatury a dalších informačních zdrojů, které jsou všechny citovány. V disertační práci jsem také použil texty a informace z článků, kterých jsem autor nebo spoluautor.

I herewith declare that I have personally penned this doctoral thesis. I have only used the mentioned sources and utilities and have marked parts copied from elsewhere, either literally or by content as such. I have also used texts and information from my own co-authored publications.

**Veera Venkata Satya Varaprasad Jakka**

## **Bibliographic quote**

VEERA VENKATA SATYA VARAPRASAD JAKKA. “Computational Simulation of Mechanical Behaviour of Endothelial Cells“, Brno University of Technology, Faculty of Mechanical Engineering, 2022. Supervisor: prof. Ing. Jiří Burša, Ph.D.

*Dizertační práce je dostupná v tištěné podobě na oddělení vědy a výzkumu Fakulty strojního inženýrství Vysokého učení technického v Brně, Technická 2896/2, 616 69 Brno.*

## **Acknowledgments**

I wish to express my deep gratitude to my supervisor prof. Ing. Jiří Burša, Ph.D. for all his guidance and support throughout my research. His creative ideas and constant encouragement to attend many conferences, internships, and networking events around the world made my PhD program one of the most rewarding experiences possible.

I would also like to thank all my committee members for taking time out from their busy schedules and reviewing my work. Additionally, I am also grateful to the Faculty of Mechanical Engineering at the Brno University of Technology and its staff for their support in all possible ways. I sincerely acknowledge the financial support from the Brno University of Technology which helped me to stay focused. I sincerely appreciate and thank all my lab mates Ondřej Lisický, Jiří Jagoš, Lucie Orlová, Jiří Vaverka, and Jiří Fischer for their time to time helpful tips. I would like to thank my friends Sudhir Kumar Kondepoti, Surya Teja Madala and Sai Jagan Yalamanchili for their support and encouragement towards the successful completion of PhD program. Last but not the least, I would like to thank my parents who during these years have comforted me morally and encouraged me to achieve my goals.



## Table of Contents

<b>1. Introduction</b>	<b>1</b>
1.1. General background	1
1.1.1. The artery wall	1
1.1.2. Endothelium and its role in atherosclerosis	2
1.1.3. Endothelial cells	2
1.2. Motivation of the study	3
1.3. Objectives of the doctoral thesis	3
<b>2. State of the art</b>	<b>5</b>
2.1. Cytoskeletal components	5
2.2. Experimental methods for measuring cell mechanics	5
2.3. Cell mechanics modelling approaches	5
2.4. Non-linear constitutive models	7
2.4.1. Neo-Hooke Model	8
2.4.2. Mooney-Rivlin Model	9
2.4.3. Model Arruda-Boyce	10
2.5. Summary	11
<b>3. Literature review of mechanical behaviour of endothelium cells and its simulation</b>	<b>12</b>
3.1. Mechanical Stresses and Fluid Dynamics	13
3.2. Shear Stress Patterns in Stenotic Arteries	15
3.3. Experimental tests of endothelial cells	16
3.3.1. Tensile test Experimental setup.	16
3.3.2. Compression Test Experimental setup	17
3.4. Endothelial Cell Culture devices	18
3.4.1. Modified Cone and Plate Viscometer	18
3.4.2. Parallel Plate Flow Chamber	19
3.4.3. Tubular Models	20
3.4.4. Existing experimental Limitations	20
<b>4. Finite element bendo-tensegrity model of endothelial cell</b>	<b>21</b>
4.1. Structure and Geometries of hexagonal endothelial cell model variants	21
4.1.1. Material properties of flat model	25
4.2. Spherical model of suspended endothelial cell	26
4.3. Modification of the FE model for adherent endothelial cell	27
4.3.1. Material Properties of adherent model	29

<b>5. Finite element simulations of endothelial cell</b>	<b>31</b>
5.1. Simulations of Suspended cell model	31
5.1.1. Simulations of suspended cell in compression and its experimental validation.	31
5.1.2. Simulations of suspended cell in tension and its experimental validation	34
5.1.3. Role of cytoskeletal components	37
5.1.4. Summary and discussion of suspended cell model	37
5.2. Simulations of adherent cell model	39
5.2.1. Simulations of adherent cell in compression and its experimental validation	39
5.2.2. Role of cytoskeletal components	41
5.3. Simulation of flat cell model	42
5.3.1. Simulations of regular flat and domed cell in compression	42
5.3.2. Simulations of regular flat and domed cell in shear	45
5.4. Simulations of flat cell in different variants under physiological conditions	47
5.5. Simulation of cell debonding during cyclic loads	55
5.5.1. Results of debonding	56
<b>6. Conclusions</b>	<b>63</b>
6.1. Additional ideas for future works	64
<b>Bibliography</b>	<b>66</b>
<b>List of Figures</b>	<b>73</b>
<b>List of Tables</b>	<b>77</b>
<b>Abbreviations</b>	<b>78</b>
<b>Appendices</b>	

# 1. INTRODUCTION

## 1.1. General background

Living cells are themselves the universe and can be considered one of the most complex forms of matter. The initial step in understanding how living cells respond to applied stresses was to study their mechanical behaviour and interactions with the extracellular environment. Cells in living organisms are constantly subjected to a variety of mechanical stimuli, which cause them to change their shape, function, and behaviour. New experimental methodologies combined with robust computational approaches capable of modelling the mechanical response of cells at different temporal and spatial scales are opening new avenues for understanding cell mechanics and mechanobiology. Research on cell mechanics is very important for two main reasons. First, cells are constantly exposed to physical stress and strain caused by external physical forces that govern the health and function of the human body [1], and second, Biomechanical studies can give quantitative information on the changes in cell mechanical properties as diseases progress. In the developed world, atherosclerosis is the main cause of morbidity and mortality. It is characterised by the progressive narrowing and hardening of medium and large arteries, which can eventually lead to ischemia of the heart, brain, or extremities, leading to infarction [2]. The biology of the artery wall, disease genesis, and cell mechanisms that have been linked to the onset of atherosclerosis are discussed in this chapter. Understanding the cellular responses due to the haemodynamic environment is important for understanding the initiation of atherogenesis.

### 1.1.1. The artery wall

The artery's structure is divided into three layers: tunica intima, tunica media, and tunica adventitia (see [Figure 1.1.](#)). The tunica intima is a very thin layer that covers the artery wall's innermost section. A thin layer of endothelial cells in direct contact with flowing blood acts as an active barrier to material transport between the flowing blood and the artery wall. A layer of connective tissue lies beneath this single layer of endothelial cells. The internal elastic lamina is the intima's outermost layer, composed of a fenestrated network of elastin and collagen fibres. The tunica media is the thickest layer of the arterial wall, located in the middle. The arterial wall's stiffness, strength, and structural integrity are provided by this layer, which is made up primarily of smooth muscle cells organized concentrically but also contains elastin and collagen fibres. The medial layer's composition is highly influenced by the artery's size and age. The left anterior descending coronary artery, for example, comprises a higher number of smooth muscle

cells when it comes to aligning the heart. Finally, the tunica adventitia, the outermost layer, is made up of connective tissue, collagen, and elastic fibres; it is separated from the media by a thin layer of elastic tissue known as the external elastic lamina. The adventitia layer protects the artery from severe deformation when it is overloaded, and it also contains vasa vasorum, which are small blood vessels that provide oxygen, metabolites, and nutrition to the arterial wall, all of which are necessary for its survival. These vessels may pass through the media layer as well.

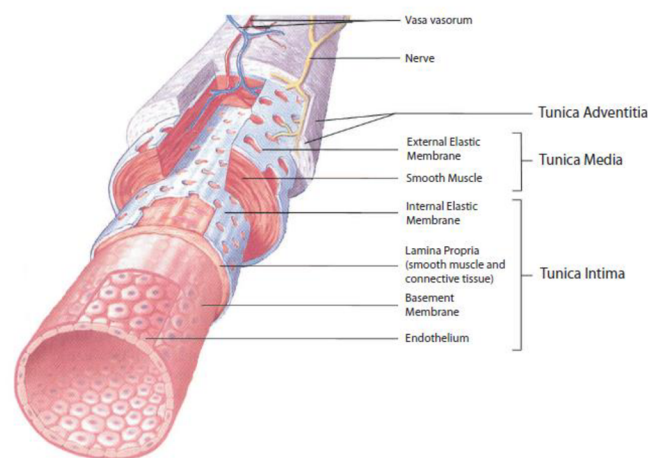


Figure 1. 1: Successive layers of the arterial wall. Figure adapted from [3]

### 1.1.2. Endothelium and its role in atherosclerosis

The endothelium is an important player in the pathobiology of atherosclerosis. The endothelium is a monolayer of cells that lines the inside walls of arteries, acting as a barrier between the flowing blood and the arterial wall. Initially, this layer was considered to act as a passive barrier between the flowing blood and the artery wall, but it has since been found that the opposite is true. [4] was the first to reveal this in an in vitro investigation on isolated rabbit arteries. They observed that when arteries with an intact endothelium are given acetylcholine, they dilate, but when this layer is removed, the vessel constricted under the same conditions. The endothelium reacts to the current haemodynamic and biochemical environment by triggering a variety of cellular responses. Additionally, this cell layer has been strongly implicated in the pathobiology of atherosclerosis through its regulatory functionality.

### 1.1.3. Endothelial cells

The basic architecture of endothelial cells is constructed from membranes, organelles and cytosol. The plasma membrane is the cell's outermost protective coating; it is a semipermeable lipid bilayer surface coating that regulates the flow of matter between the extracellular and

intracellular environments, particularly in the form of ions and molecules. A number of integral membrane proteins can be found on the membrane's surface (or ion channels). Non-gated ion channels govern plasma membrane permeability, ligand gated ion channels activate in response to ligand binding, and flow sensitive ion channels are among them. These react to the current haemodynamic situation. The cytoplasm, which makes up the majority of the cell volume and is made up of cytosol and organelles, is an area within the cell. The cytosol is the fluid part of the cytoplasm that is mostly made up of proteins. The cytoskeleton, a 3D internal scaffolding network connected inside the cytosol that provides mechanical rigidity and strength to the cell, holds the cells actual structure together. Actin filaments, intermediate filaments, and microtubules make up this network. Actin filaments are of particular significance because they play a role in force transmission, and their reorganization allows for morphological changes in shape and orientation in response to changing environmental conditions.

## **1.2. Motivation of the study**

Cells convert various types of energy and signals, maintain, and modify their internal structure, and react to external stimuli. They have structural features related to intracellular components that allow them to tolerate both physiological and mechanical shocks within the body. Mechanobiology is the study of the relationship between mechanical forces and biological processes. Several in vivo and in vitro investigations have demonstrated the importance of mechanical stress on cellular processes as cell proliferation, contractility, and apoptosis [5]. Mechanotransduction is the process by which cells convert mechanical signals into biochemical reactions. It is separated into two parts: mechanical response and biochemical response. For a better knowledge of cell physiology, researchers are studying both intracellular load transfer mechanisms and mechanotransduction. Cell forces, intracellular structures, and cell behaviour are all interconnected phenomena, and quantifying them with computational models will help us better understand how they interact.

## **1.3. Objectives of the doctoral thesis**

The main objective of the thesis is to investigate and to model the mechanisms that determine the intracellular force propagation and the mechanical behaviour of endothelium cell and its structural components. More specifically formulated as follows:

- To investigate the cell response to distinct global mechanical stimuli by simulating mechanical behaviour of isolated endothelial cell such as:
  - tension and compression of a suspended endothelial cell for validation
  - compression for adherent and flat endothelial cells

- shear of the flat endothelial cell
- To investigate the mechanical contribution of cytoskeletal components to cell mechanics, individually and synergistically by simulating disruption of cytoskeleton and its components.
- To investigate the mechanical response of the flat cell within the endothelium layer under physiological conditions in arterial wall.
- To investigate the cell response in debonding during cyclic stretches using 3-D finite element simulations. For this purpose, the created 3-D finite element model will be expanded by cohesive elements capable to simulate gradual debonding from the substrates under cyclic load.

## 2. STATE OF THE ART

### 2.1. Cytoskeletal components

Living cells are extremely complex entities with several structural components such as the cytoskeleton, cell membrane (CM), nucleus, and cytoplasm. The structural rigidity and rheology of the cytoskeleton, as well as its mechanical interaction with the extracellular environment, have a substantial impact on cell activity. The cytoskeletal network is comprised of three types of components that are distributed throughout the cytoplasm: actin filaments (AFs), microtubules (MTs), and intermediate filaments (IFs). These components are interconnected to one other, to the nucleus, and to the CM, despite their differences in characteristics [6]. Their structural organization determines the cytoskeleton's response to both external and internal mechanical stimuli. Actin-myosin contractility causes pre-tension and pre-stress in the cell, which is countered mostly by MTs and partially by the extracellular matrix (ECM) to which the cell is tethered [7]. As a result, the cytoskeleton determines the mechanical properties of cell deformation required for various cellular processes to be regulated.

### 2.2. Experimental methods for measuring cell mechanics

With the advancement of micro rheological tools in recent decades, precise quantitative mechanical measurements of single living cells have been available. The passive measurement methods and the active measurement methods are the two primary categories of these approaches. The former investigates the motion of particles injected into the cell as a result of thermal fluctuations, whereas the latter involves applying forces directly to the cell. The active methods are further divided into two types of experiments: those that apply a mechanical stimulus to a localized portion of the cell, such as atomic force microscopy (AFM) [8], magnetic twisting cytometry (MTC), and those that apply a mechanical stimulus to the entire cell, such as microplate stretchers [9], microplate manipulation ([10]; [11]) etc. Active approaches are recommended over passive ones because passive methods may damage the cell and impact its interior by causing changes in the cytoskeletal framework.

### 2.3. Cell mechanics modelling approaches

Since computational modelling allows for complete control over the shape and organization of individual cytoskeletal components, it may be used to investigate the mechanisms behind cell responses to a variety of mechanical stimuli. ([12]; [13]; [14]; [15]; [16]; [17]; [18]; [10]; [19]; [20]; [21]; [22]; [23]; [24]; [25]). Existing computational modelling approaches for cell mechanics can be divided into two groups: continuum approaches and microstructural approaches.

When the shortest length scale of interest is substantially larger than the space over which the cell's structures and properties vary appreciably, continuum techniques are used. The coarse-graining approach is used in continuum mechanics to localize microscopic stress-strain connections, resulting in a constitutive relationship and deformation description of the material that can be applied at the macroscopic scale [1]. These are broadly classified as liquid drop models and the material models such as elastic, viscoelastic, biphasic, and active continua.

The cytoskeleton is a fundamental component in cell mechanics, according to microstructural studies. The cellular tensegrity model, which depicted the cytoskeleton as a linked network of cables in tension representing AFs and struts in compression representing MTs, is one of the most widely used models in this class [7]. This model has successfully predicted viscosity modules of the cytoskeleton ([22], [23], [24]) as well as experimentally observed features of cell mechanical behaviour such as strain hardening [26]. However, this model does not consider other cellular components such as nucleus, cytoplasm, and CM.

The hybrid modelling approach using FE analysis has been proposed for more reliable formulation of cell mechanical behaviour [25]. Using the same method, ([17], [18]) proposed a more complicated cell model with 210-members tensegrity structure that successfully simulates both tensile and AFM indentation testing.

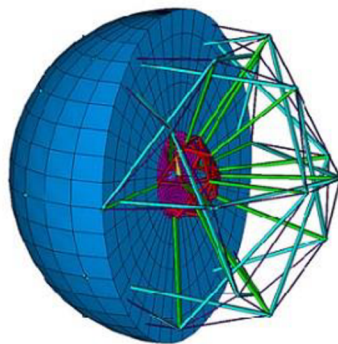


Figure 2. 1: Tensegrity FE model of suspended cell by ([17]; [18]) including nucleoskeleton (purple), cytoplasm (blue) and discrete elements representing cytoskeleton structure.

The suspended cell model depicted in Fig. 2.1 was based on the realistic shape of cell and includes all cytoskeletal components. Some of the recent models in this category are multi-structural model [15] self-stabilizing tensegrity structure based model [16] spring network cell model [19] granular cell model [20], etc. None of these models take into account the active cell responses, where the cytoskeletal fibres undergo polymerization and depolymerisation during loading.



The cytoskeletal tensegrity models presented in the literature do not account for the flexural behaviour of MTs. Thus, MTs appear too stiff. In order to compensate this problem, the most sophisticated hybrid model was created recently by using the bendo-tensegrity concept for modelling smooth muscle cells as shown in [Fig. 2.2](#) from [27].

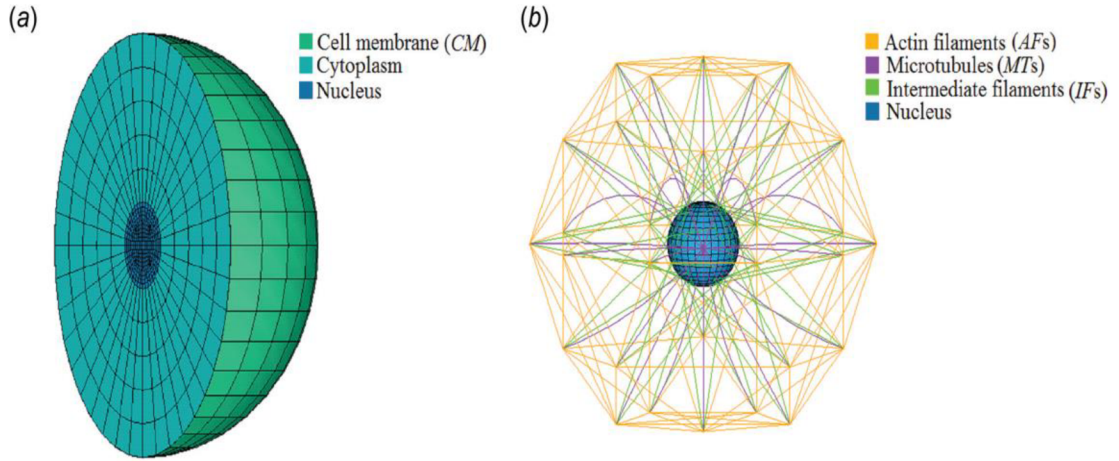


Figure 2. 2: Sections of continuous elements (a) and structural arrangement of cytoskeletal components (b) with respect to the nucleus for suspended cell model. From [27]

Recent active approaches studies have successfully solved this issue by adding the cell's inherent active nature into computational modelling, such as the bio-chemo-mechanical mode [28], dynamic stochastic model [29], kinematic model [30] etc. Although contemporary models in this class have formulations to describe both passive and active cell responses, they do not explain the role of additional cytoskeletal components like MTs, IFs, and so on.

## 2.4. Non-linear constitutive models

A material is said to be hyperelastic if there exists an elastic potential  $W$  (or strain energy density function SEDF) that is a scalar function of one of the strain or deformation tensors, whose derivative with respect to a strain component determines the corresponding stress component.

$$S_{ij} = \frac{\partial W}{\partial \epsilon_{ij}}$$

Where,  $S_{ij}$  - the folder 2nd Piola-Kirchhoff stress tensor

$W$ - is a function of the specific strain energy per unit undeformed volume

$\epsilon_{ij}$  are components of Green-Lagrange strain tensor

They do not take into account for the dissipative release of energy as heat while straining the material and perfect elasticity is assumed at all stages of deformations. They are characterized

by a relatively low elastic modulus and high bulk modulus and used in a wide variety of structural applications. Some of the most common applications to the hyperelastic models are:

- (i) The rubbery behaviour of a polymeric material
- (ii) Polymeric foams that can be subjected to large reversible shape changes
- (iii) Biological materials

Rubber as well as other hyperelastic materials are widely employed for structural purposes in a wide range of sectors, from tyres to aerospace. The most attractive property of rubbers is their ability to experience large deformation under small loads and to retain their initial configuration without considerable permanent deformation after load is removed [31]. Their stress-strain behaviour is very nonlinear, and a simple elasticity modulus is no longer adequate. Therefore, characterization of elastic behaviour of highly extensible, nonlinear materials is of great importance [32].

The constitutive behaviour of hyperelastic material is derived from its SEDF ‘ $W$ ’ based mostly on three strain invariants  $I_1$ ,  $I_2$  and  $I_3$ . It is the energy stored in the material per unit of reference volume (volume in the initial configuration) as a function of strain at that point in material [33].

$$W = f(I_1, I_2, I_3)$$

Where  $I_1$ ,  $I_2$  and  $I_3$  are invariants of right Cauchy-Green deformation tensor defined in terms of principal stretch ratios  $\lambda_1$ ,  $\lambda_2$  and  $\lambda_3$  as follows:

$$\begin{aligned} I_1 &= \lambda_1^2 + \lambda_2^2 + \lambda_3^2 \\ I_2 &= \lambda_1^2 \lambda_2^2 + \lambda_2^2 \lambda_3^2 + \lambda_3^2 \lambda_1^2 \\ I_3 &= \lambda_1^2 \lambda_2^2 \lambda_3^2 \end{aligned}$$

If hyperelastic materials are considered incompressible, i.e.  $I_3 = 1$  then only two independent strain measures remain, namely  $I_1$  and  $I_2$ . Otherwise these invariants should be isovolumetric ( $\bar{I}_1, \bar{I}_2$ ) and the volume member with compressibility parameter “ $d$ ” is used in the SEDF formulation.

#### 2.4.1. Neo-Hooke Model

This model is a special case of Mooney-Rivlin form with  $C_{01} = 0$  and can be used when material data is insufficient. It's easy to use and can make accurate approximations at low strains. But it cannot capture the upturn of the stress strain curve.

This model introduces specific strain energy in the form of

$$W = \frac{G}{2} (\bar{I}_1 - 3) + \frac{1}{d} (J - 1)^2$$

Where,

$G$  = initial shear modulus

$\bar{I}_1$  = Modified first invariant of the right Cauchy-Green deformation tensor

$d = 2/K$  compressibility parameter of the material, when  $K$  is the bulk modulus of elasticity and

$J$  = third invariant of the deformation gradient tensor

Since, the shape change in this model is described by a single elastic constant, the model is accurate only for strains less than 50%.

## 2.4.2. Mooney-Rivlin Model

### 2.4.2.1. Mooney-Rivlin 2-parametric Model

Two parameters phenomenological model that works well for moderately large stains in uniaxial elongation and shear deformation. But, it cannot capture the upturn (S-curvature) of the force-extension relation in uniaxial test and the force-shear displacement relation in shear test. This model works with incompressible elastomers with strains up to 100% and introduces a specific SEDF in the form:

$$W = C_{10}(\bar{I}_1 - 3) + C_{01}(\bar{I}_2 - 3) + \frac{1}{d}(J - 1)^2$$

Where  $C_{10}$ ,  $C_{01}$  are material parameters

$\bar{I}_1$  = isovolumetric first invariant of the right Cauchy-Green deformation tensor

$\bar{I}_2$  = isovolumetric second invariant of the right Cauchy-Green deformation tensor

$d$  = compressibility parameter of the material, the relationship

$K$  = is the bulk modulus of elasticity

$J$  = third invariant of the deformation gradient tensor.

The stress-strain curve cannot show strain stiffening (inflexion point) and the model can be commonly used for polymers and rubber for an automobile tire.

### 2.4.2.2. Mooney-Rivlin 5-parametric Model

This model works with incompressible elastomers with strain up to 100-200% and introduces a specific strain energy in the form of

$$W = C_{10}(\bar{I}_1 - 3) + C_{01}(\bar{I}_2 - 3) + C_{20}(\bar{I}_1 - 3)^2 + C_{11}(\bar{I}_1 - 3)(\bar{I}_2 - 3) + C_{02}(\bar{I}_2 - 3)^2 + \frac{1}{d}(J - 1)^2$$

Where  $C_{10}$ ,  $C_{01}$ ,  $C_{20}$ ,  $C_{02}$  are material parameters

$\bar{I}_1$  = Modified first invariant of the right Cauchy-Green deformation tensor

$\bar{I}_2$  = Modified second invariant of the right Cauchy-Green deformation tensor

$d$  = compressibility parameter of the material, the relationship

$K$  = is the bulk modulus of elasticity

$J$  = third invariant of the deformation gradient tensor.

This model is applicable even when the stress-strain curve shows an inflexion point.

### 2.4.2.3. Mooney-Rivlin 9-parametric Model

This model introduces specific strain energy in the form of

$$W = C_{10}(\bar{I}_1 - 3) + C_{01}(\bar{I}_2 - 3) + C_{20}(\bar{I}_1 - 3)^2 + C_{11}(\bar{I}_1 - 3)(\bar{I}_2 - 3) + C_{02}(\bar{I}_2 - 3)^2 \\ + C_{30}(\bar{I}_1 - 3)^3 + C_{21}(\bar{I}_1 - 3)^2(\bar{I}_2 - 3) + C_{12}(\bar{I}_1 - 3)(\bar{I}_2 - 3)^2 \\ + C_{03}(\bar{I}_2 - 3)^3 + \frac{1}{d}(J - 1)^2$$

Where  $C_{10}, C_{01}, C_{20}, C_{02}, C_{11}, C_{03}, C_{30}, C_{21}, C_{12}$  and are material parameters

$\bar{I}_1$  = Modified first invariant of the right Cauchy-Green deformation tensor

$\bar{I}_2$  = Modified second invariant of the right Cauchy-Green deformation tensor

$d$  = compressibility parameter of the material, the relationship

$K$  = is the bulk modulus of elasticity

$J$  = third invariant of the deformation gradient tensor.

This model is applicable even for complex shapes of stress-strain curves but must be supported, in addition to simple tension test, also with equibiaxial and shear tests.

### 2.4.3. Model Arruda-Boyce

This model is structure-based, unlike previous models based on purely phenomenological description of the material responses, and introduces the energy threshold stress stretching structure  $\lambda_L$  chains

$$W = G \left[ \frac{1}{2}(\bar{I}_1 - 3) + \frac{1}{20\lambda_L^2}(\bar{I}_1^2 - 9) + \frac{11}{1050\lambda_L^4}(\bar{I}_1^3 - 27) \right. \\ \left. + \frac{19}{7000\lambda_L^6}(\bar{I}_1^4 - 81) + \frac{519}{673750\lambda_L^8}(\bar{I}_1^5 - 243) \right] \\ + \frac{1}{d} \left( \frac{J^2 - 1}{2} - \ln J \right)$$

Where,

$\mu$  = initial shear modulus

$\lambda_L$  = marginal structural chain elongation

$d$  = compressibility parameter of the material

$K$  = is the bulk modulus of elasticity and the relationship

$\bar{I}_1$  = Modified first invariant of the right Cauchy-Green deformation tensor

J = third invariant of the deformation gradient tensor.

For  $\lambda_L$  tending to infinity we get the Neo-Hooke model.

Well suited for rubbers with strain up to 300% and provides good prediction in case of lack of material data.

## **2.5. Summary**

The presented models use Hooke's law for modelling the cytoskeletal components (linear elastic material properties) because the cytoskeletal components are represented with discrete (1D) elements which are not supported (in the applied ANSYS software) to use hyper elastic material properties. On the other hand, the continuum part (hyper elastic materials) is modelled by using Neo-Hooke hyper elastic model because this is the simplest hyper elastic model that requires only one material constant (Shear modulus) derived from any tests whereas other models require more parameters to define their mechanical response which are not available in the literature.

### **3. LITERATURE REVIEW OF MECHANICAL BEHAVIOUR OF ENDOTHELIUM CELLS AND ITS SIMULATION**

The endothelium is a continuous, single cell-thick membrane, which lines blood vessels and forms part of the tunica intima. They lay on a connective tissue basement membrane that connects them to the tunica media (comprised mainly of elastin, collagen, and smooth muscle cells). The tunica adventitia, the vessel wall's outermost layer, is mostly connective tissue strengthened by collagen fibres.

Endothelial cells are normally flat and elongated in the direction of blood flow, measuring 0.2-0.5  $\mu$ m thick, 10-15  $\mu$ m broad, and 25-50  $\mu$ m long, with a centrally positioned oval or spherical nucleus that is slightly elevated in comparison to the rest of the cell [34].

The endothelium is a unique multifunctional tissue with significant basal, inducible metabolic and synthetic functions in addition to its role as a selective permeability barrier. It responds to both physical and chemical stimuli, such as mechanical forces. These cells play a role in regulating hemostasis/thrombosis, vasoconstriction/vasodilation, as well as immunological and inflammatory responses.

The endothelial cells that line the lumen surface of blood vessels are exposed to at least two different mechanical forces: fluid shear stress generated by blood circulation, and periodic stretching and relaxing caused by blood pulsation-induced diameter oscillations [35].

The luminal surface of mammalian arteries is lined with a continuous coating of endothelial cells. In vivo, periodic oscillations in vessel diameter are caused by the pulsations of blood flow in arteries, forcing the vessel wall to expand and relax in a cyclic pattern. As a result of blood flow, the endothelium lining is subjected to fluctuating fluid shear stress. Endothelial cells of arteries are elongated and oriented in the direction of the blood flow ([36]; [37]), whereas endothelial cells of large veins are polygonally shaped and are not aligned as shown in the [Fig. 3.1.](#)

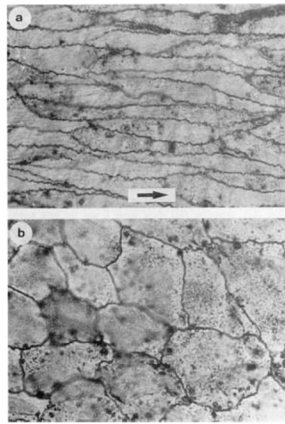


Figure 3. 1: Arrangement of endothelial cells lining the luminal surface of arteries and veins (silver nitrate staining), a) Strongly elongated and oriented endothelial cells in human thoracic aorta. The direction of blood flow is indicated by the arrow. Bright field; magnification,  $\times 225$ . b) Polygonally shaped endothelial cells of human saphenous vein. Sample was obtained after bypass surgery. Bright field; magnification,  $\times 350$ . This picture is adopted from [35]

Atherosclerosis can cause stenosis, or narrowing of the lumen of blood vessels, which can lead to pro-thrombotic regions. Shear stress can stimulate both vascular cells and blood components in stenotic areas. Cellular interactions play a crucial part in a variety of biological processes inside the cardiovascular system [38]. They are quite particular and are influenced by a variety of circumstances, including hemodynamic forces. For blood components to adhere to the vessel wall, a balance of dynamic forces (forces acting on cells) and adhesive forces is required (interactions of receptors and ligands from one cell to another). Understanding the interaction of hemodynamic factors with vascular cell biology is crucial to understanding cardiovascular diseases. This section will go through the mechanical stresses that the arterial wall is subjected to, the shear stress patterns found in stenotic arteries, and the hemodynamic effects on endothelial cells.

### 3.1. Mechanical stresses and fluid dynamics

The vascular tree is subjected to various types of forces. Blood pressure fluctuations, artery motion, and fluid shear all exert stresses on vascular cells. Factors like artery architecture, blood pulsatility, and tissue mechanical characteristics all influence stress levels.

Although vascular cells respond to cyclic strain and hydrostatic pressure, endothelial cells are more sensitive to wall shear stress. Shear stress is a force that is applied parallel to the vessel in the direction of blood flow, and it is expected to have major physiologic and pathological responses by affecting blood components and endothelial cells that are in direct contact with

flowing blood. For a Newtonian fluid, shear stress ( $\tau$ ) is proportional to the dynamic viscosity ( $\mu$ ) of the fluid and to the speed at which adjacent layers of fluid slide past each other, i.e. the shear rate  $\frac{d\vartheta}{dy}$  as seen in the equation below.

$$\tau = \mu \frac{d\vartheta}{dy} = \mu \dot{\gamma} \quad (1)$$

Where  $\vartheta$  is flow velocity along the boundary,

$y$  is height above the boundary

The wall shear rate ( $\dot{\gamma}$ ) in a laminar steady flow tubular vessel, assuming an incompressible, and Newtonian fluid, can be calculated as:

$$(\dot{\gamma}) = \frac{32Q}{\pi D^3} \quad [39] \quad (2)$$

where  $D$  is the diameter and  $Q$  is the volumetric flow rate. Combining equation 1 and 2 gives a reasonable estimate of the mean wall shear stress in straight arteries.

$$\tau = \frac{32\mu Q}{\pi D^3} \quad (3)$$

The velocity profiles, shear stress and shear rate patterns are shown in [Fig. 3.2](#). For laminar flow in straight tubular vessels.

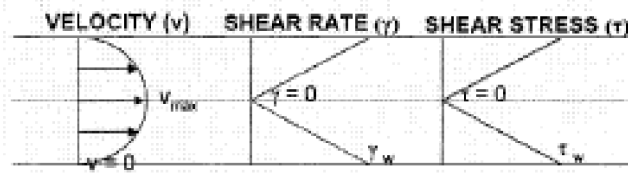


Figure 3.2: Laminar fully developed blood flow in a tubular vessel [39]

Non-dimensional fluid characteristics can be used to simulate genuine (physiological) conditions in real-world studies. For steady flow, these parameters include the Reynolds number ( $Re$ ), which measures the ratio of inertial to viscous forces and is represented in equation (4).

$$Re = \frac{\rho V D}{\mu} \quad (4)$$

Where  $\rho$  is density and  $V$  is the average velocity. These equations can only crudely estimate the dynamics in blood vessels.

Blood is a suspension that can behave like a non-Newtonian fluid, and its viscosity varies depending on factors like haematocrit, aggregation, plasma viscosity, and the deformability of red blood cells, and blood behaves as a Newtonian fluid at shear rates greater than  $200 \text{ s}^{-1}$  and has a viscosity of approximately  $3.5 \text{ cP}$  ( $0.0035 \text{ kg}/(\text{m} \cdot \text{s}) = 0.0035 \text{ Pa} \cdot \text{s}$ ) [40]. Blood viscosity



increases with a substantial effect below 20 Pa.s when the shear rate decreases due to red blood cell cross-linking (Rouleaux formation). Blood viscosity has been studied extensively, and various mathematical models, such as the Carreau, power law, Casson, and expanded power law models, have been developed to quantitatively represent it [41].

### 3.2. Shear stress patterns in stenotic arteries

Complex patterns of blood flow can be observed in arteries with stenosis. Endothelial cells which line the vessel lumen are particularly sensitive to wall shear stress. Fig. 3.3 depicts an idealized asymmetric stenosis shear stress profile for a fully developed laminar flow of an incompressible Newtonian fluid. It has a fluid acceleration region near the stenosis's throat, as well as a post-stenosis low-velocity recirculation region with a reattachment point ([42]; [43]). Variations in shear stress in this region can alter blood components and endothelial cells, resulting in thrombosis and atherosclerosis progression.

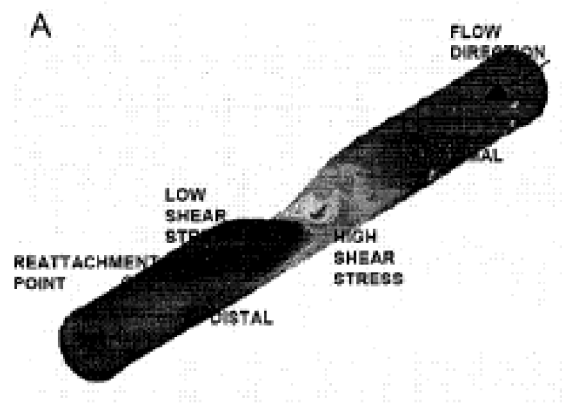


Figure 3. 3:Shear stress patterns in the asymmetric stenosis model as computed in a numerical Simulation (A) [42].

Longer blood component interaction, higher residency time, and endothelium adherence of circulating elements such as lipoproteins, monocytes, and platelets may be favoured by fluid velocity. High shear stresses at the stenosis's throat can activate blood components, and the recirculation zone's low velocity allows for lengthier interactions between blood components and endothelial cells, culminating in the formation of a thromb.

Shear stress triggers a variety of physiological, pharmacological, and gene regulatory responses in various vascular cells, which may have an impact on the formation and progression of atheroma in stenotic areas.

Mechanical forces, specifically stress concentrations and fluid shear stresses, may play a key role in atherogenesis, based on the localized distribution of atherosclerotic lesions. Because lifestyle and risk factors are prevalent across the vasculature, they cannot explain this

distribution. Areas where stress concentrations occur and blood flow is known to be disrupted, such as bifurcations and curvatures, are atheroprone. The coronary arteries, the primary branches of the aortic arch, the visceral arterial branches of the abdominal aorta, and the terminal abdominal aorta and its branches are preferred places in the arterial tree ([44]; [45]). These areas are characterized by disturbed flow with low and high shear stress magnitudes, as well as significant temporal and geographical oscillations. Because atherosclerotic plaques are frequently found in specific regions, damage to the endothelium is assumed to be the cause. According to the response-to-injury hypothesis [2] atherosclerosis starts with endothelial cell injury. Endothelial cells can be stimulated by local blood flow perturbations, resulting in a pro-atherogenic cell phenotype [46].

Endothelial cell shape and function have been the subject of numerous scientific studies in recent years. The nature of shear stress and its impact on endothelial cell activation or dysfunction, which leads to atherosclerotic plaque formation, remain unknown. The purpose of these experiments was to determine cellular responses to shear stress caused by fluid movement. The detection of the effects of shear stress on the arterial wall, as well as the development of endothelial cells in an artery-like shape, is a critical step in understanding the pathophysiology of vascular disease.

### **3.3. Experimental tests of endothelial cells**

#### **3.3.1. Tensile test experimental setup.**

Micro tensile testing of individual cells are carried out with a tensile test equipment that they developed before [47] and refined for this investigation. A round-shaped floating cell is grabbed using a pair of cantilevers displaced by the micromanipulators. The cantilever, which is made up of a carbon fibre and a glass rod, is handcrafted: a thin carbon fibre with an 8 $\mu$ m diameter is bonded to the tip of a 1 mm diameter glass rod with an epoxy adhesive to achieve the length indicated below. By altering the carbon fibre length, they create two types of cantilevers: deflectable and non-deflectable. The length of the carbon fibre at the tip of a glass rod for the deflectable cantilever is set to 2–3mm. The deflectable cantilever is easily bent since it is so thin. A cross-calibration approach is used to obtain the spring constant for cantilever bending [48]. The carbon fibre for the non-deflectable cantilever is set to a length of 100  $\mu$ m. This is so short that the non-deflectable cantilever has a relatively large spring constant and hence does not bend against a force of less than 10  $\mu$ N that appears in this experiment.

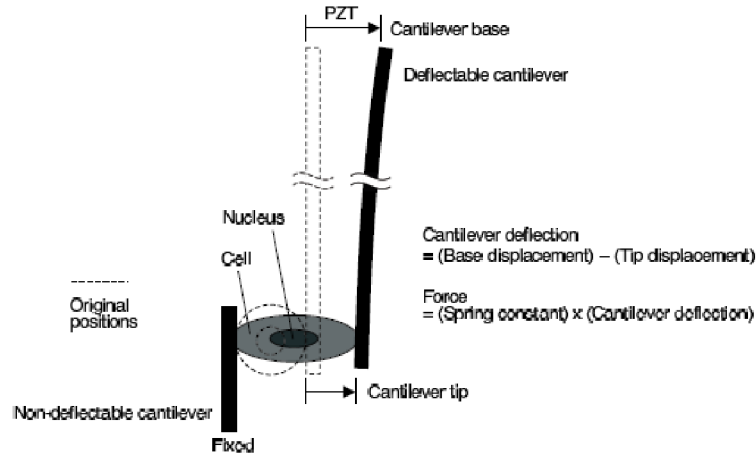


Figure 3. 4: A single cell's tensile test is depicted in this diagram. The cantilever and the cell are not depicted in precise relative scale, and the cantilever deflection is exaggerated [47].

### 3.3.2. Compression test experimental setup

The untreated rigid microplate is positioned beneath a suspended endothelial cell or a nucleus that has settled down due to gravity in the observation chamber. The microplate is kept in this position for around 2 minutes, or until the cell or nucleus sticks to it. The observation medium is then replaced with medium containing 10% fetal calf serum and 20mM HEPES. The mechanical test is performed right away on round cells and nuclei. For the so-called spread cells, a custom-made mechanism connects the chamber and the rigid microplate, which is then moved to an incubator (37<sup>0</sup> C, 5% CO<sub>2</sub>) [49]. The chamber is returned to the microscope and the microplate is re-attached to the steel arm after a 45-minute incubation time, which is long enough to stimulate cell spreading. Compression is imposed by pushing the rigid microplate holding the cell or nucleus by 2.5 μm per 10 s towards the flexible microplate after initial contact with the flexible microplate, as demonstrated in [Fig.3.5](#). For the first 2.5 μm displacement of the rigid microplate, the stiffness of the flexible microplate is set to achieve a compression of the cell or nucleus on the order of 1.5 μm and a deflection of the flexible microplate of around 1 μm. This is equivalent to a total compression of 50–60%. Relaxation is accomplished by removing the rigid microplate in the same time sequence as before. Depending on the cell, the complete cycle (loading and emptying) takes 1.5 to 3 minutes. To quantify solely passive mechanical qualities and eliminate cellular adaptation, the mechanical test is performed in the shortest period possible. Throughout each 10 s step, the applied forces and consequent cell or nuclei deformation remain constant. Digital video images of round cell are shown in [Fig. 3.6](#).

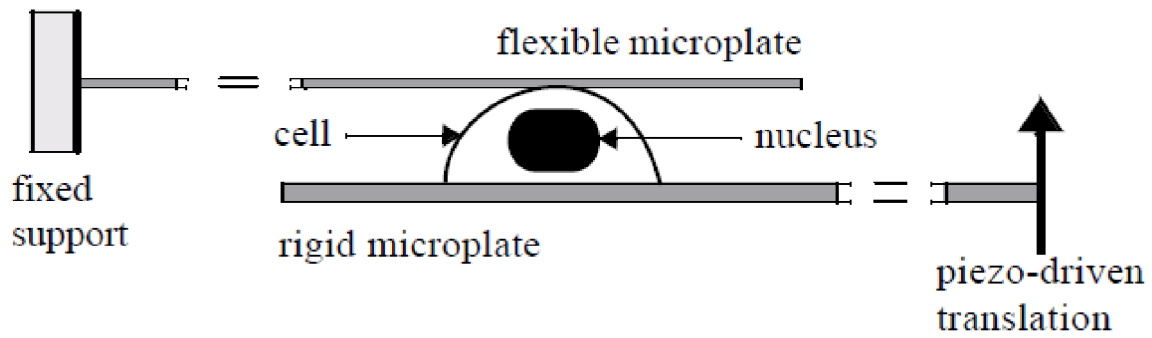


Figure 3. 5: Schematic diagram of the Compression test of a single cell from [50]

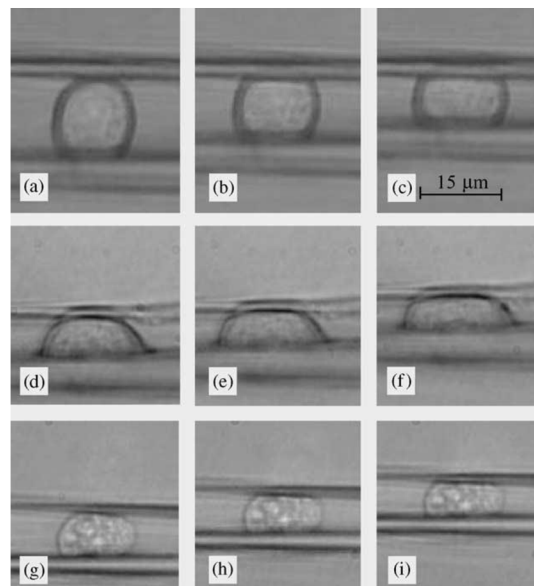


Figure 3. 6: Digitized video images of a round cell (a–c), a spread cell (d–f), and an isolated nucleus (g–i) exposed to compression. This picture is taken from the [50]

### 3.4. Endothelial cell culture devices

Endothelial cells have been investigated for their ability to respond to shear stress in devices inspired by viscometers with different arrangements. Modified cone and plate or Couette viscometers, as well as parallel-plate flow chambers, were used in the experiments. Tubular devices have only been studied in a small number of cases.

#### 3.4.1. Modified cone and plate viscometer

In a cone and plate viscometer as shown in [Fig. 3.7](#), shear is created between a flat plate and a cone with a low angle, in a design similar to a Couette viscometer. Endothelial cells are grown on a flat plate or in a series of glass coverslips. Rotation of the cone with respect to the stationary base plate produces uniform fluid shear strains in the cultivated endothelium monolayers. In vitro models of the cone and plate can incorporate both pulsatility and spatial gradients. Applied

shear stresses [51] in the range of 0 - 1.5 Pa modifying the viscosity, cone angle, and rotational speed in three different patterns, i.e. steady, periodic and oscillating (non-periodic) shear stress. Rapid sinusoidal changes of shear stress at 60 cycles/min (1 Hz) were produced by tilting the cone with respect to the axis of rotation resulting in a slight wobble in the cone rotation, creating pulsatile flow ([52]; [53]; [54]).

[55] Glued coverslips into a stainless-steel ring with a protuberance in the form of a rectangular bar that disrupted flow downstream of the bar. The constant laminar shear stress was re-established further downstream. Each ring's bar was aligned in the radial direction, requiring almost concentric flow to ensure that the streamlines strike the bar at a perpendicular angle, resulting in complicated spatial shear stress patterns ([55]; [56])

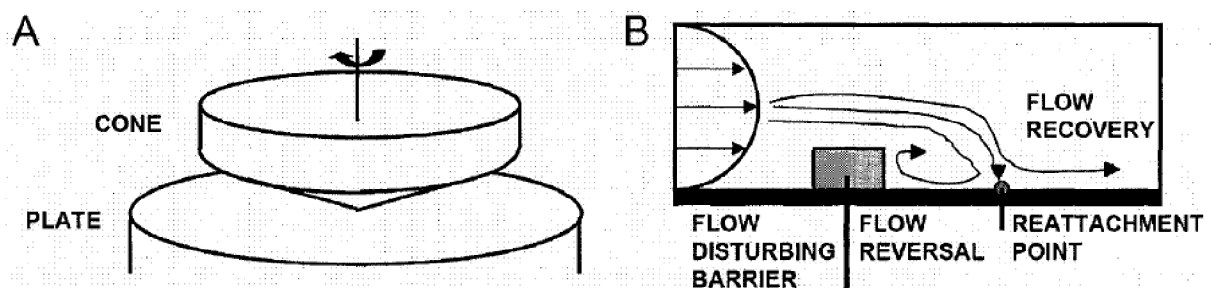


Figure 3. 7: Cone and plate viscometer, original (A) [52] and modified with a step (B) [55]

### 3.4.2. Parallel plate flow chamber

A microscope slide or coverslip is used to culture endothelial cells in parallel plate flow chambers (see Fig. 3.8). On both sides of the flow chamber, endothelial cells are generated. The culture media is then pumped through the chamber, creating a well-defined wall shear stress on the surface of the endothelial cells. To limit the effects of the entrance zone, the inlet and outflow are perpendicular to the flow direction ([57]; [58]; [59]). The apparatus's height to width ratio is usually quite minimal. This enables for the use of infinite parallel plates, for which the fluid mechanics are well understood.

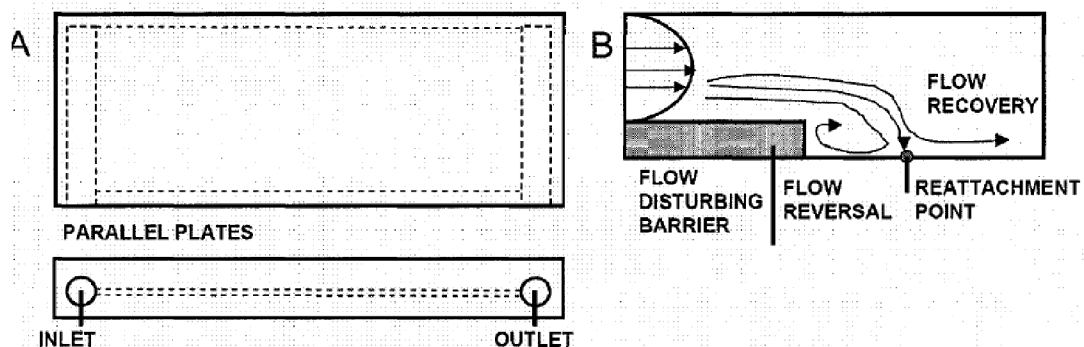


Figure 3. 8: Parallel plate chamber, original (A) [57] and modified with a step (B) [59]

Modified a parallel plate flow chamber by placing a rectangular obstacle perpendicular to the flow field [59]. Numerical software was used to calculate the flow separation, reattachment, and recovery point details. The cells were exposed to a shear stress of 1.4 Pa, a Reynolds number of 20, and a complex hemodynamic environment similar to that of a cone and plate with disrupting bar, resulting in a flow separation zone and a reattachment point. The presence of large spatial gradients and a complicated shear stress distribution (constant over the width) mimics stenotic areas. Pulsatility was added to the parallel plate flow chamber, and the influence of temporal wall shear stress gradients on endothelial cell morphology was investigated [60]. It has been found that machining flaws can cause shear stress fluctuations of up to 11 percent within a chamber [61]. When the study is conducted on different parts of the same plate or when only a few endothelial cells are examined, this can lead to considerable inaccuracies

### **3.4.3. Tubular models**

Cells have been investigated using tubular models to determine endothelial function within an arterial geometry [62]. This is a better model in terms of geometry, but it's still a model with well-defined fluid dynamics. None of these models have presented images of endothelial cells growing in them [63], nor have they examined spatial gradients in wall shear stress.

Endothelial cells have also been cultured in distensible membranes ( [64]; [35]) and compliant tubes, and then stretched rapidly in specially developed cyclic strain apparatus to replicate the rhythmic deformation of the artery wall associated with systolic-diastolic pressure variations ( [65]; [66]; [67]). Endothelial cultures with no fluid flow have also been subjected to hydrostatic pressure [62]. The impact of shear stress on endothelial vasoactive substance production was investigated using compliant models [63].

### **3.4.4. Existing experimental limitations**

Endothelial cells' responses to idealized hemodynamic conditions have been studied extensively. In response to shear, cultured endothelial cells change their shape, gene expression, signalling, and metabolism ( [46]; [68]; [55]; [69]). The hemodynamic studies are far from realistic, making it difficult to relate these data to in vivo endothelial cell responses. Our ability to investigate cellular mechanics has advanced significantly. Unfortunately, our failure to reproduce mechanical stimuli may be complicating our comprehension of the in vivo response.

## 4. FINITE ELEMENT BENDO-TENSEGRITY MODEL OF ENDOTHELIAL CELL

### 4.1. Structure and geometries of hexagonal endothelial cell model variants

The concept of “bendo-tensegrity” was proposed by [70] recommending an alteration to contemporary cytoskeletal tensegrity models that considers the flexural response of MTs. In the current study implementing this concept with hybrid modelling approach, a FE bendo-tensegrity model of suspended endothelial cell is proposed, with topology being similar to the model of vascular smooth muscle cell by [27]. The hypothesis of this work is that the proposed bendo-tensegrity model of flat cell that can describe the cellular structural behaviour and determine cell’s global response to distinct mechanical stimuli. It is not only important to study the cell response to global deformation of extracellular environment but also if it responds differently depending on the stimulus.

Two different geometries of endothelial cell models within an arterial wall were introduced in [71], based on a flat (constant cell thickness of  $0.5\ \mu\text{m}$  [72]) and domed (non-constant thickness, tapered from the centre to the edges) regular hexagons. However, while the ratio of longitudinal and circumferential dimension of a regular hexagonal cell [72] (see Fig. 4.1(b)) is 0.87, the “in situ” endothelial cells are irregular, elongated in the direction of blood flow [73]. Therefore, we modified the model geometry to mimic better the natural shape of endothelial cells in arteries and used a ratio of 0.96 in our simulations for the so called elongated shapes [74] [75].

In the four created geometry variants, the structure of the model is the same. The endothelial cell model encompasses the nucleus and cytoplasm surrounded by the CM (Fig. 4.1.) and cytoskeletal components like AFs, MTs, and IFs (Fig.4.3.). For the proposed model implementing the hybrid modelling approach, the continuum parts (nucleus, cytoplasm) were modelled using continuous (volume) elements circumscribed by a thin layer of shell elements (representing CM) and the cytoskeletal components were modelled using discrete (beam or truss) elements.

Endothelial cells are  $0.5\ \mu\text{m}$  thick,  $15\ \mu\text{m}$  wide and  $50\ \mu\text{m}$  long and have a centrally located oval or round nucleus slightly raised compared to the rest of the cell. Endothelial cells are usually flat and elongated in the direction of blood flow [34]. Both cytoplasm and nucleus were modelled with eight-node hexahedral isoperimetric elements. A thin flexible layer circumscribing the cytoplasm referred to as the CM was modelled with four-node quadrilateral shell elements on the outer surface of the cytoplasm, with thickness of  $0.01\ \mu\text{m}$  [76] and no bending stiffness.

The computational model of flat endothelial cell is presented in the following [Fig. 4.1](#).

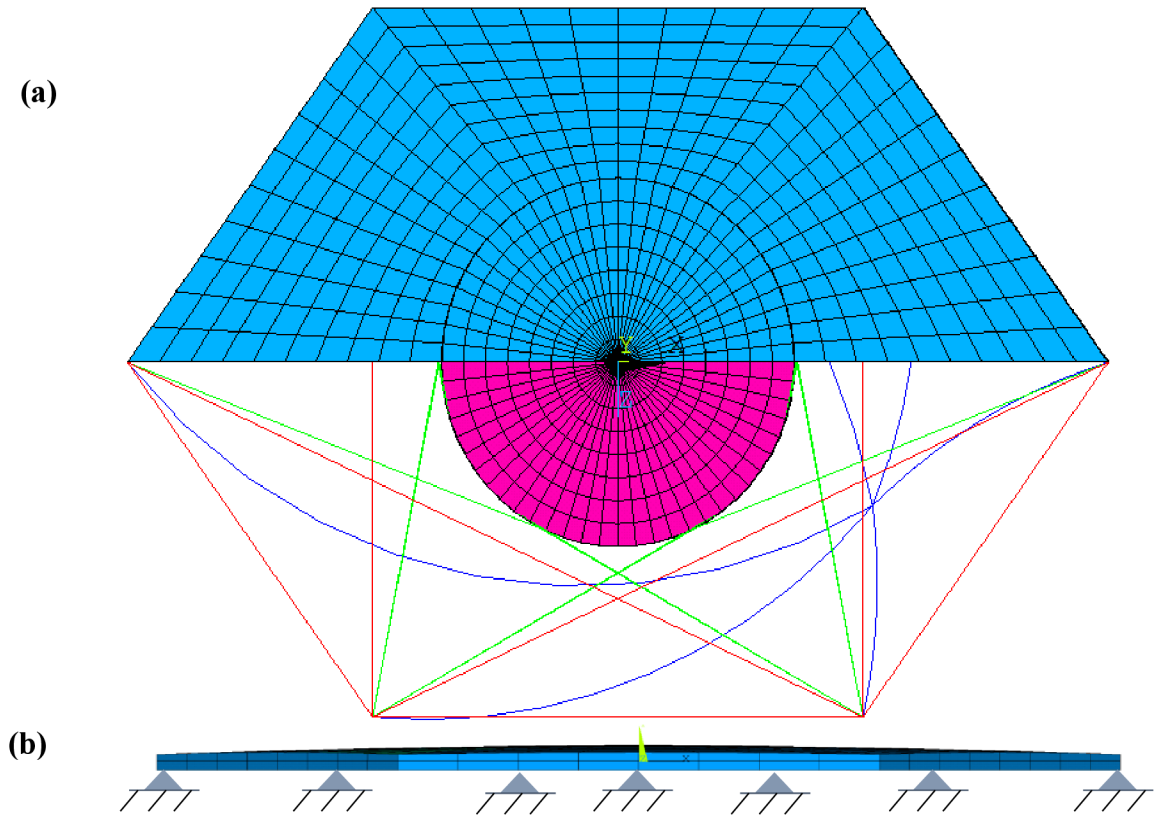


Figure 4. 1: Finite element hybrid model of endothelial cell representing (a) the continuum mesh and the cytoskeletal components of the elongated flat model with AFs (red), IFs (green), and MTs (blue) (b) front view of the domed cell model with supports and varying thickness.

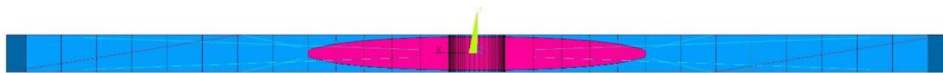


Figure 4. 2: Sectional view of the hybrid model representing nucleus on the centre.

In a real cell, MTs of unequal lengths originate from the centrosome located near the nucleus and emanate outward through the cytoplasm till the cortex where they interact with other cytoskeletal filaments at focal adhesions (FAs). It is now evident that MTs do not have compression-only behaviour but they appear highly curved (buckled) in living cells under no external load. This indicates that compressive forces in MTs induce substantial bending solely by the action of prestressed AFs; this is referred to as the “bendo-tensegrity” concept [70]. Implementing this concept, the MTs of varying curvature were modelled using beam elements, originating from a single node near the nucleus (representing the centrosome) and further extending till the FAs to form a star-like shape. Every FA was connected to the centrosome with only one MT and it was ensured that they do not penetrate the nucleus.



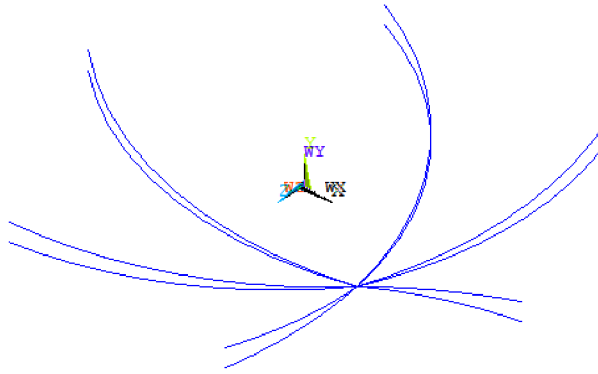


Figure 4. 3: MTs architecture in the proposed computational model.

IFs are scattered throughout the intracellular space, connecting the FAs to the nucleus. On stretching these filaments become straight and behave stiffer, thus contributing to the cell mechanics only at large strains (above 20%) ([77]; [78]). To incorporate their waviness, the IFs were modelled as truss elements resisting only tensile loads under elongations higher than 20% (Fig. 4.5 a) and all the IFs were equally strained for simplification. In this way, these truss elements behave like wavy fibres although they are modelled straight in contrast to real IFs as depicted. For better transmission of mechanical stimuli to the nucleus and its stabilization at the centre of the cell, each FA is connected to the nucleus via at least one IF circumscribing the nucleus. To create a realistic model geometry without modelling the contact between the IF and nucleus, the circumscribing part of the IF is assumed to be included in the nucleus model and thus not modelled separately. To mimic their real structural arrangement, each IF was modelled as two fibres originating from the same FA and being tangential to the nucleus thus creating a dense network in perinuclear region.

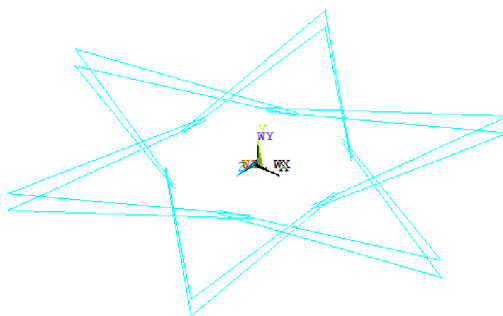


Figure 4. 4: IFs architecture in the proposed computational model.

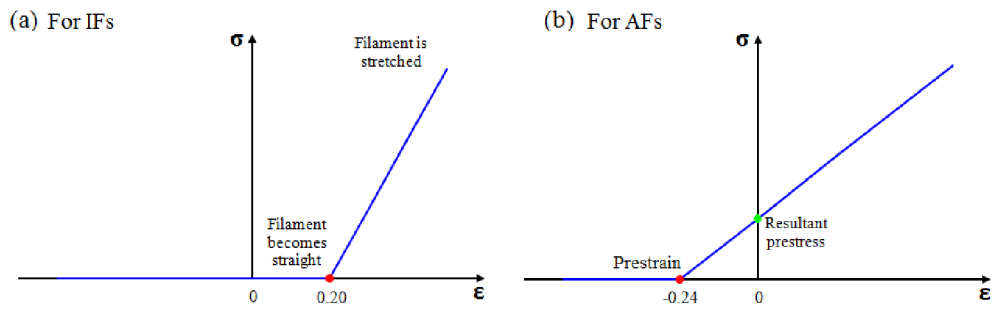


Figure 4. 5: Stress-strain relationship defining the mechanical behaviour of (a) IFs with applied positive strain and (b) AFs with applied negative strain (pre-strain) in their undeformed configurations.

AFs filaments were modelled as truss elements shown in [Fig.4.6](#) that resist only tensile loads. Truss elements are one-dimensional (1D) line elements that have 2 nodes, axial stiffness, and only 3-DOFs (translational) in each node. Thus, they were selected to represent the mechanical behaviour of AFs and IFs that behave in similar way as ropes.

AFs are internally prestressed (i.e. stressed even without application of an external load); to achieve this in the proposed models, experimentally measured prestrain of 24% ([\[47\]](#), [\[79\]](#)) was assigned to them generating the initial force (prestress) essential for cell shape stability ([Fig. 4.5 b](#)). For simplification, this prestrain was equal in all AFs of the model. To achieve the synergistic effect of cytoskeletal components, the elements representing AFs, MTs, and IFs were connected by sharing the same end nodes at the CM representing FAs.

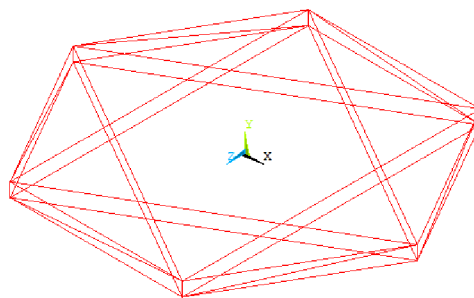


Figure 4. 6: AFs architecture in the proposed computational model.

In this way, the element types used for modelling cytoskeletal components were chosen to represent their idealized structural role in a realistic manner and are summarized in [Table 4.1](#). It is decisive for mechanical response of the model because the mechanical behaviour of living cells is mainly determined by the cytoskeletal filaments ([\[7\]](#); [\[80\]](#)).

All the details of FE models of flat endothelial cells are published in conference paper, see [Appendix D](#). The general overview of computational models of endothelial cells are presented in other conference proceedings, see [Appendix E](#).

#### **4.1.1. Material properties of flat model**

For the proposed model implementing the hybrid modelling approach, the continuum parts (nucleus, cytoplasm) were modelled using continuous (volume) elements circumscribed by a thin layer of shell elements (representing CM) and the cytoskeletal components were modelled using discrete (beam or truss) elements.

For the elasticity of cell components modelled using continuous elements, a Neo-Hookean hyper elastic incompressible/compressible description was used. The reason for adopting Neo-Hookean hyper elastic model is that it is the simplest hyper elastic model which can be defined by a single parameter corresponding to shear modulus (or also by bulk modulus if being compressible), whereas other hyper elastic models require more input parameters that cannot be obtained from experiments published in literature. Also, its predictive capability is better than that of the higher order (Mooney-Rivlin) models which is important especially with a lack of experimental data from multiaxial tests. This model is recommended if the strains do not exceed 50% and no strain stiffening occurs. The values of shear modulus of continuous components recalculated from the published Young's modules are summarized in [Table 4.2](#).

BEAM188 is a linear (2-node) beam element in 3-D with six degrees of freedom at each node (three translations and three rotations). Linear, large rotation, and/or large strain nonlinear applications are well-suited for the beam elements. BEAM188 includes stress stiffness terms, by default, in any analysis with NLGEOM, ON. The stress stiffness terms provided enable the elements to analyse flexural, lateral and torsional stability problems (using eigenvalue buckling or collapse studies with arc length methods).

Thus, the MTs are able to resist tensional as well as compressive forces with their flexural (buckling) behaviour taken into consideration. MTs are modelled as curved beams which requires at least three nodes to define their geometry.

Cell component	Elastic modulus, E (Pa)	Poisson's ratio, $\nu$	Diameter (nm)	Finite element specification	Nature
Microtubules (MTs) [81]	$1.2 \times 10^9$	0.3	25/17 (outer/inner)	BEAM188	Curved Beams
Actin filaments (AFs) [82]	$2.2 \times 10^9$	0.3	7	LINK180	Tension only
Intermediate filaments (IFs) [82]	$2.0 \times 10^9$	0.3	10	LINK180	Tension only

Table 4. 1: Elastic properties of discrete components of cell model.

As the one-dimensional line elements do not support hyper elasticity in ANSYS software, homogenous, isotropic, and linear elastic material properties were considered for all the cytoskeletal components; their elastic parameters taken from the literature are summarized in [Table 4.1.](#)

Component Name	Young's Modulus E (Pa)	Shear Modulus G (Pa)	Bulk Modulus K (Pa)	Finite element specifications
Cytoplasm [50]	$0.5 \times 10^3$	$0.17 \times 10^3$	$2.77 \times 10^3$	SOLID 185
Nucleus [50]	$5 \times 10^3$	$1.7 \times 10^3$	$27.77 \times 10^3$	SOLID 185
Cell membrane (CM) [76]	$1 \times 10^6$	$0.33 \times 10^6$	Infinity	SHELL 181

Table 4. 2: Hyper elastic properties of continuous components of cell model

## 4.2. Spherical model of suspended endothelial cell

The experiments [50] show a spherical shape of suspended cells used in most mechanical tests. In order to validate the mechanical response of endothelial cell, we rearranged the shape of flat endothelial cell model into the spherical cell model as shown in [Fig.4.7](#); for this purpose, we assumed the same volume of the cell.

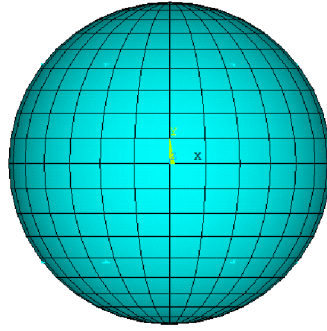


Figure 4. 7: Spherical model of suspended endothelial cell

The dimensions are recalculated by equating volume of regular hexagonal prism to the volume of a sphere. From this, the diameter of cytoplasm is  $7.4 \mu\text{m}$  and diameter of nucleus is  $3.0 \mu\text{m}$ .

### 4.3. Modification of the FE model for adherent endothelial cell

Implementing the bendo-tensegrity concept [70] with fusion of continuum and discrete approaches, a FE bendo-tensegrity model of adherent cell [27] modified from the suspended cell model incorporating Microtubules (MTs), Actin Bundles (ABs), Intermediate filaments (IFs), nucleus, cytoplasm, and Actin cortex (AC) is proposed in the current study. The unique features of this structural model keep fundamental principles governing cell behaviour, including cellular prestress and interaction between the cytoskeletal components with their more realistic morphological representation for cell in adherent state.

In this study, the simulation of compression test with the proposed FE adherent cell model was performed to validate the model with modified geometry and structure. Images of cytoskeletal protein distributions and in situ microscopic observations of cell shape in adherent state (Fig. 4.8 a) were used to develop a 3D adherent cell model (Fig. 4.8 b) and the architecture of its cytoskeletal components.

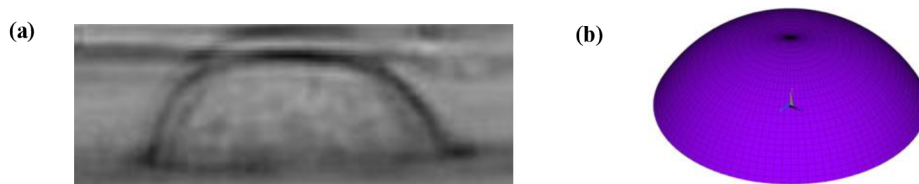


Figure 4. 8: Typical images of: (a) an adherent cell on a rigid microplate [50] and (b) corresponding proposed FE adherent cell model.

The adherent cell model is slightly distinct from the suspended cell model. It encompasses the nucleus and cytoplasm enclosed by the Actin Cortex and cytoskeletal components like ABs, MTs, and IFs (Fig. 4. 9). For this model, the approximate geometry was based on the rules

described by [25]. The maximum diameter of our model axisymmetric cell was 20 microns, while the maximum height was 8 microns. The model nucleus had a flat ellipsoidal shape with a maximum diameter of 8 microns and a height of 4 microns based on the experimental observations [50]. The experimentally measured thickness of the cortical layer is 0.2  $\mu\text{m}$  (i.e. 20 times thicker than the cell membrane itself) was chosen for our model ([21]; [83]) and the values are consistent with another study on endothelial cells [84].

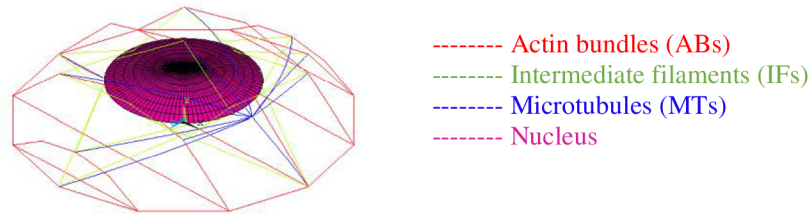


Figure 4. 9: Structural arrangement of cytoskeletal components with respect to the nucleus. The cytoplasm and nucleus were both meshed with four-node tetrahedral solid elements due to the geometric complexity of the cell configuration. A thin layer of actin-gel at the cell surface, referred to as AC, was modelled with four-node quadrilateral shell elements with no bending stiffness, using an equivalent approach as reported by [15]. For this model, the topological distribution of both MTs and IFs was retained analogous to that of the suspended cell model. In contrast, however, in a cell adhered to a rigid substrate thick ABs were observed localized at the cell periphery running almost uniformly in the longitudinal direction ([15]; [47]) as depicted in Fig. 4.10 b.

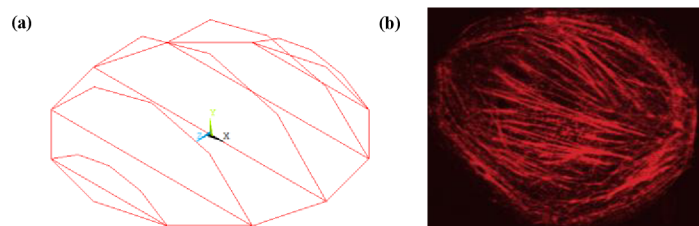


Figure 4. 10: (a) architecture in the proposed computational model and (b) Microscopic fluorescence image of the architecture of ABs cited from [85]

These bundles were modelled using truss elements (Fig. 4.10 a) that resist only tensile loads and are arranged along the AC with both ends anchored to it at FAs together with elements representing MTs and IFs. Similarly, to AFs in the spherical model, ABs are internally prestressed; to achieve this in the proposed model, the prestress caused by the 24% prestrain (

[47]; [15]) was assigned to them generating the initial force essential for cell shape stability. For simplification, all the ABs in the model were prestressed equally.

Cell Component	Element Type	Element definition
Microtubules (MTs)	Beam	Beam188
Actin bundles (ABs)	Truss	Link180
Intermediate filaments (IFs)	Truss	Link180
Actin cortex (AC)	Shell	Shell181
Cytoplasm	Continuous(volume)	Solid185
Nucleus	Continuous(volume)	Solid185

Table 4. 3: Mesh properties of the adherent cell model in ANSYS

The element types chosen for modelling cytoskeletal components to represent their idealized structural role are summarized in [Table 4.3](#).

#### 4.3.1. Material properties of adherent model

Material properties have been set mostly identical with the suspended cell model presented in [Table 4.1](#) and [Table 4.2](#); differences are highlighted in bold in [Table 4.4](#), and [Table 4.5](#). Due to the difficulty of obtaining elastic parameters of cellular components from a single cell type, those employed in the current study were acquired from literature for distinct cell types measured using various experimental techniques.

Cell component	Elastic modulus, E (Pa)	Poisson's ratio, $\nu$	Diameter (nm)
Microtubules (MTs) [81]	$1.2 \times 10^9$	0.3	(outer/inner) 25/17
<b>Actin bundles (ABs) [47]</b>	<b><math>0.34 \times 10^6</math></b>	<b>0.3</b>	<b>250</b>
Intermediate filaments (IFs) [82]	$2.0 \times 10^9$	0.3	10

Table 4. 4: Elastic properties of discrete components of adherent cell model

Cell component	Elastic modulus, E (Pa)	Calculated shear modulus, G (Pa)
Cytoplasm [50]	$0.5 \times 10^3$	$0.17 \times 10^3$
Nucleus [50]	$5 \times 10^3$	$1.7 \times 10^3$
<b>Actin cortex (AC) [86]</b>	<b><math>2 \times 10^3</math></b>	<b><math>0.67 \times 10^3</math></b>

Table 4. 5: Hyper elastic properties of continuous components of adherent cell model



## 5. FINITE ELEMENT SIMULATIONS OF ENDOTHELIAL CELL

### 5.1. Simulations of suspended cell model

To validate the proposed bendo-tensegrity model of a suspended cell, compression and tensile tests of endothelial cells were simulated and compared with experimental results from literature.

#### 5.1.1. Simulations of suspended cell in compression and its experimental validation.

The compression test of a suspended cell done with microplates was simulated to compare with the cell response to compression. The simulation was performed in several successive steps, mimicking the experiment [50]. The spherical shape of the cell with prestressed AFs serves as the initial state and the microplates are supposed rigid. To avoid further nonlinearities related to contact, the cell was fixed in the central node of the cell in all directions and compressed vertically on both sides (top and bottom side) of the cell by applying vertical displacements to the nodes on both sides in order to flatten the area being in contact with the microplates and to achieve 50% deformation of the cell. Further details of the compression test with suspended cell can be found in [Appendix C](#) where, however, a smooth muscle cell was simulated instead of endothelial cell.

To assess the impact of cytoskeleton, the simulations were repeated with models with individual cytoskeletal components being removed and with a continuum model without any cytoskeleton.

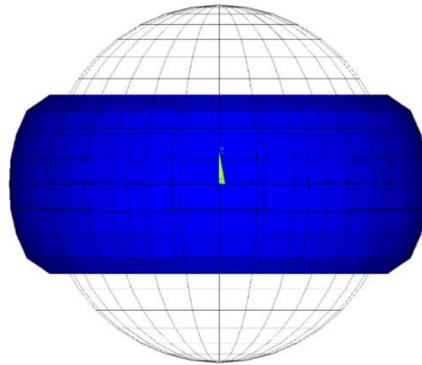


Figure 5. 1: Suspended cell model during consecutive steps in simulation of Compression test at 50% compression (blue) and unloaded state (wire frame)

The force-deformation (%) curve calculated from compression test simulation is in good agreement with the non-linear responses of the experimental curves obtained from the compression test of cultured endothelial cells [50], as depicted in [Fig. 5.2](#) and thus validates the proposed bendo-tensegrity model of a suspended cell. The slope of the simulated force-

deformation curve increased with increase in cell compression, similar to that observed in the experiments.

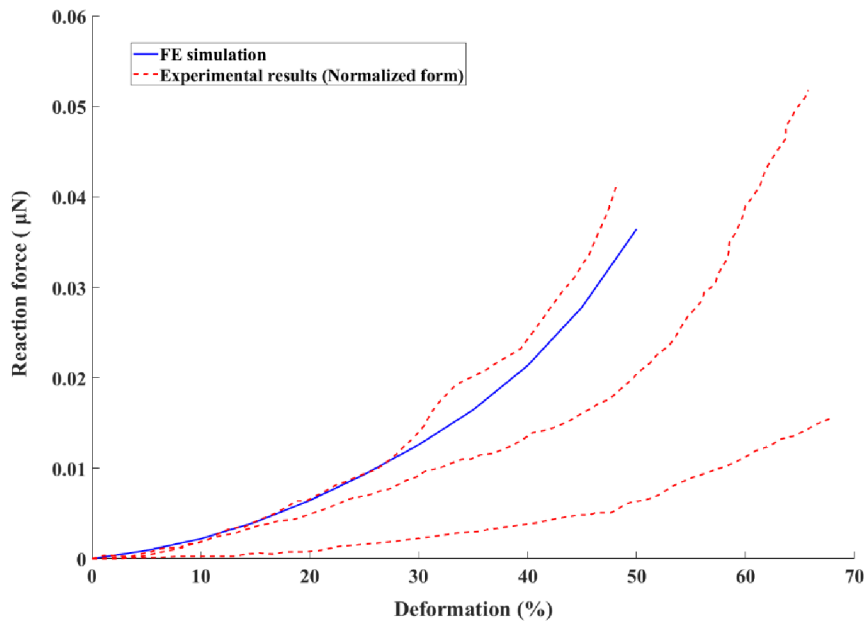


Figure 5. 2: Comparison of simulated force-deformation (%) curve with the experimental curves taken from a study by [50] investigating the biomechanical properties of a single endothelial cell using a micromanipulation technique.

During simulation of compression test, the nucleus appears elongated perpendicularly to the loading direction concomitant of cell compression, analogous to that observed in experiments [50]. MTs localized in the central region perpendicular to the direction of loading were merely straightened, while the others remain bended (Fig. 5.3 c). MTs in the direction perpendicular to compression that became less curved resist tensile forces and generate low positive stresses, while those ones that were bended more due to compressive forces generate low negative stresses; this effect highlights the influence of the shape of MTs on cell deformation.

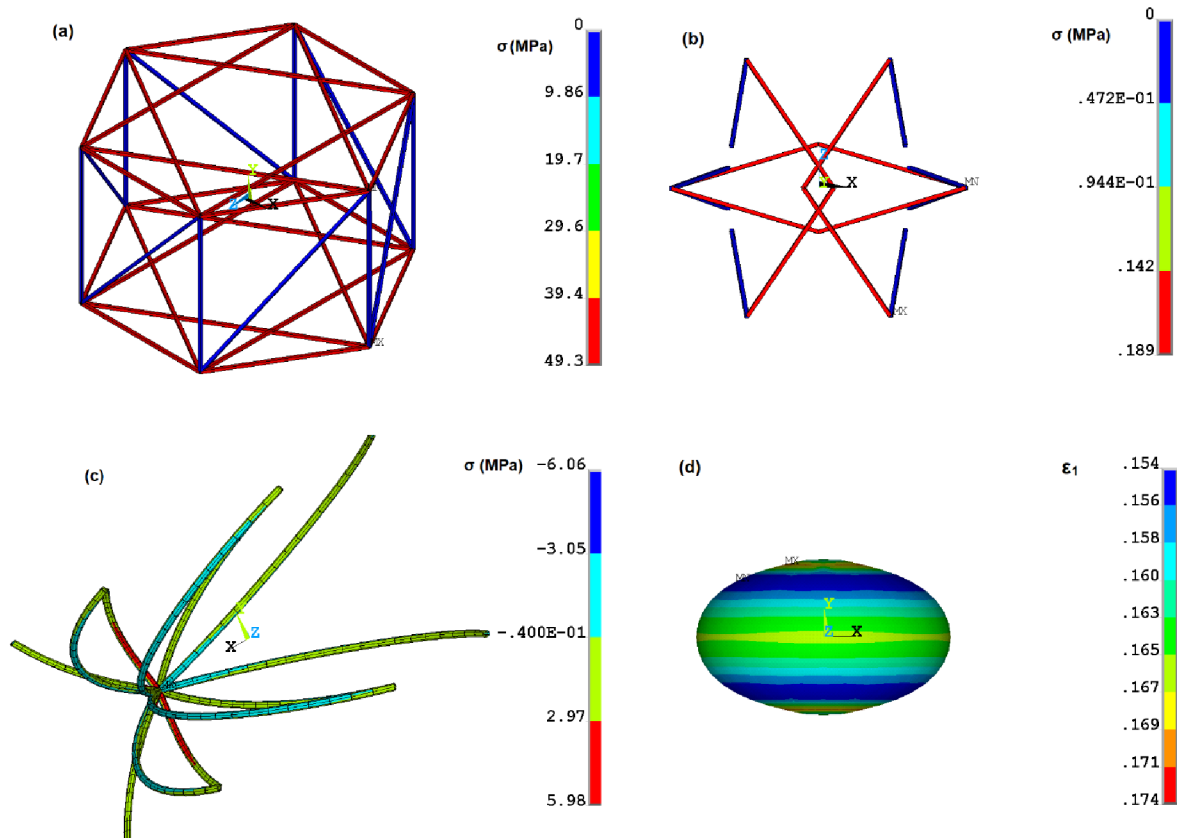


Figure 5. 3: Simulation results of 50% cell compression: Stresses in (a) AFs (b) IFs and (c) MTs; (d) distribution of first principal strain in the continuous elements representing nucleus.

The proposed model can predict correlation of cellular mechanical properties and stress/strain distribution within the specific cytoskeletal components during compression. AFs reoriented perpendicularly to the loading direction resist tensile forces and generate high stresses ([Fig. 5.3 a](#)) consequently increasing stiffness of the entire cell. The number of these reoriented filaments increased with cell compression that in turn increased the cell stiffness gradually as observed experimentally by [\[50\]](#).

IFs reoriented perpendicularly to the direction of compression were slightly uncoiled from their assumed initial waviness and exhibited very lower positive stresses induced ([Fig.5.3 b](#)). This quantitative characterization of nucleus deformation could be hypothetically decisive for transducing mechanical signals into changes in gene expression for 50% cell compression (global deformation).

Under 50% compression, the reaction force of the cell model without cytoskeleton was 1.32 times lower than the model with cytoskeleton ([Fig. 5.2](#)), highlighting its role in characterizing the compressive properties of cell. When MTs were removed the model showed an approximately 1.08 times decrease in the cell reaction force compared to the hybrid model.

When IFs being removed the model showed an approximately 1.04 times decrease in the cell reaction force compared to the hybrid model. When AFs were removed, the maximum reaction force of the cell model without AFs was 1.20 times lower than the hybrid model. Even though AFs are tension bearing elements, they play a vital role in maintaining the cell stiffness during compression, similar to that observed experimentally by [10].

### 5.1.2. Simulations of suspended cell in tension and its experimental validation

The tensile test of a suspended cell with rigid micropipettes was simulated for comparison of the cell response to stretching.

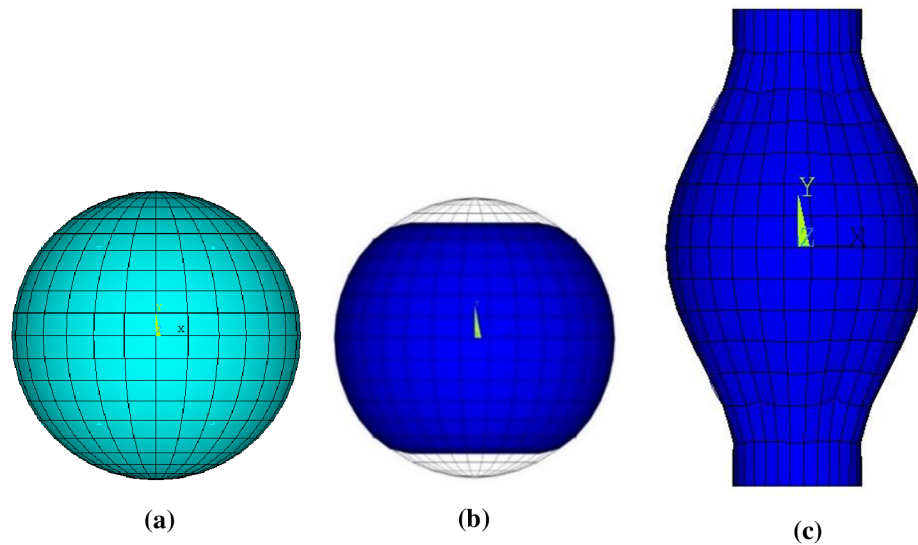


Figure 5. 4: The suspended cell model during consecutive steps in simulation of tensile test:

(a) spherical cell, (b) compressing the cell by 20% and (c) stretching the cell 50%

The simulation was performed in several steps, mimicking the experiment [87]. In the first step, contact between the spherical cell (with prestressed AFs) and both micropipettes were established by compressing the cell by approximately 20%. In the second load step, the cell was elongated to achieve zero reaction forces in the micropipettes; this shape serves then as the initial (unloaded) state of the cell. In the final step, displacement was applied to the nodes of the top and bottom surfaces in order to achieve 50% tensile strain of the model. The reaction force was assessed as the sum of forces at the nodes of the either top or the bottom surface of the cell. The distance between micropipettes in the state with zero reaction force was taken as the unloaded length of cell and therefore, it differs from the cell diameter.

The force-elongation curve calculated from tensile test simulation is in good agreement with the non-linear responses of the experimental curves obtained from the tensile test of cultured Bovine aortic endothelial cells [87], as depicted in [Fig. 5.5](#).

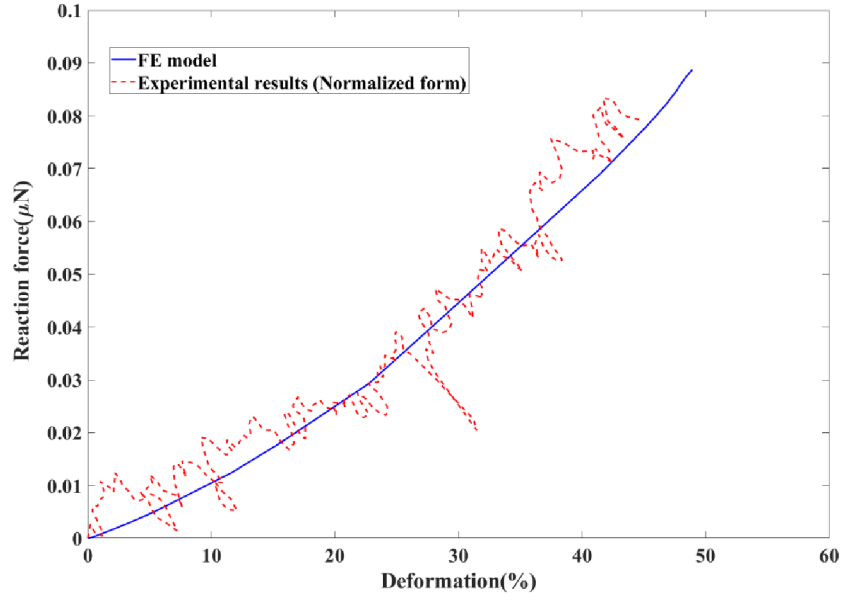


Figure 5. 5: Comparison of simulated force-deformation (%) curve with the experimental curves taken from a study by [87], measuring the tensile properties of cultured Bovine aortic endothelial cells.

The cell diameter in the experiments differs from our model, thus for comparison the experimental results are normalized to the same diameter; in reaction force it was as  $F_N = F \left[ \frac{D}{D_{exp}} \right]^2$  and the normalized deformation is given as  $\Delta l_N = \Delta l \left[ \frac{D}{D_{exp}} \right]$ .

where  $D$  is diameter of the suspended cell model and  $D_{exp}$  is the cell diameter in the experimental results.

The stiffness of the hybrid model of suspended cell in tension was evaluated as the ratio of conventional stress ( $\sigma$ ) to conventional strain ( $\epsilon$ ) being proportional to the slope of the resulting force-elongation curve. The conventional stress is given as:

$$\sigma = \frac{f}{a}$$

Where,  $f = 0.0765 \mu N$  was the reaction force of cell at the stretched edge and  $a = 42.9866 \mu m^2$  was the (maximal undeformed) cross-sectional area of cell.

With reference to [Fig. 5.5](#), the stiffness of 3.17 kPa calculated for the FE model ( $D=7.4 \mu m$ ), is in good accordance with the stiffness of  $2.6 \pm 0.7$  kPa calculated for the experimental cell sample.

The proposed model can predict the relation between cellular mechanical response to stretching and stress/strain distributions within the specific cytoskeletal components. During cell

stretching, the randomly oriented AFs were likely to be aligned in the direction of stretch. This passive realignment gradually increased the overall reaction force of the cell, causing the force-elongation curve to be non-linear ([19]; [88]). During cell stretching some of the MTs were merely straightened out, while others remain bended (Fig. 5.6.c). MTs that were straightened and aligned in the direction of stretch resist tensile forces and generate high stresses, while the ones that were bended due to compressive forces generate negative stresses; this effect highlights the influence of the shape of individual MTs on cell deformation. High stresses in straightened MTs can be attributed to the large difference between their flexural and tensional stiffness, which may significantly contribute to the non-linearity of cell responses. High stresses were observed also in AFs (Fig. 5.6.a) that were aligned in the direction of stretch and resist tensile forces. IFs aligned in the direction of stretch were linearized from their assumed initial waviness and exhibited high strains, while only low stresses were observed in the ones oriented in longitudinal direction and zero stress occurs in the others which remain wavy.

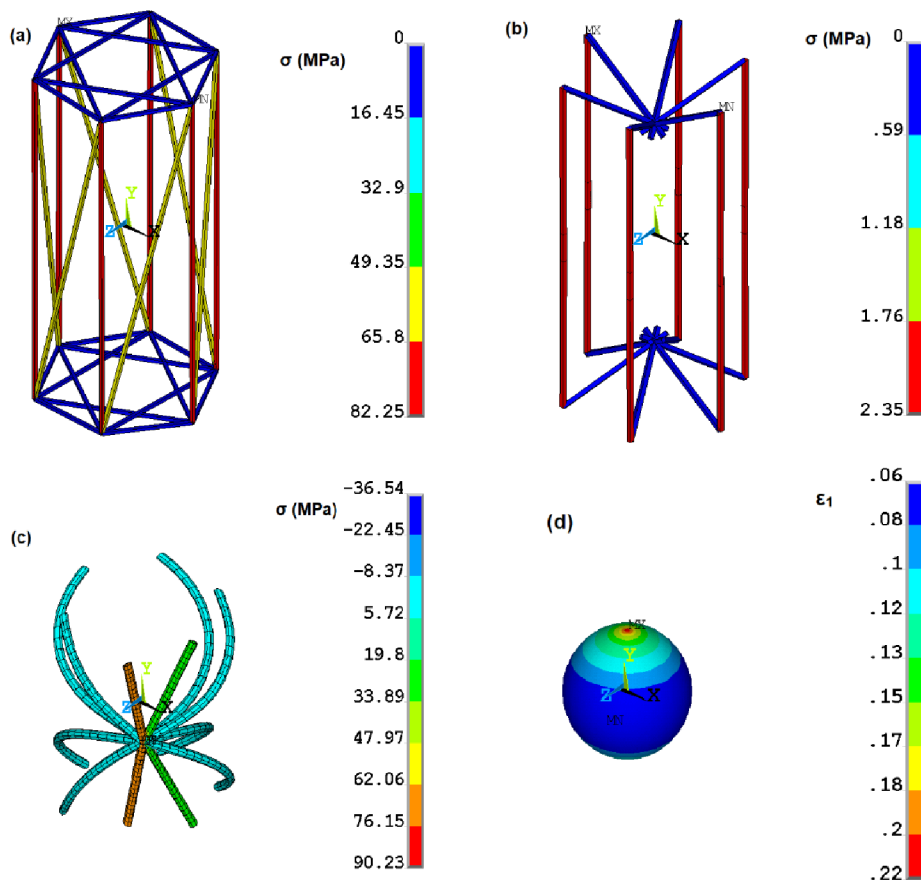


Figure 5. 6: Simulation results of 50% cell elongation: axial stress distribution in (a) AFs (b) IFs and (c) MTs; (d) distribution of first principal strain representing nucleus.

### 5.1.3. Role of cytoskeletal components

The role of each cytoskeletal component in cell stiffness was investigated via removal of this component from the hybrid model as illustrated in [Fig. 5.7](#) comparing the stiffness of the modified models, i.e. the total reaction force under the same (maximum) deformation. The results in [Fig. 5.7 \(a\)](#) show that the stiffness of the spherical model in compression decreases by some 32% when all the cytoskeleton components are removed; the contribution of AFs to the stiffness appears to be the highest: compared to the reaction force of the hybrid model, removal of AFs reduced the reaction force of the cell model by 20%. These rather contra-intuitive result relates to volume incompressibility of the cytoplasm and a consequent increase in lateral dimensions of the cell under compression.

In simulations of the tensile test of the spherical model, the maximum reaction force of the cell model without cytoskeleton was by 66% lower than that for the hybrid model (see [Fig. 5.7 \(b\)](#)), and both AFs and MTs played a vital role in this decrease.

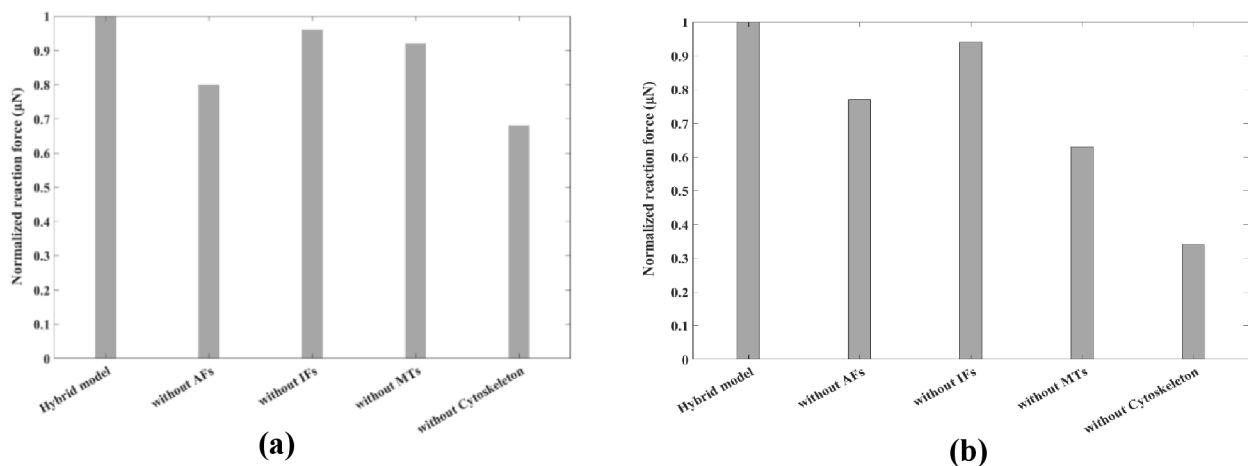


Figure 5. 7: Contribution of cytoskeletal components in spherical cell model to its stiffness (a) in compression, (b) in tension. The reaction force is normalized to 1 with respect to that from hybrid model.

### 5.1.4. Summary and discussion of suspended cell model

The proposed bendo-tensegrity model of suspended cell describes the response of cytoskeletal components and cell as a whole to distinct mechanical stimuli (tension and compression), thus satisfying the initial hypothesis. The proposed model predicted the relation between cellular mechanical response and stress/strain distributions within the specific cytoskeletal components under different loading conditions. For simulation of both tests, it provides quantitative characterization of nucleus deformation.

The compression test simulations revealed that although being tension-bearing elements, AFs contribute significantly even to the compressive response of a cell. Thus, the proposed bendo-tensegrity model identifies the cytoskeletal components that influence the global mechanical response of suspended cell depending on the type of mechanical loading.

Thus, the proposed suspended cell model based on the bendo-tensegrity concept provides new insights into the interdependence of cellular mechanical properties, the mechanical role of components of cytoskeleton, and the nucleus deformation under different mechanical loading conditions.

The presented models aim at realistic simulation of the deformation of cell, primarily focusing on mimicking its structure to obtain realistic nucleus deformation. It is well established that cells respond to mechanical stimuli in a variety of ways that range from changes in cell morphology to activation of biochemical responses, which affect the cell's phenotype. The nucleus plays a central role in defining cell responses thus the current study provides an insight into its deformation by means of FE modelling of distinct single cell mechanical tests. The nucleus deformation (maximum first principal strain,  $\epsilon_1$ ) was observed for 50% global deformation for compression is 0.176 and for tension 0.218.

The tensile test simulation results demonstrated that the bended MTs were highly compliant with lower stresses, whereas the straight ones (being in tension only) showed much higher stresses ([Fig. 5.6 \(c\)](#)), highlighting the significant contribution of MTs arranged in loading direction to the cell stiffness during stretching. When stretched by approximately 50 % the suspended cell model gave the reaction force of 0.0765  $\mu\text{N}$  that evaluated the cell stiffness of 3.17 kPa, which is in good agreement with normalized stiffness of  $2.6 \pm 0.7$  kPa measured for cultured bovine aortic endothelial cells [87]. The effect of cytoskeletal components in tension and compression test simulations demonstrated that removal of AFs reduced the cell stiffness by approximately 23% and 20%. This difference in stiffness might be attributed to the treatment with cytochalasin D that resulted in disruption of not only the deep actin fibres but also an actin meshwork beneath the CM [10]. As a result, the cell stiffness was reduced substantially during experiments in contrast to the simulations.

The cellular tensegrity models envision AFs as tension supporting cables and MTs as compression supporting struts [7]. Although these models successfully explain several observations in cell mechanics, the excessive compression stiffness of the struts introduces non-realistic artifacts in tension test simulations, as shown by ([17]; [18]). The previous tensegrity-based models neither take into account the influence of flexural behaviour of MTs nor predict the impact of individual cytoskeletal components. The proposed bendo-tensegrity models



modify this structural concept by taking into account both flexural (buckling) as well as tensional behaviour of MTs and they enable us to change their stiffness by changing their curvature.

Although the proposed models have some advantages over the previous models, they have certain limitations as well. The structural arrangement of cytoskeletal components does not capture their true complexity and dynamic behaviour as observed in living cells. These models also do not take into consideration the viscoelastic nature of cell. Due to their passive nature, they are not able to capture the active responses of cell such as remodelling of AFs and MTs exhibited under mechanical loading. However, this remodelling occurs in longer time periods than duration of the considered experiments thus they cannot be captured by the experimental response.

## 5.2. Simulations of adherent cell model

### 5.2.1. Simulations of adherent cell in compression and its experimental validation

The boundary conditions (see [Fig. 5.8](#)) are applied by mimicking the experimental approach [50] investigating the behaviour of a single endothelial cell under compression using a micromanipulation technique.

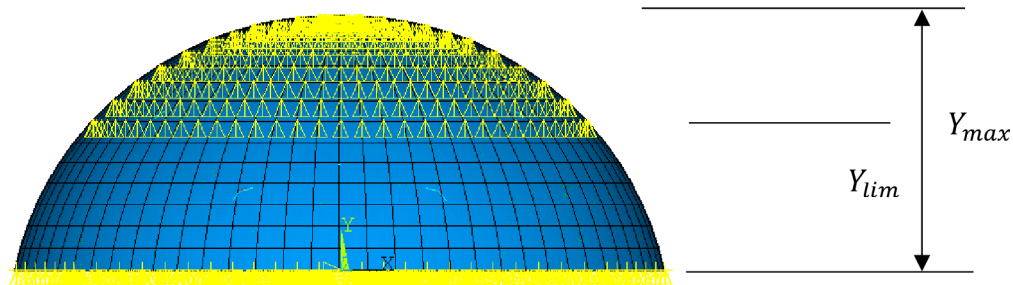


Figure 5. 8: FE model of an adherent cell in the Compression test, with constraints and displacement load applied on the top of the cell. (front view).

The initial shape of the cell model was truncated sphere being close to the real shape of the adherent cell. The cell was then compressed vertically on its top side by applying vertical displacements to the nodes in order to flatten the area coming gradually into contact with the microplates and to achieve the total 50% deformation of the cell. The reaction force was evaluated as the sum of forces at nodes of top side of the cell.

To validate the adherent cell, the simulation of compression test was performed by mimicking the experiments by [50]. Results of the simulation are presented in [Fig. 5.9](#) (undeformed and

deformed mesh on the cell surface), and [Fig. 5.10](#) (first and third principal strains in the nucleus).

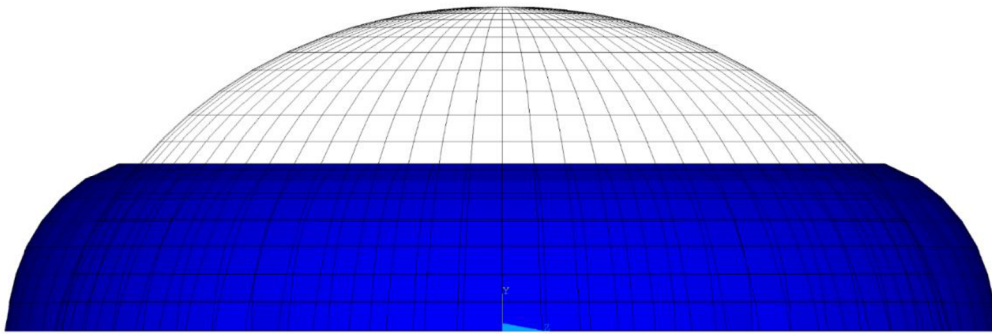


Figure 5. 9: Adherent cell model in simulation of Compression test: unloaded shape of truncated sphere in wire frame and final shape with 50% compression of the cell in solid blue color.

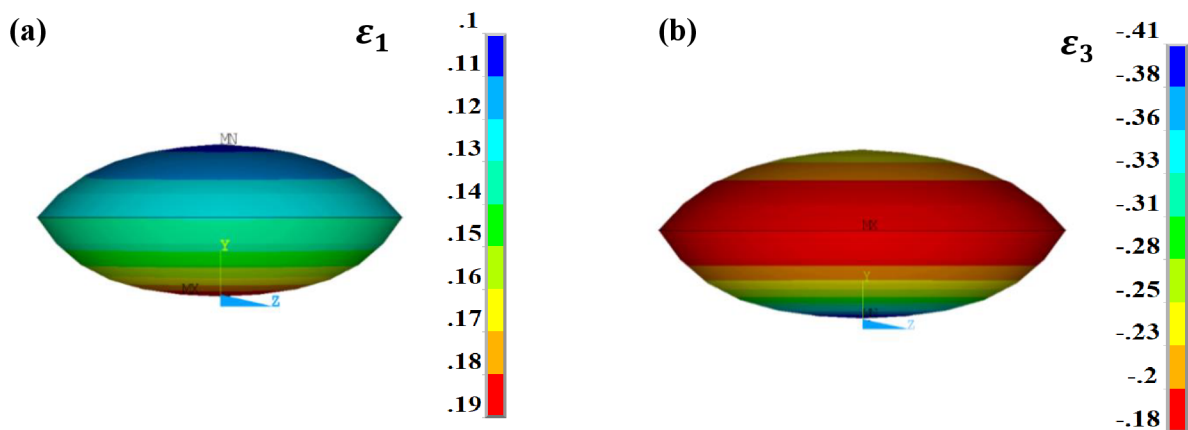


Figure 5. 10: Distribution of (a ) first principal strain (b) third principle strain in the nucleus of adherent endothelial cell.

The force-deformation curve calculated from compression test simulation is in good agreement with the non-linear responses of the experimental curves obtained from the compression test of cultured endothelial cells [50], as depicted in [Fig. 5.11](#). And thus, validates the proposed bendotensegrity model of adherent cell. The slope of the simulated force-deformation curve increased with increase in cell compression, similar to that observed in the experiments.

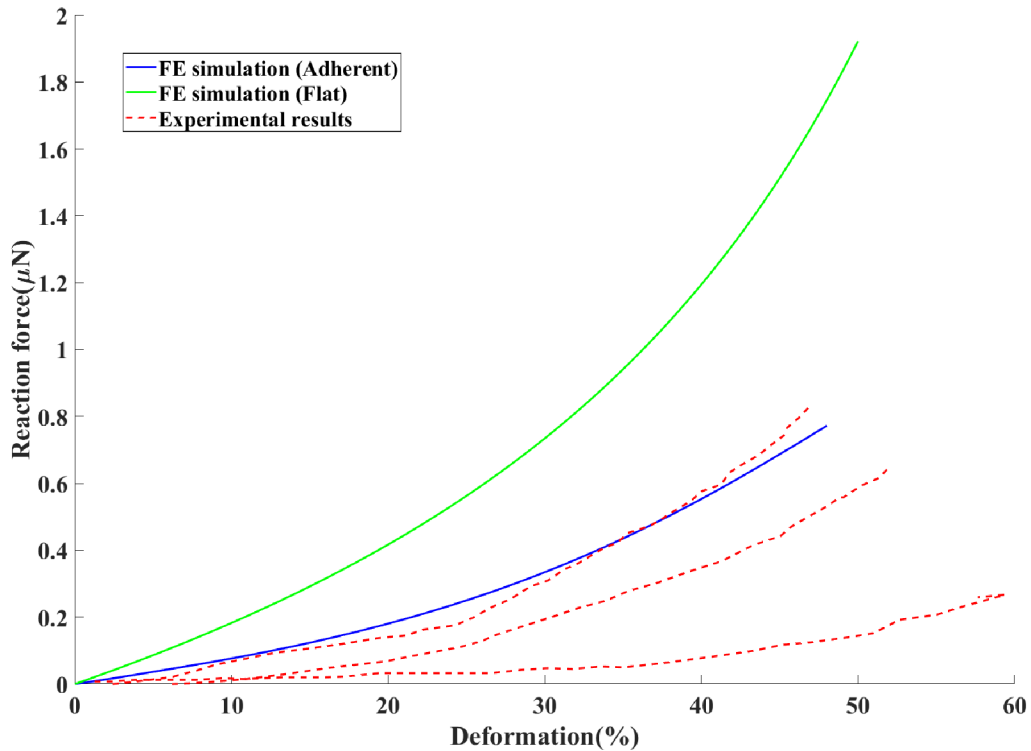


Figure 5. 11: Comparison of simulated force-deformation curves obtained with the adherent cell and flat cell models with the experimental curves taken from the study by [50].

The quantitative characterization of nucleus deformation could be hypothetically decisive for transducing mechanical signals into changes in gene expression for 50% cell compression (global deformation).

### 5.2.2. Role of cytoskeletal components

The role of each cytoskeletal component in cell stiffness was investigated via removal of this component from the hybrid model as illustrated in [Fig. 5.7](#) comparing the stiffness of the modified models, i.e. the total reaction force under the same (maximum) deformation. The results in [Fig. 5.12](#) show that the stiffness of the adherent model in compression decreases by some 32% when all the cytoskeleton components are removed; the contribution of AFs to the stiffness appears to be the highest: compared to the reaction force of the hybrid model, removal of ABs reduced the reaction force of the cell model by 20%. These rather contra-intuitive result relates to volume incompressibility of the cytoplasm and a consequent increase in lateral dimensions of the cell under compression.

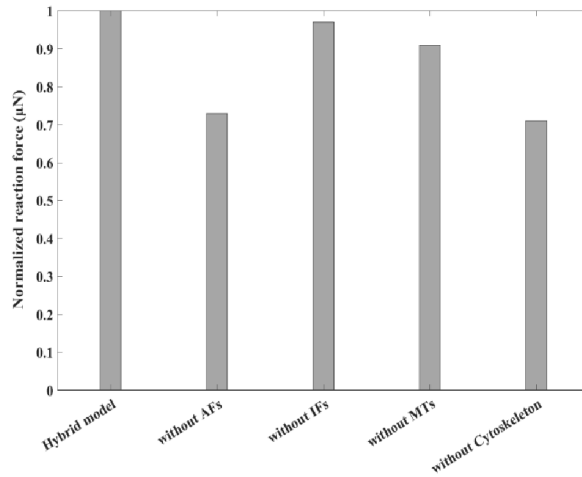


Figure 5. 12: Contribution of cytoskeletal components in adherent cell model to its stiffness (a) in compression. The reaction force is normalized to 1 with respect to that from hybrid model.

### 5.3. Simulation of flat cell model

#### 5.3.1. Simulations of regular flat and domed cell in compression

The compression test of a regular flat endothelial cell model was simulated to investigate the cell response to compression. The simulation was performed in several successive steps, mimicking the experiment [50]. The cell model was then compressed vertically (in thickness direction) on top and bottom side of the cell to achieve 50% deformation of the cell. The reaction force was evaluated as sum of reaction forces on either top or bottom surface nodes.

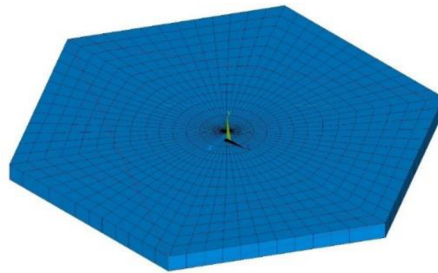


Figure 5. 13: FE model of undeformed shape of regular flat hybrid endothelial cell

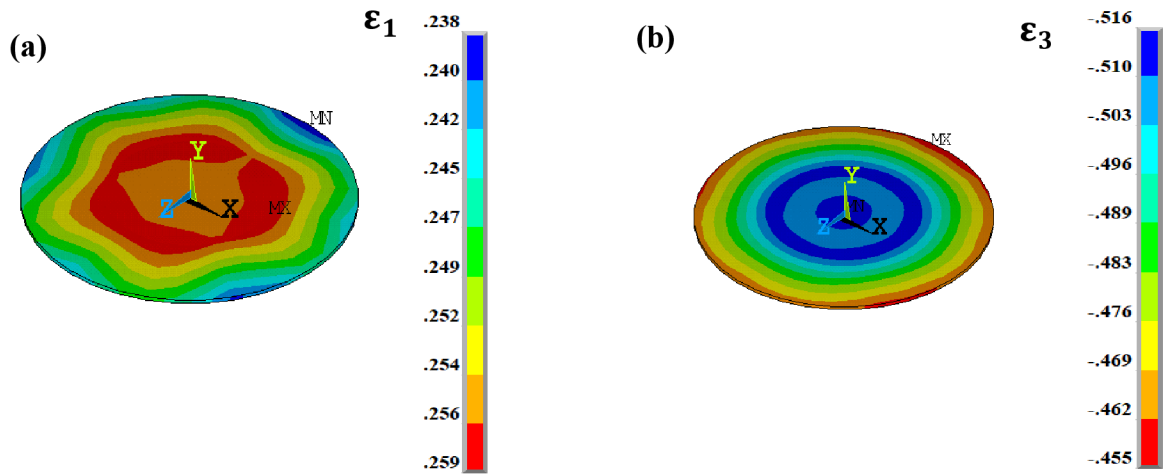


Figure 5. 14: Distribution of (a) first principal strain (b) third principle strain in the nucleus of flat endothelial cell in isometric view.

The stiffness of the flat model is several times higher than the adherent model (Spread cell) presented in experimental results from [50]. The reason is evidently in the different shape of the flat model which corresponds to a very short hexagonal prism with its upper hexagonal face being in full contact with the microplate. In contrast, the experiment was done with a single cell cultivated in vitro on a substrate which results in a different shape with the top contact area being much smaller.

Investigation done with adherent and flat cell models under compression brought results qualitatively similar to those with the spherical model under compression, as illustrated in [Fig. 5.15.](#)

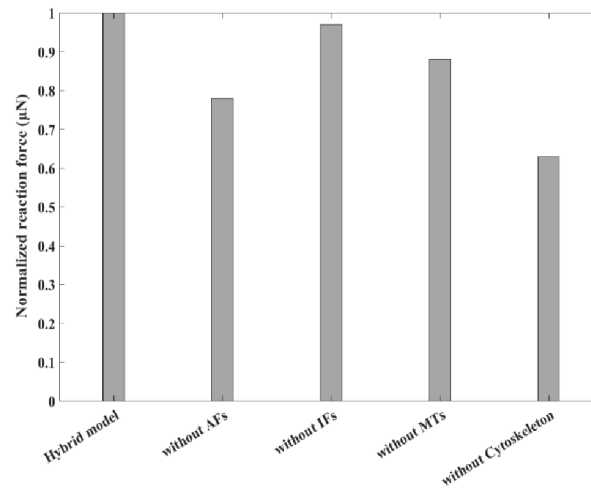


Figure 5. 15: Contribution of cytoskeletal components in cell models to their stiffness in compression flat model. The reaction force is normalized to 1 with respect to that from hybrid model.

The role of cytoskeletal filaments and discussions related to the results are explained in [Appendix A](#).

### 5.3.2. Simulations of regular flat and domed cell in shear

The shear test of a flat endothelial cell model was simulated to investigate the cell response to shearing load. The flat shape endothelial cell model presented in Fig.6.5. In this simulation, all the nodes of bottom hexagonal face were fixed in all directions. The cell was then loaded on the top side by prescribed constant displacements in x-direction (in all the surface nodes in top side) in order to achieve shear deformation of the cell. The resultant reaction force was evaluated as the sum of forces at nodes of the top side of the cell. The boundary conditions of the flat endothelial cell are shown in [Fig. 5.16](#) and 15% shear deformation is shown in [Fig. 5.17](#). The distribution of first principal stress in nucleus is presented for flat and domed in the [Fig. 5.19](#).

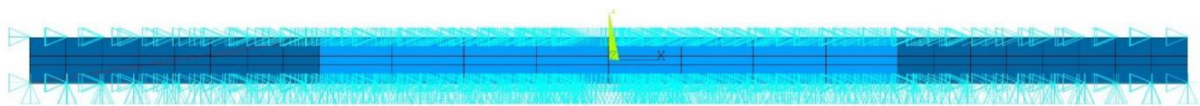


Figure 5. 16: Boundary conditions of flat endothelial cell for shear

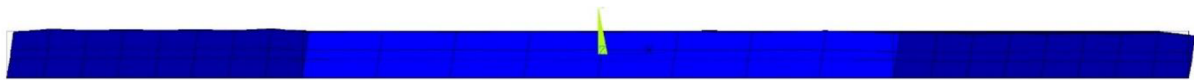


Figure 5. 17: Shear deformation of regular flat endothelial cell

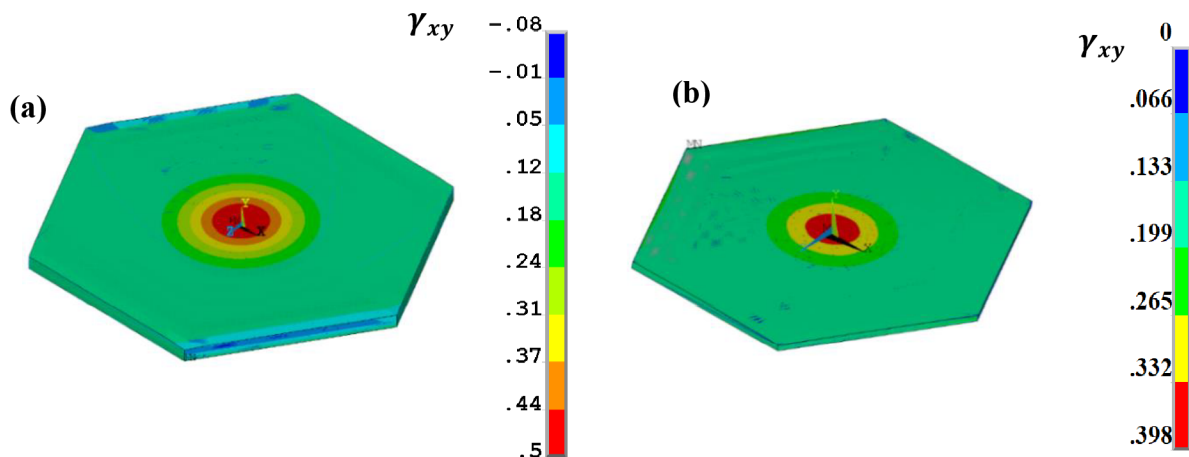


Figure 5. 18: Distribution of shear strain in xy direction of flat endothelial cell at 15% shear deformation in isometric view. (a) regular flat (b) regular domed

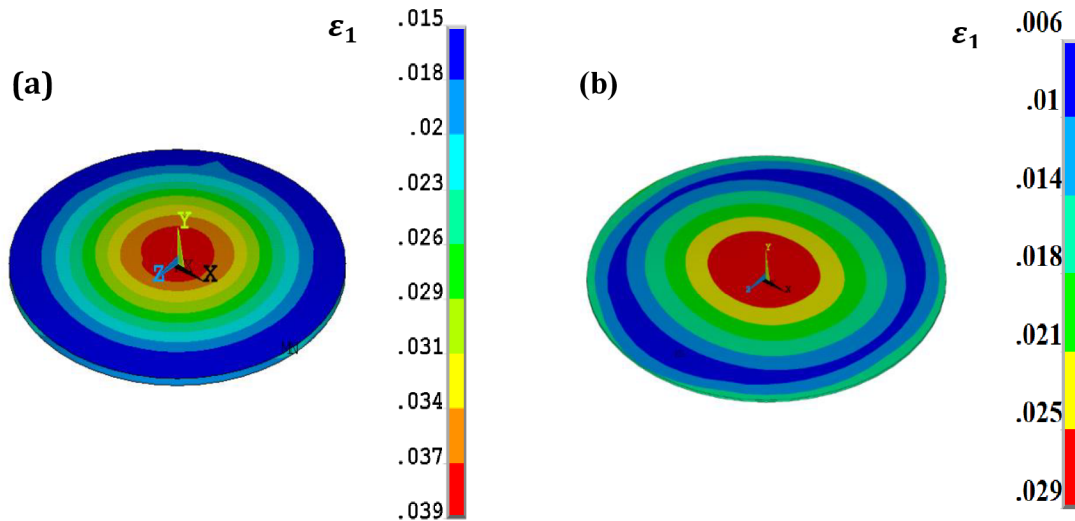


Figure 5. 19: Distribution of first principal strain in the nucleus of regular endothelial cell at 15% shear deformation in isometric view (a) regular flat (b) regular domed

The maximum shear strain in xy plane within the whole cell is about 0.5 (see [Fig. 5.18](#)). However, the nucleus undergoes much lower strains (some 0.04, see [Fig. 5.19](#)) as it is 10 times stiffer than the cytoplasm and the shear deformation is concentrated in the cytoplasm above and below the nucleus. Evidently, the transmission of strain to nucleus is much lower in shear than under the other loading conditions.

The total reaction force (F) is calculated by taking a sum of reactions on nodes of top hexagonal plane; its resulting value is 759 pN.

Area of regular hexagon is  $405.95 \mu\text{m}^2$  @ side length of  $12.5 \mu\text{m}$

The resultant shear stress is  $\tau = \frac{\text{Resultant Force}}{\text{Area of hexagon}}$  which is equal to  $1.87 \text{ Pa}$

This shear stress is within the physiological range of wall shear stresses in arteries. The detailed information about the simulations of Flat cell model in shear are addressed in a journal paper, see [Appendix A](#).



## 5.4. Simulations of flat cell in different variants under physiological conditions

The “in situ” physiological load of an arterial endothelial cell comprehends blood pressure and the corresponding circumferential strain, axial pre-stretch intrinsic for arteries and shear load from the blood flow [89]. While all the other physiological conditions can be found in literature, the circumferential strain depends, in addition to the blood pressure, on dimensions and material properties of the arterial wall and its layers. As intima is very thin and mechanically irrelevant in healthy arteries [90], we used only two layers representing media and adventitia of different arteries to calculate circumferential deformations of the endothelium.

The dimensions of media and adventitia (inner  $R_1$ , interface  $R_2$  and outer  $R_3$  radiuses, see [Fig. 5.20 \(a\)](#) of the chosen arteries are specified in [Table 5.2](#).

The arterial wall was modelled as axisymmetric using quadratic elements with material properties described by a 3rd order ( $N = 3$ ) hyper-elastic incompressible Yeoh model with strain energy potential given as:

$$W = \sum_{i=1}^N C_{i0} (\bar{I}_1 - 3)^i$$

where  $\bar{I}_1$  is the 1st invariant of right Cauchy-Green deformation tensor and  $C_{i0}$  are stress like material parameters. Note that the neo-Hookean model used for continuous cell components is a specific case of Yeoh model for  $N = 1$ . The material parameters of media and adventitia (according to [90]) are specified in [Table 5.1](#).

Tissue	Material Constants [kPa]		
	$C_{10}$	$C_{20}$	$C_{30}$
Media	122.3	0	337.7
Adventitia	88.7	0	45301.4

Table 5. 1: Hyper-elastic material properties of arterial layers [90]

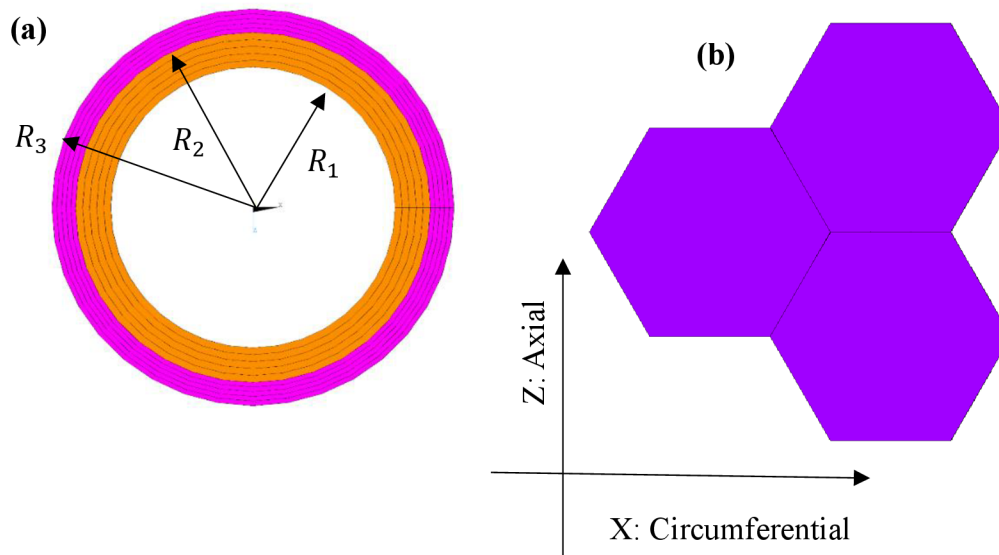


Figure 5. 20: (a) Finite element mesh (in axial view) of the arterial wall model with media (orange) and adventitia (pink) layers. (b) Arrangement of hexagonal endothelial cells on the inner surface of the artery used for transmission of deformation between the artery and cell model.

Boundary conditions for these simulations are given by blood pressures of 10, 16, 20 kPa corresponding to diastolic, systolic, and hypertensive values, respectively. Axial pre-strains of 0, 0.05, 0.1, 0.2 and 0.3 typical for aorta are applied; they are known to decrease with age [91]. In this model, no shear load is applied because its mechanical impact on the rather stiff arterial layers is negligible.

Resulting circumferential strains on the arterial inner surface (endothelium) for different arteries and combination of loads typical for older individuals (0 % axial pre-strain, 20 kPa blood pressure) are presented in [Table 5.2](#). For application within the cell model, typical dimensions of common or internal carotid arteries were chosen with their values of 2.83 mm, 3.53 mm and 4 mm, respectively [92]. The solved combinations of boundary conditions and the resulting circumferential strains on the inner surface covering all the range of physiological biaxial loads of the endothelial cell are summarized in [Tab. 5.3](#).

Artery (location)	Middle of thoracic aorta	Distal AA	Renal artery	Iliac artery	Carotid artery
Inner radius[mm]	11.20	8.25	2.3	4.8	2.83
Wall thickness [mm]	2.05	2.3	1.05	2.00	1.17
Strains [%]	11.9	11.3	7.5	10.28	9.2

Table 5. 2: Dimensions of different arteries and circumferential strains on their inner surface (endothelium) under zero axial pre-strain and blood pressure of 20 kPa – a combination typical for older individuals

Axial pre-strain (%) / Pressure (kPa)	Circumferential strain (%) at a given pressure and axial pre-strain
0/10	4.6
0/16	7.5
0/20	9.2
5/10	2
5/16	5
5/20	6.6
10/10	-0.1
10/16	1.1
10/20	2.49
20/10	-8
20/16	-7.4
20/20	-6.8
30/10	-13
30/16	-12.6
30/20	-12.5

Table 5. 3: Axial and circumferential strains of endothelium used to formulate boundary conditions of the individual cell model in the circumferential direction

All the four geometries of the model (flat and domed, regular and elongated hexagons) were analysed under different biaxial deformation, i.e., with fifteen different combinations of axial and circumferential strains, and in three consecutive load steps: under biaxial extension (Bi), with addition of blood pressure (BiP), and with blood pressure and shear load (BiPS) acting on

the luminal surface. Thus, we obtained 180 solutions in total. It is worth to mention, that the biaxial extension applies the circumferential strain calculated using the carotid artery model with the chosen blood pressure, thus addition of the blood pressure itself on the inner surface represents a minor modification only.

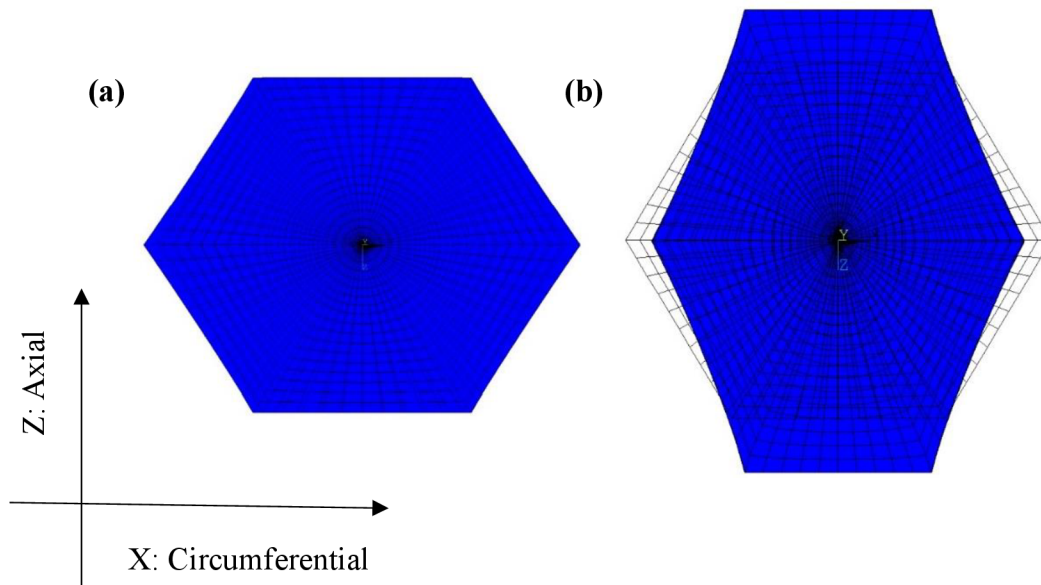


Figure 5. 21: Examples of the deformed shapes of regular flat endothelial cell model variant Bi under extreme biaxial strains according to Tab. 5.3: (a) 0/20 and (b) 30/10

Illustrative examples of deformed shapes of the regular flat model in variant Bi under minimum and maximum distortion are shown in [Fig. 5.21](#).

As the nucleus deformation is considered to be decisive for mechanotransduction [27], [93], [94] and [95] examples of distribution of first principal strain in nucleus are presented in Appendix B and their maximum values for all the solved cell models are summarized in [Table 5.4](#) and [Table 5.5](#).

Model variant	Axial pre-strain [%]	Pressure [kPa]	First principal strain in nucleus for the regular model variant					
			Flat model			Domed model		
			Bi	BiP	BiPS	Bi	BiP	BiPS
0/10	0	10	0.055	0.060	0.160	0.052	0.048	0.138
0/16	0	16	0.088	0.090	0.175	0.083	0.071	0.148
0/20	0	20	0.107	0.110	0.193	0.101	0.083	0.155
		Pulsations	+0.052	+0.050	+0.033	+0.049	+0.035	+0.017
5/10	5	10	0.067	0.070	0.140	0.064	0.058	0.119
5/16	5	16	0.071	0.070	0.155	0.067	0.057	0.129
5/20	5	20	0.075	0.080	0.167	0.070	0.057	0.129
		Pulsations	+0.008	+0.010	+0.027	+0.006	-0.001	+0.010
10/10	10	10	0.122	0.112	0.136	0.119	0.107	0.130
10/16	10	16	0.121	0.120	0.140	0.121	0.111	0.133
10/20	10	20	0.119	0.124	0.144	0.118	0.111	0.137
		Pulsations	-0.003	+0.012	+0.008	-0.001	+0.004	+0.007
20/10	20	10	0.220	0.197	0.231	0.218	0.187	0.225
20/16	20	16	0.220	0.204	0.230	0.218	0.188	0.225
20/20	20	20	0.221	0.201	0.230	0.218	0.191	0.225
		Pulsations	+0.001	+0.004	-0.001	+0.000	+0.004	+0.000
30/10	30	10	0.31	0.277	0.326	0.308	0.263	0.317
30/16	30	16	0.31	0.279	0.326	0.308	0.264	0.317
30/20	30	20	0.31	0.280	0.326	0.308	0.264	0.317
		Pulsations	+0.000	+0.003	+0.000	+0.000	+0.001	+0.000

Table 5. 4: The first principal strains in the nucleus in the calculated cases for regular hexagonal endothelial cell. Pulsations represent the cyclic increase of the first principal strain in nucleus between blood pressures of 10 and 20 kPa.

Model variant	Axial pre-strain [%]	Pressure [kPa]	First principal strain in nucleus for the elongated model variant					
			Flat model			Domed model		
			Bi	BiP	BiPS	Bi	BiP	BiPS
0/10	0	10	0.052	0.055	0.115	0.052	0.049	0.164
0/16	0	16	0.085	0.085	0.123	0.085	0.073	0.172
0/20	0	20	0.104	0.092	0.144	0.104	0.087	0.178
		Pulsations	+0.052	+0.037	+0.039	+0.052	+0.038	+0.014
5/10	5	10	0.066	0.066	0.095	0.066	0.062	0.145
5/16	5	16	0.071	0.072	0.112	0.069	0.067	0.154
5/20	5	20	0.075	0.075	0.120	0.072	0.067	0.160
		Pulsations	+0.009	+0.009	+0.025	+0.006	+0.005	+0.015
10/10	10	10	0.122	0.113	0.126	0.122	0.107	0.141
10/16	10	16	0.124	0.12	0.128	0.124	0.113	0.145
10/20	10	20	0.126	0.119	0.130	0.125	0.111	0.150
		Pulsations	+0.004	+0.006	+0.004	+0.003	+0.004	+0.009
20/10	20	10	0.220	0.202	0.237	0.224	0.194	0.228
20/16	20	16	0.22	0.203	0.237	0.224	0.193	0.229
20/20	20	20	0.22	0.204	0.238	0.224	0.193	0.229
		Pulsations	+0.000	+0.001	+0.001	+0.000	-0.001	+0.001
30/10	30	10	0.312	0.279	0.338	0.316	0.272	0.322
30/16	30	16	0.313	0.28	0.337	0.316	0.275	0.322
30/20	30	20	0.313	0.282	0.337	0.316	0.276	0.322
		Pulsations	+0.001	+0.003	-0.001	0.000	+0.004	0.000

Table 5. 5: The first principal strains in the nucleus in the calculated cases for elongated hexagonal endothelial cell. Pulsations represent the cyclic increase of the first principal strain in nucleus between blood pressures of 10 and 20 kPa.

The whole force-displacement curves for models loaded with the highest and lowest axial prestrain (cases 30/20 and 0/20) are shown in [Fig. 5.22](#); as we apply here the circumferential strain calculated based on blood pressure in the artery, the curves represent dependences of the forces on blood pressure from 0 up to 20 kPa under constant axial pre-strain. Thus, they enable us to evaluate the force pulsations in the endothelial layer.

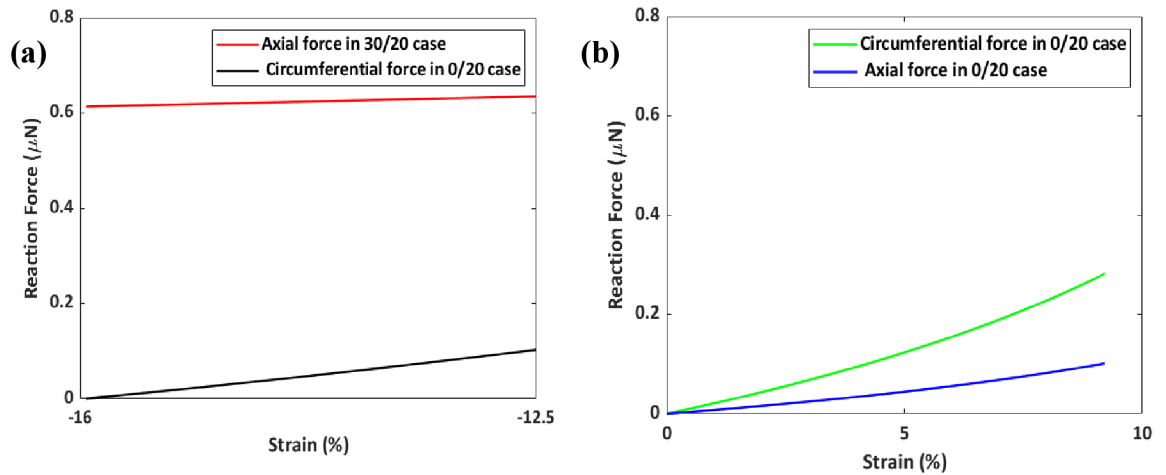


Figure 5. 22: Simulated dependences of biaxial tension forces (variant Bi) on the increasing blood pressure (between 0 and 20 kPa) recalculated into circumferential strain of the cell. (a), 30/20 case, (b) 0/20 case.

As there are no experimental results for biaxial loading conditions in available literature for validation, we compared our results for approximately equibiaxial loading conditions with our compression test simulations for flat and adherent endothelial cells published in [71] and with experimental results for cell compression [50]. It is known that for incompressible materials (product of all the three stretches equals 1) the deformations under equibiaxial tension and uniaxial compression are the same. The out-of-plane engineering strain of the 5/20 model (5% axial and 6.6% circumferential strains give nearly equibiaxial deformation) is approximately 11 %. In this way the simulated curves were recalculated and plotted in Fig. 5.23 as functions of strain in radial (out-of-plane) direction. The stiffness in equibiaxial tension is similar to that in uniaxial compression but the curves are more non-linear due to higher cell distortion (curved edges occur, see Fig 5.21 (b)).

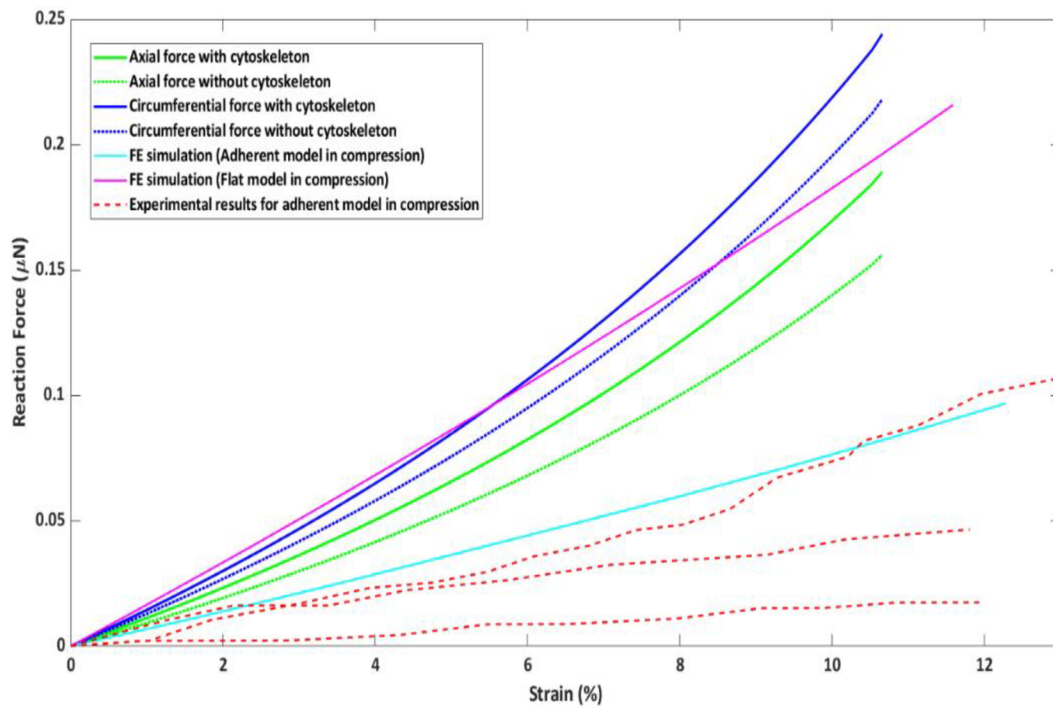


Figure 5.23: Comparison of simulated force-deformation curves for regular flat equibiaxial strain (5/20) models (with and without cytoskeleton) with simulated and typical experimental results in compression [71] [50].

The role of cytoskeletal filaments and discussions related to the results are explained in [Appendix B](#).



## 5.5. Simulation of cell debonding during cyclic loads

A continuum mechanics technique is used in this chapter to simulate cell-substrate adhesion and its debonding under cyclic loads. A cell adhesion is ensured through interaction of adhesion molecules; explicitly, molecules on the cell surface known as integrins or receptors connect with molecules on the ECM surface known as ligands to form a bond. For an adhered cell, the receptor-ligand bonds can be very numerous.

The cohesive zone modelling framework is employed, which was originally created in the field of elastic-plastic fracture mechanics. Cohesive zone modelling, first proposed in [96], [97] entails a continuum representation of an interface layer in which interfacial failure is represented by a specific phenomenological constitutive relation.

Studies [98], [99], [100], [101] have employed cohesive zone models to describe fracture in metallic, ceramic, and composite materials when the failure modes entail the nucleation, growth, and coalescence of flaws. Interface traction vs. displacement relationships are typically established so that as the interfacial separation grows, the traction across the interface reaches a maximum value and then diminishes, leading eventually to total decohesion. The determination of a size scale representative of the physical mechanism that leads to decohesion is fundamental to the execution of such a model.

The cell geometry, shown in [Fig. 4.8 \(b\)](#), is based on the experimental data of [50] for endothelial cells. Based on experimental boundary conditions [102], [103], [104], the cells are bonded to a silicone substrate that is cyclically stretched from 0% to 5% nominal axial strain via a sinusoidally changing displacement boundary condition at a frequency of 1 Hz. With Poisson's ratio of 0.4 and Young's modulus of 0.25 MPa, the silicone substrate is considered to act as a linear elastic material by [105]. To model the cell-substrate contact, cohesive zone formulations are used.

The modelling of an interface by the introduction of discrete elements (cohesive elements) between two surfaces that are meant to have zero separation in the starting condition is known as the cohesive zone formulation. The cohesive model's constitutive formulation is based on two classes of definitions: potential based (the definition of the cohesive zone law is based on the definition of an interface potential, which represents the work done to separate two opposing surfaces having contact at an interface by [100]) and non-potential based. While the first derivatives of an interface potential function must be computed to obtain the traction–separation relationships, the traction–separation relationships in non-potential based systems are not obtained from a potential function.

The concept of a continuous interface between two surfaces is being used in cohesive zone models (in this case the cell and substrate). An interface potential function  $\emptyset$  is a measure of the energy necessary to apply a displacement leap  $\delta$  to the surfaces on either side of the interface and it prescribes the interface constitutive behavior as follows:

$$\emptyset(\Delta_n, \Delta_t) = \emptyset_n + \emptyset_n \exp\left(-\frac{\Delta_n}{\delta_n}\right) \left\{ \left[1 - r + \frac{\Delta_n}{\delta_n}\right] \frac{1 - q}{r - 1} - \left[ q + \left(\frac{r - q}{r - 1}\right) \frac{\Delta_n}{\delta_n} \right] \exp\left(-\frac{\Delta_t^2}{\delta_t^2}\right) \right\}$$

$$r = \frac{\Delta_n^*}{\delta_n}, \quad q = \frac{\emptyset_t}{\emptyset_n}$$

where  $\emptyset_n$  is the work of normal separation and  $\emptyset_t$  is the work of tangential separation;  $\Delta_n$  and  $\Delta_t$  are the normal and tangential displacement jumps respectively, across the interface;  $\delta_n$  and  $\delta_t$  are normal and tangential characteristic lengths for the interface.  $\Delta_n^*$  is the value of  $\Delta_n$  following complete shear separation under the condition of normal traction being zero.

From the potential  $\emptyset$  the interface traction–separation relationships between interfacial tractions and displacement jumps can be derived as follows:

$$T = \frac{\partial \emptyset(\Delta)}{\partial \Delta}$$

The individual components of the traction are obtained from the following equations.

$$T_n = -\frac{\partial \emptyset(\Delta)}{\partial \Delta_n}$$

$$T_t = -\frac{\partial \emptyset(\Delta)}{\partial \Delta_t}$$

The Cohesive zone formulations are implemented in ANSYS software and the characteristic interface lengths of  $\delta_n = 25$  nm and  $\delta_t = 35$  nm are used based on ligand–receptor bond lengths reported in literature by [106]. Based on experimental measurements of bonding strength and density, a mode I interface strength of  $\sigma_{max} = 4$  kPa was determined by [107]. At the cell–substrate interface, mode II strength is greater than mode I strength, resulting in  $\tau_{max} = 20$  kPa. The cohesive zone formulation by [100] is utilized to model the behaviour of the interface between the endothelial cell and a silicone substrate in this study. The use of cohesive zone modelling in this way, where the major separation mode is the breakage of receptor–ligand interactions, is quite interesting.

### 5.5.1. Results of debonding

Two examples of debonding of the cell from the substrate under various cyclic loading conditions are demonstrated in the [Fig. 5.24](#).

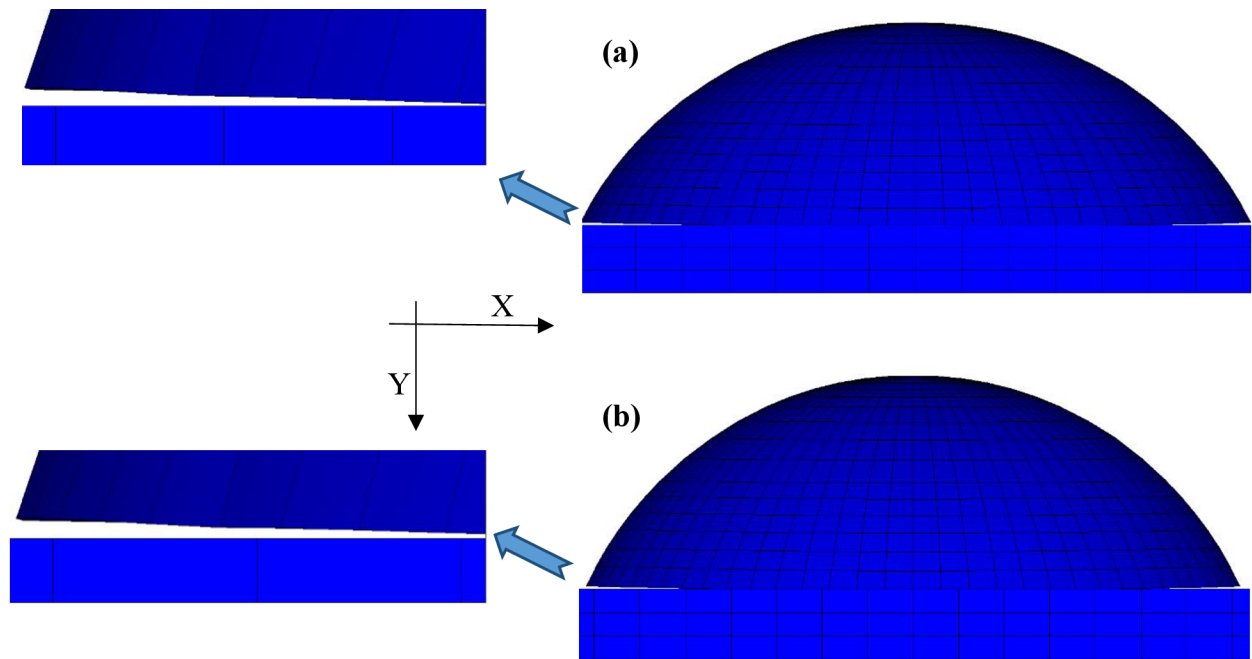


Figure 5. 24: Mixed mode separation is computed at bottom of the (a) 1st cycle (b) 30th cycles reaching 5 % strain.

The normal tractions, normal displacements and tangential tractions computed at the cell-substrate interface at the 1<sup>st</sup> and 30<sup>th</sup> loading cycles are shown in [Fig. 5.25](#), [Fig. 5.26](#) and [Fig. 5.27](#).

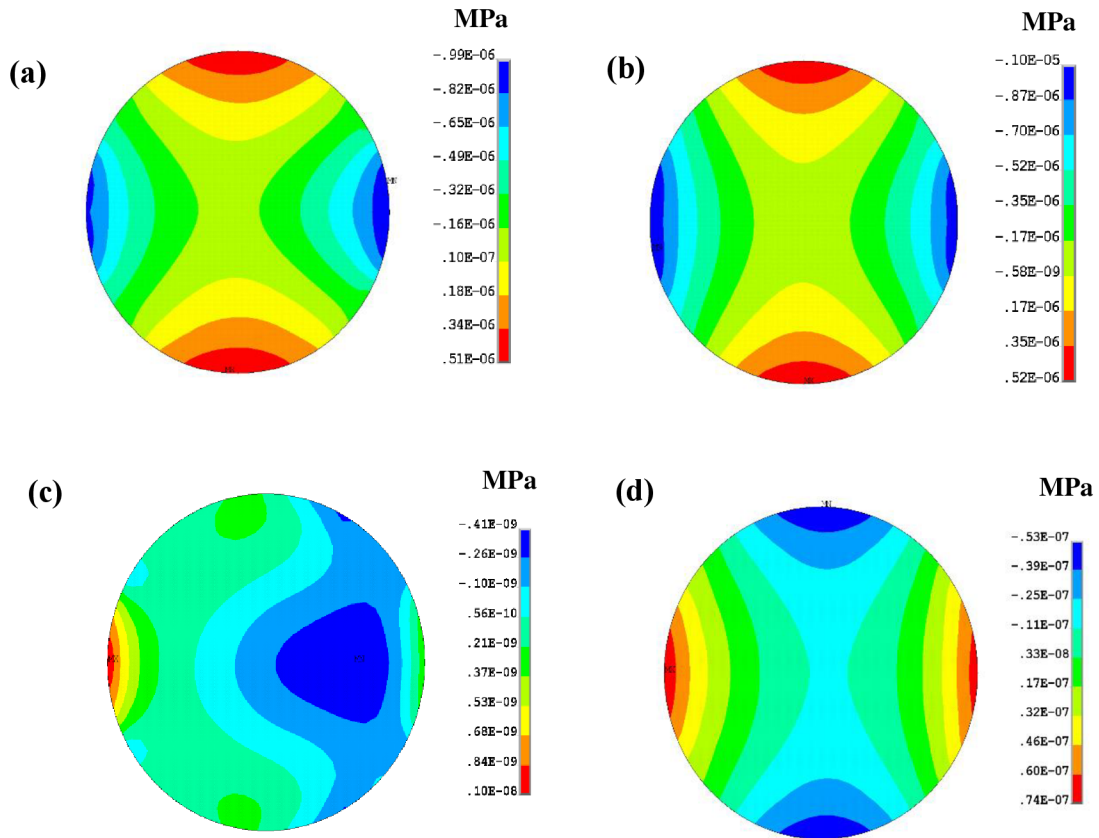


Figure 5. 25: The computed normal tractions (a) at the top of the 1st cycle (b) at the top of the 30<sup>th</sup> cycle (c) at the bottom of 1st cycle (d) at the bottom of 30<sup>th</sup> cycle. (Top View), Due to downwards orientation of the y axis, the normal tractions with maximum magnitude are negative and shown in blue colour.

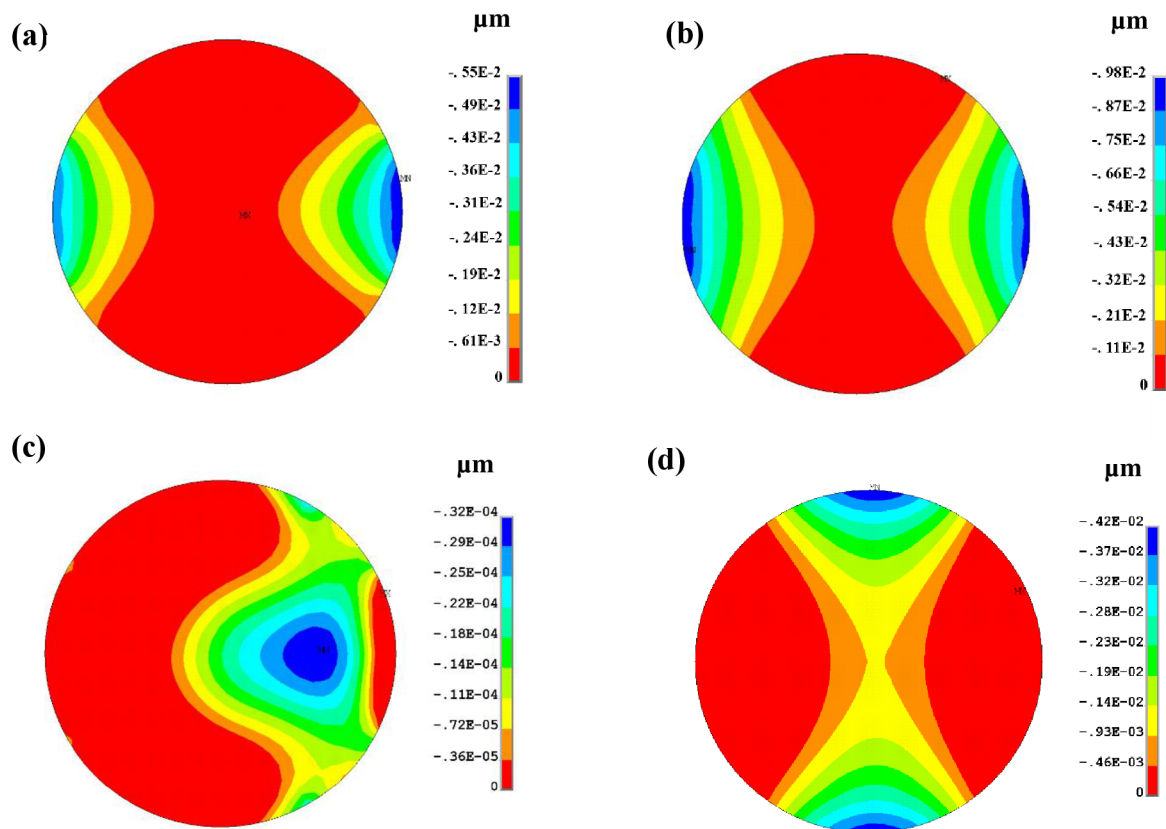


Figure 5. 26: The computed normal displacements (a) at the top of the 1st cycle (b) at the top of the 30<sup>th</sup> cycle (c) at the bottom of 1st cycle (d) at the bottom of 30<sup>th</sup> cycle. (Top View), Due to downwards orientation of the y axis, the normal displacements with maximum magnitude are negative and shown in blue colour.

In the top of the cycle (the loaded state) we can see the nearly symmetric distributions as shown in [Fig. 5.25 \(a\)](#) and [Fig. 5.26 \(a\)](#). The asymmetric distributions for [Fig. 5.25 \(c\)](#) and [Fig. 5.26 \(c\)](#) in the bottom of the first cycle (the unloaded state) change into symmetric ones after 5 cycles. This asymmetry is not significant in tangential tractions ([Fig. 5.27 \(a\)](#)).

While the top values of both normal and tangential tractions do not change significantly between the 1st and 30th cycle ([Fig. 5.25 \(a\)](#), [Fig. 5.25 \(b\)](#) and [Fig. 5.27 \(a\)](#), [Fig. 5.27 \(b\)](#)), their bottom values after the 1st cycle, which can be considered as residual tractions, are lower by orders. However, these residual values increase significantly with repeated loading.

In contrast, the normal displacements (separation) increase significantly in the subsequent cycles as shown in [Fig. 5.26 \(a\)](#) and [Fig. 5.26 \(b\)](#) while, in the unloaded state they don't exceed a few nanometers.

The asymmetry of the responses may be explained by the non-symmetric cytoskeleton shape explicitly related to the position of centrosome in the model.

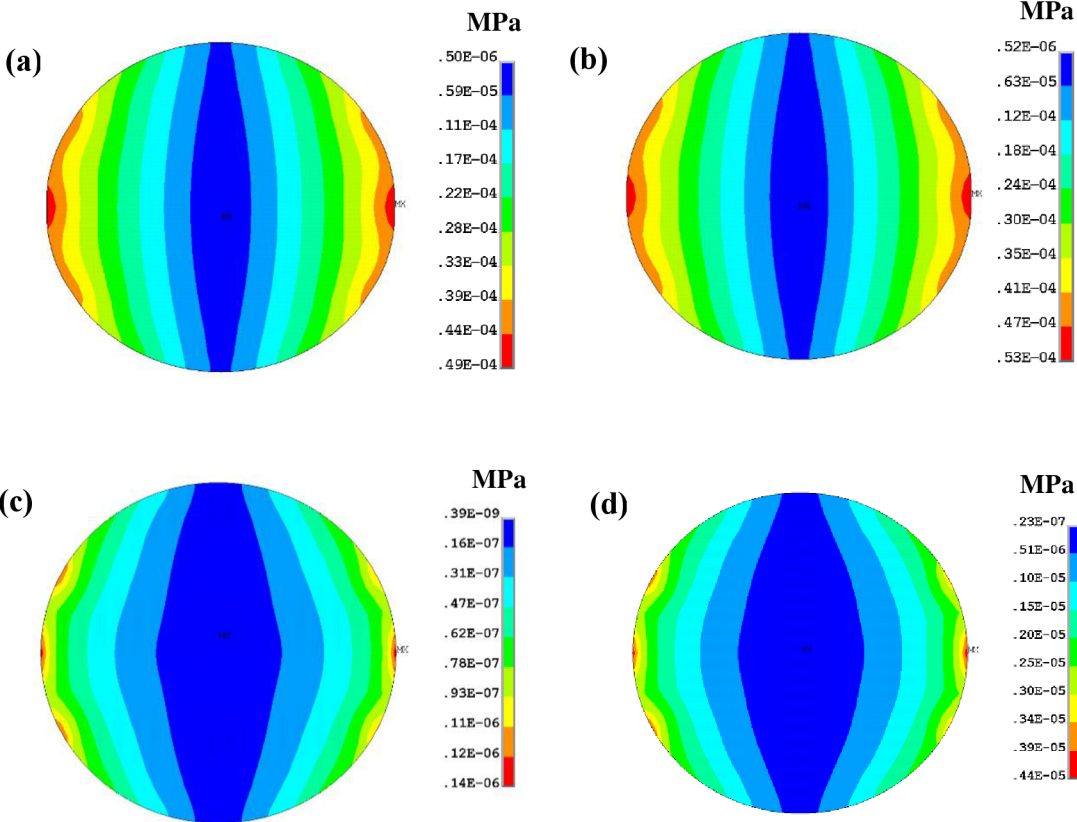


Figure 5. 27: The computed tangential tractions (a) at the top of the 1st cycle (b) at the top of the 30<sup>th</sup> cycle (c) at the bottom of 1st cycle (d) at the bottom of 30<sup>th</sup> cycle. (Top View)

[Fig. 5.28](#) illustrates a complete history of normal separation demonstrating the cyclic character of the debonding process. The contact edge opening (i.e., normal displacement or separation) when the substrate is fully extended is increasing with the number of cycles, as can be seen in [Fig. 5.28](#), due to the increasing upwards push on the contact edge at the start of each cycle causing the increasing tensile strain concentration. It must be emphasised that normal separation and normal traction values presented in [Fig. 5.28](#) and [Fig. 5.29](#). (With a dashed lines) are obtained after the substrate has returned to its unloaded shape at the end of each cycle.

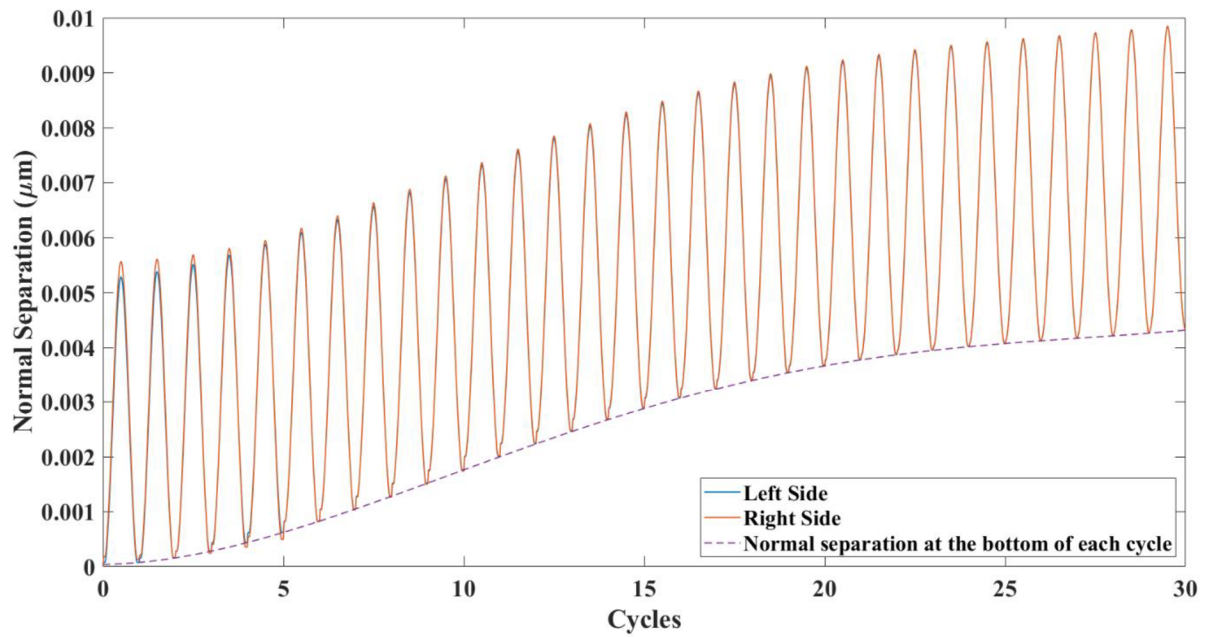


Figure 5. 28: Full history of normal separation during 30 cycles for both sides of deformation.

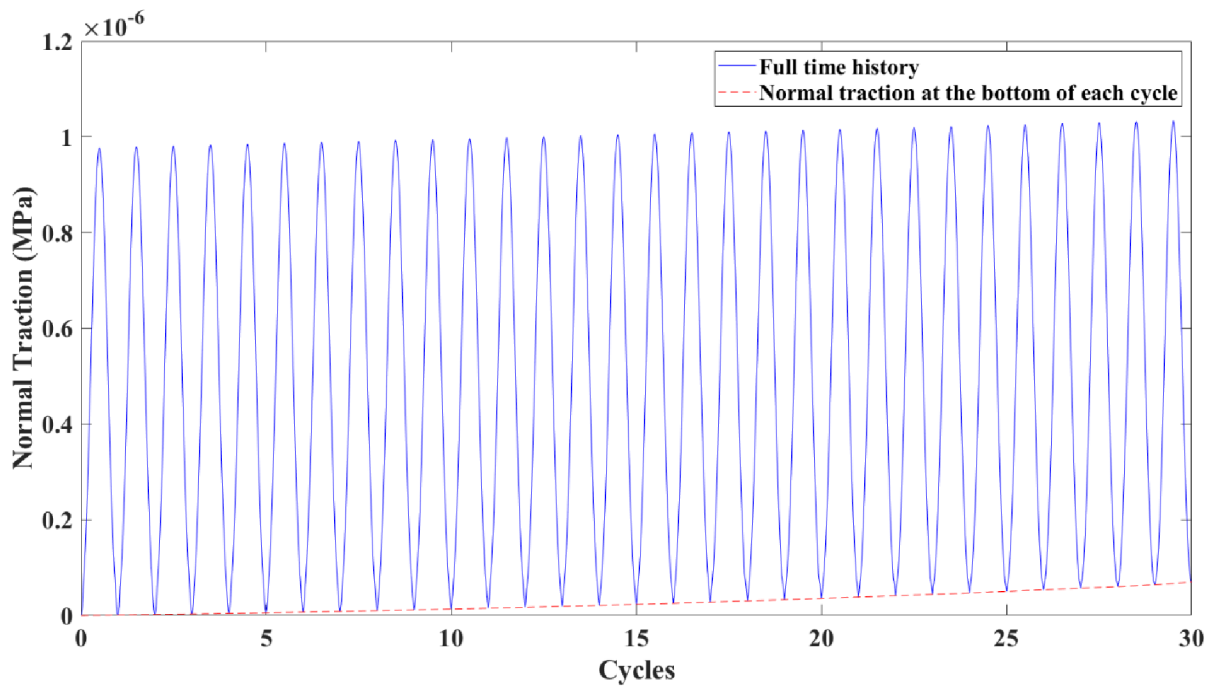


Figure 5. 29: Normal traction during all the 30 cycles. (The dashed line represents the bottom values of each cycle representing residual tractions).

[Fig. 5.30](#). shows contour plots of the strain component in the direction of stretching at the top of the 30th cycle when the substrate is fully extended. The cell surface to the right of the contact edge is at an angle to the substrate, which causes the cell to lift upwardly toward the contact edge.

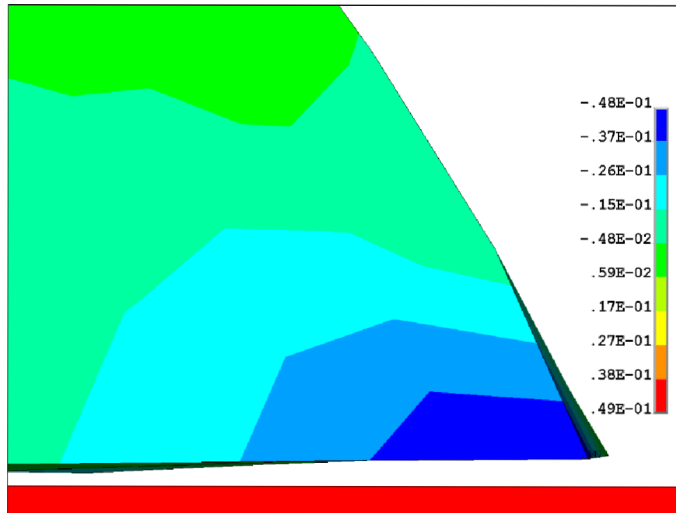


Figure 5. 30: Contour plot of the strain component in the direction of substrate stretching at the top of the 30th cycles.



## 6. CONCLUSIONS

The present thesis was aimed towards a realistic computational modelling of cytoskeleton and endothelial cell as a whole. The FE bendo-tensegrity model of smooth muscle cell created in the previous doctoral thesis [27] was modified to mimic specific shapes, properties and cytoskeletal arrangement of endothelium cells. It investigates the passive behaviour of endothelial cells by studying their cytoskeletal mechanics in suspended and adherent states. In this study, five mechanical tests of single cell were simulated and in three cases i.e., tensile test of suspended cell with micropipettes, compression test of suspended cell with microplates, and compression of adherent model were compared with corresponding published experimental data. In addition, compression and shear of the flat model were simulated to elucidate the global cell response. Also, we investigated the mechanical response of the flat cell within the endothelium layer in its realistic shape under physiological conditions in arterial wall. Finally, we investigated the cell response in debonding during cyclic stretches using 3-D finite element simulations. The findings of this thesis predict and explain distinct cellular behaviours that emerge from mutual interaction between specific cytoskeletal components observed under different experimental conditions. The main findings of this thesis can be summarized as follows:

- The proposed models provide simulation of the cell mechanical responses during tension and compression and aid to illustrate the mechanical role of individual cytoskeletal components including stress/strain distribution within them, and offer quantitative information on the nucleus deformation hypothetically decisive for mechanotransduction.
- The mechanical response of the flat cell within the endothelium layer under physiological conditions in arterial wall is assessed. The impact of individual components of loads on the nucleus deformation (more specifically on the first principal strain) was investigated because we believe it might influence mechanotransduction. Also, the role of the cytoskeleton and its constituents in the mechanical response of the endothelial cell was assessed. The results show (i) the impact of pulsating blood pressure on cyclic deformations of the nucleus, which increase substantially with decreasing axial pre-stretch of the cell, (ii) the importance of relatively low shear stresses in the cell response and nucleus deformation. Not only the pulsatile blood pressure but also the wall shear stress may induce significant deformation.

- The cell response in debonding during cyclic stretches using 3-D finite element simulations revealed that 5% axial strain applied on the substate is sufficient to induce debonding of the cell from the substrate. The debonding starts in the first cycle and that the crack created in the mixed mode (opening + shear) propagates more and more during the following cycles.
- The models predict the role of specific cytoskeletal components in force transmission across the cell based on external mechanical stimuli. The effect of the cytoskeleton's mechanical role revealed that AFs and MTs play a critical part in cell stiffness, which increases with stretching. Even though AFs are tension bearing elements, they have been found to contribute significantly to the compressive characteristics of the cell.
- The proposed cell models consider the different structure and organization of actin protein in suspended cells, emphasizing how this affects the interpretation of force-deformation measurements.
- As a result, the proposed models may aid in a better understanding of cellular mechanical processes such as mechanotransduction and cytoskeleton remodelling.

All the conclusions of this thesis have been summarized and submitted to the conference at ESB 2022. See [Appendix F](#).

## 6.1. Additional ideas for future works

Out of scope of the formulated objectives of the doctoral thesis, the followings are recommended to be investigated:

- The majority of in vitro investigations measure cell deformation over time or on a frequent basis. Cells deform in response to external mechanical stimuli, displaying both solid-like elastic and fluid-like viscous behaviour. As a result, cells and their components are better defined as viscoelastic materials, and the mechanical responses that may be evaluated vary depending on the time scale. [108]. Viscoelastic characteristics for continuous components could be defined in the proposed models using a conventional linear solid model.
- Including the centrosome in the proposed models could explain the relationship between nucleus and MTs, following the strategy proposed in [20] utilizing granular media, although little is known about centrosome dynamics. To do this, computer simulations with or without the centrosome might be run, allowing for a better understanding of the centrosome's role in cell dynamics under various loading circumstances.

- Using a cytoskeletal remodelling description presented in [28], active cell responses might be included into the proposed models, following the method of [14]. The remodelling process is driven by three interconnected events: an activation signal that causes actin polymerization and myosin phosphorylation, the tension-dependent assembly of actin and myosin into stress fibres (SFs), and the tension-generating cross-bridge mechanics between actin and myosin filaments.
- Finally, the model is intended to be used for assessment of the impact of wall shear stress in arteries on endothelium cells. Through their response to hemodynamic forces, endothelial cell dysfunction has been related to atherosclerosis. Endothelial cells are composed in a monolayer, in this manner further advances are needed to investigate the perception of loads by a population of cells.

## **BIBLIOGRAPHY**

- [1] C. T. Lim, E. H. Zhou and S. T. Quek, "Mechanical models for living cells," *Journal of biomechanical*, vol. 39, no. 2, pp. 195-216, 2006.
- [2] R. Ross, "Atherosclerosis: an inflammatory disease.," *The New England Journal of Medicine*, vol. 340, pp. 115-127, 1999.
- [3] R. R. Seeley, T. D. Stephens and P. Tate, *Anatomy and physiology*, Boston: McGraw Hill, 2003.
- [4] R. Zawadzki and R. Furchgott, "The obligatory role of endothelial cells in the relaxation of arterial smooth muscle by acetylcholin," *Nature*, vol. 288, p. 373–376, 1980.
- [5] P. A. Janmey, "The Cytoskeleton and Cell Signaling: Component Localization and Mechanical Coupling," *the American Physiological Society*, vol. 78, no. 3, 1998.
- [6] R. Lebiš, "Computational Modeling of Mechanical Behavior of the Cell.," Brno, 2007.
- [7] D. Ingber, "Cellular tensegrity: defining new rules of biological design that govern the cytoskeleton.," *Journal of cell science*, vol. 104, pp. 613-27, 1993.
- [8] A. Pillarisetti, J. Desai, H. Ladjal, A. Schiffmacher, A. Ferreira and C. Keefer, "Mechanical phenotyping of mouse embryonic stem cells: increase in stiffness with differentiation.," *Cell Reprogram*, vol. 13, no. 4, pp. 371-80, 2011.
- [9] K. Nagayama, Y. Nagano, M. Sato and T. Matsumoto, "Effect of actin filament distribution on tensile properties of smooth muscle cells obtained from rat thoracic aortas," *Journal of biomechanics*, vol. 39, no. 2, pp. 293-301, 2006.
- [10] Y. Ujihara, M. Nakamura, H. Miyazaki and S. Wada, "Contribution of actin filaments to the global compressive properties of fibroblasts," *Journal of the Mechanical Behaviour of Biomedical Materials*, vol. 14, pp. 192-198, 2012.
- [11] B. V. Nguyen, Q. Wang, N. J. Kuiper, A. J. El Haj, C. R. Thomas and Z. Zhang, "Strain-dependent viscoelastic behaviour and rupture force of single chondrocytes and chondrons under compression.," *Biotechnology letters*, vol. 31, no. 6, pp. 803-9, 2009.
- [12] H. Ghaffari, M. S. Saidi and B. Firoozabadi, "Biomechanical analysis of actin cytoskeleton function based on a spring network cell model," *Journal of Mechanical Engineering Science*, 2016.
- [13] F. Xue, A. Lennon, K. McKayed, V. Campbell and P. Prendergast, "Effect of membrane stiffness and cytoskeletal element density on mechanical stimuli within cells: an analysis of the consequences of ageing in cells," *Computer Methods in Biomechanics and Biomedical Engineering*, vol. 18, no. 5, pp. 468-76, 2015.
- [14] E. P. Dowling and J. P. McGarry, "Influence of Spreading and Contractility on Cell Detachment," *Annals of Biomedical Engineering*, vol. 42, p. 1037–1048, 2014.
- [15] S. Barreto, C. Clausen, C. Perrault, D. Fletcher and D. Lacroix, "A multi-structural single cell model of force-induced interactions of cytoskeletal components.," *Biomaterials*, vol. 34, no. 26, pp. 6119-26, 2013.
- [16] D. Kardas, U. Nackenhorst and D. Balzani, "Computational model for the cell-mechanical response of the osteocyte cytoskeleton based on self stabilizing tensegrity structures. Biomec Model Mechanobio," *Biomechanics and Modeling in Mechanobiology*, vol. 12, pp. 167-83, 2013.

- [17] J. Bursa, J. Holata and R. Lebis, "Tensegrity finite element models of mechanical tests of individual cells," *Technology health care*, vol. 20, no. 2, pp. 135-150, 2012.
- [18] J. Bursa, R. Lebis and P. Janicek, "FE models of stress-strain states in vascular smooth muscle cell," *Technology health care*, vol. 14, no. 4,5, pp. 311-20, 2006.
- [19] Y. Ujihara, M. Nakamura, H. Miyazaki and S. Wada, "Proposed spring network cell model based on a minimum energy concept," *Annals of Biomedical Engineering*, vol. 38, no. 4, pp. 1530-8, 2010.
- [20] B. Maurin, P. Cañadas, H. Baudriller, P. Montcourrier and N. Bettache, "Mechanical model of cytoskeleton structuration during cell adhesion and spreading," *Journal of Biomechanics*, vol. 41, no. 9, pp. 2036-41, 2008.
- [21] G. Unnikrishnan, U. Unnikrishnan and J. Reddy, "Constitutive material modeling of cell: a micromechanics approach," *Journal of Biomechanical Engineering*, vol. 129, no. 3, p. 315–23, 2007.
- [22] P. Cañadas, V. Laurent, P. Chabrand, D. Isabey and S. Wendling Mansuy, "Mechanisms governing the visco-elastic responses of living cells assessed by foam and tensegrity models," *Medical & Biological Engineering & Computing*, vol. 41, no. 6, pp. 733-9, 2003.
- [23] P. Cañadas, V. Laurent, C. Oddou, D. Isabey and S. Wendling, "A cellular tensegrity model to analyse the structural viscoelasticity of the cytoskeleton," *Journal of Theoretical Biology*, vol. 218, pp. 155-173, 2002.
- [24] P. Cañadas, S. Wendling Mansuy and D. Isabey, "Frequency response of a viscoelastic tensegrity model: Structural rearrangement contribution to cell dynamics," *Journal of Biomechanical Engineering*, vol. 128, no. 4, pp. 487-495, 2006.
- [25] J. G. McGarry and P. J. Prendergast, "A three-dimensional finite element model of an adherent eukaryotic cell," *European Cells & Materials*, vol. 7, p. 27–33, 2004.
- [26] M. C. D. Stamenovic, "The role of prestress and architecture of the cytoskeleton and deformability of cytoskeletal filaments in mechanics of adherent cells: a quantitative analysis," *Journal of Theoretical Biology*, vol. 201, no. 1, pp. 63-74, 1999.
- [27] Y. D. Bansod, T. Matsumoto, K. Nagayama and J. Bursa, "A Finite Element Bendo-Tensegrity Model of Eukaryotic Cell," *ASME Journal of Biomechanical Engineering*, 2018.
- [28] V. S. Deshpande, R. M. McMeeking and A. G. Evans, "A bio-chemo-mechanical model for cell contractility," *Proceedings of national academy of science of the U.S.A.*, vol. 03, no. 38, p. 14015–14020., 2006.
- [29] R. De, A. Zemel and S. and Safran, "Dynamics of cell orientation," *Nature Physics*, vol. 3, p. 655–659, 2007.
- [30] R. Kaunas and H. J. Hsu, "A kinematic model of stretch-induced stress fiber turnover and reorientation," *Journal of theoretical biology*, vol. 257, pp. 320-30, 2009.
- [31] H. F. Brinson and L. C. Brinson, *Polymer engineering science and viscoelasticity: an introduction.*, Springer Verlag, 2008.
- [32] G. AN, *Engineering with rubber: how to design rubber components*, Munich: Hanser Gardener Publication, 2000.
- [33] H. M. a. S. B. Ali A, "A review of constitutive models for rubber-like materials.," *American Journal of Engineering and Applied Sciences*, vol. 3, no. 1, pp. 232-239, 2010.

- [34] B. Sumpio and R. J. D. A. Timothy, "Cells in focus: endothelial cell," *The International Journal of Biochemistry & Cell Biology*, vol. 34, no. 12, pp. 1508-1512, 2002.
- [35] P. C. Dartsch and E. Betz, "Response of cultured endothelial cells to mechanical stimulation," *Basic research in cardiology*, vol. 84, no. 3, pp. 268-81, 1989.
- [36] B. Langille L and A. S.L, "Relationship between blood flow direction and endothelial cell orientation at arterial branch sites in rabbits and mice," *Circulation Research*, vol. 48, pp. 481-488, 1981.
- [37] M. Levesque, D. Liepsch, S. Moravec and R. Nerem, "Correlation of endothelial cell shape and wall shear stress in a stenosed dog aorta.," *Arteriosclerosis*, vol. 6, pp. 220-229, 1986.
- [38] K. Konstantinos, K. Sharad and V. M. Larry, "Biomechanics of cell interactions in shear fields," *Advanced Drug Delivery*, vol. 33, p. 141-164, 1998.
- [39] R. Darby, *Chemical Engineering Fluid Mechanics*, vol. II, 2001.
- [40] D. A. McDonald, *Blood Flow in Arteries*, vol. II, Baltimore: Williams & Wilkins, 1974, p. 496.
- [41] B. Johnston, P. Johnston, S. Corney and D. Kilpatrick, "Non-Newtonian blood flow in human right coronary arteries: steady state simulations," *Journal of Biomechanics*, vol. 37, no. 5, p. 709-720, 2004.
- [42] N. J. Zhang, A. L. Bergeron, Q. Yu, C. Sun, L. V. McIntire, J. A. Lopez and J. F. Dong, "Platelet aggregation and activation under complex patterns of shear stress," *Thrombosis and Haemostasis*, vol. 88, pp. 817-821, 2002.
- [43] A. Bruel, G. Ortoft and H. Oxlund, "Inhibition of cross-links in collagen is associated with reduced stiffness of the aorta in young rats," *Atherosclerosis*, vol. 140, pp. 135-145, 1998.
- [44] M. E. DeBakey, G. M. Lawrie and D. H. Glaeser, "Patterns of atherosclerosis and their surgical significance," *Annals of Surgery*, vol. 201, pp. 115-131, 1985.
- [45] T. Asakura and T. Karino, "Flow patterns and spatial distribution of atherosclerotic lesions in human coronary arteries," *Circular respiratory*, pp. 1045-1066., 1990.
- [46] G. Garcia-Cardena, J. Comander, K. R. Anderson, B. R. Blackman and M. A. J. Gimbrone, "Biomechanical activation of vascular endothelium as a determinant of its functional phenotype," *Proceedings of national academy of sciences of the U.S.A.*, vol. 98, pp. 4478-4485, 2001.
- [47] S. Deguchi, T. Ohashi and M. Sato, "Evaluation of tension in actin bundle of endothelial cells based on preexisting strain and tensile properties measurements," *Molecular & Cellular Biomechanics*, vol. 2, no. 3, pp. 125-133, 2005.
- [48] A. K. a. T. Yanagida, "Force measurements by micromanipulation of a single actin filament by glass needles," *Nature*, vol. 334, p. 74-76, 1988.
- [49] O. Thoumine, A. Ott, O. Cardoso and J.-J. Meister, "Microplates: a new tool for manipulation and mechanical perturbation of individual cells.," *Journal of Biochemical and Biophysical Methods*, vol. 39, p. 47-62, 1999a.
- [50] N. Caille, O. Thoumine, Y. Tardy and J. Meister, "Contribution of the nucleus to the mechanical properties of endothelial cells.," *Journal of Biomechanics*, vol. 35, pp. 177-87, 2002.

- [51] P. F. Davies, A. Remuzzi, E. J. Gordon, C. F. J. Dewey and M. A. J. Gimbrone, "Turbulent fluid shear stress induces vascular endothelial cell turnover in vitro.," *Proceeding of national academy of science of the U.S.A*, vol. 83, pp. 2114-2117, 1986.
- [52] C. F. J. Dewey, S. R. Bussolari, M. A. Gimbrone and D. P. F. Jr., "The dynamic response of vascular endothelial cells to fluid shear stress.," *Journal of biomechanical engineering*, vol. 103, pp. 177-185, 1981.
- [53] P. F. Davies, C. F. J. Dewey, S. R. Bussolari, E. J. Gordon and M. A. J. Gimbrone, "Influence of hemodynamic forces on vascular endothelial function. In vitro studies of shear stress and pinocytosis in bovine aortic cells.," *Journal of Clinical Investigation*, vol. 73, pp. 1121-1129., 1984.
- [54] T. Nagel, N. Resnick, W. J. Atkinson, C. F. J. Dewey and M. A. J. Gimbrone, "Shear stress selectively upregulates intercellular adhesion molecule-1 expression in cultured human vascular endothelial cells.," *The Journal of Clinical Investigation*, vol. 94, no. 2, pp. 885-891, 1994.
- [55] T. Nagel, N. Resnick, C. F. J. Dewey and M. A. J. Gimbrone, "Vascular endothelial cells respond to spatial gradients in fluid shear stress by enhanced activation of transcription factors.," *Arteriosclerosis, Thrombosis, and Vascular Biology*, vol. 19, pp. 1825-1834., 1999.
- [56] N. Depaola, M. A. J. Gimbrone, P. F. Davies and C. F. J. Dewey, "Vascular endothelium responds to fluid shear stress gradients.," *arteriosclerosis thrombosis*, vol. 12, pp. 1254- 1257., 1992.
- [57] M. J. Levesque and R. M. Nerem, "The elongation and orientation of cultured endothelial cells in response to shear stress.," *Journal of biomechanical engineering*, vol. 107, pp. 341-347, 1985.
- [58] S. G. Frangos, V. Gahtan and B. Sumpio, "Localization of atherosclerosis: role of hemodynamics.," *Archives of Surgery*, vol. 134, pp. 1142-1149, 1999.
- [59] Y. Tardy, N. Resnick, T. Nagel, M. A. J. Gimbrone and C. F. J. Dewey, "Shear stress gradients remodel endothelial monolayers in vitro via a cell proliferation-migration-loss cycle.," *Arteriosclerosis, Thrombosis, and Vascular Biology*, vol. 17, no. 11, pp. 3102-3106, 1997.
- [60] T. K. Hsiai, S. K. Cho, H. M. Honda, S. Hama, M. Navab, L. L. Demer and C. M. Ho, "Endothelial cell dynamics under pulsating flows: significance of high versus low shear stress slew rates (d(tau)/dt).," *Annals of Biomedical Engineering*, vol. 30, pp. 646-656, 2002.
- [61] J. A. McCann, S. D. Peterson, M. W. Plesniak, T. J. Webster and K. M. Haberstroh, "Non-uniform flow behavior in a parallel plate flow chamber : alters endothelial cell responses," *Annals of Biomedical Engineering*, vol. 33, pp. 328-336, 2005.
- [62] X. Peng, F. A. Recchia, B. J. Byrne, J. S. Wittstein, R. C. Ziegelstein and D. A. Kass, "In vitro system to study realistic pulsatile flow and stretch signaling in cultured vascular cells," *American Journal of Physiology-Cell Physiology*, vol. 279, 2000.
- [63] Y. Qiu and J. M. Tarbell, "Interaction between wall shear stress and circumferential strain affects endothelial cell biochemical production," *The Journal of Vascular Research*, vol. 37, pp. 147-157, 2000.
- [64] T. Iba and B. E. Sumpio, "Morphological response of human endothelial cells subjected to cyclic strain in vitro.," *Microvascular Research*, vol. 42, pp. 245-254, 1991.

- [65] T. Ziegler, K. Bouzourene, V. J. Harrison, H. R. Brunner and D. Hayoz, "Influence of oscillatory and unidirectional flow environments on the expression of endothelin and nitric oxide synthase in cultured endothelial cells. *Arterioscler., Thrombosis, and Vascular Biology*, vol. 18, pp. 686-692, 1998a.
- [66] T. Ziegler, P. Silacci, V. I. Harrison and D. Hayoz, "Nitric oxide synthase expression in endothelial cells exposed to mechanical forces," *Hypertension*, vol. 32, pp. 351-355., 1998b.
- [67] S. Zhao, A. Suci, T. Ziegler, J. E. J. Moore, E. Burki, J. J. Meister and H. R. Brunner, "Synergistic effects of fluid shear stress and cyclic circumferential stretch on vascular endothelial cell morphology and cytoskeleton.," *Arteriosclerosis, Thrombosis, and Vascular Biology*, vol. 15, pp. 1781-1786, 1995.
- [68] M. A. J. Gimbrone, J. N. Topper, T. Nagel, K. R. Anderson and G. Garcia-Cardena, "Endothelial dysfunction, hemodynamic forces, and atherogenesis," *Annals of the New York Academy of Sciences*, vol. 902, pp. 230-239, 2000.
- [69] H. Miao, Y. L. Hu, Y. T. Shiu, S. Yuan, Y. Zhao, R. Kaunas, Y. Wang, G. Jin, S. Usami and S. Chien, "Effects of flow patterns on the localization and expression of VE-cadherin at vascular endothelial cell junctions: in vivo and in vitro investigations," *The Journal of Vascular Research*, vol. 42, pp. 77-89, 2005.
- [70] M. Mehrbod and M. Mofrad, "On the Significance of Microtubule Flexural Behavior in Cytoskeletal Mechanics," *PLoS ONE*, vol. 6, no. 10, 2011.
- [71] V. Jakka and J. Bursa, "Finite Element Simulations of Mechanical Behaviour of Endothelial Cells," *Biomed Research International*, pp. 1-17, 2021.
- [72] A. Nieto, J. Escribano, F. Spill, M. Garcia-Aznar and M. J. Gomez-Benito, "Finite element simulation of the structural integrity of endothelial cell monolayers: a step for tumor cell extravasation," *Engineering Fracture Mechanics*, vol. 224, 2020.
- [73] J. Uzarski, E. Scott and P. McFetridge, "Adaptation of endothelial cells to physiologically-modeled, variable shear stress.," *PLoS One*, vol. 8, no. 2, 2013.
- [74] S. M. and T. Ohashi, "Biorheological views of endothelial cell responses to mechanical stimuli," *Biorheology*, vol. 42, no. 6, p. 421-441, 2005.
- [75] A. Remuzzi, C. Dewey, P. Davies and M. Gimbrone, "Orientation of endothelial cells in shear fields in vitro.," *Biorheology*, vol. 21, no. 4, 1984.
- [76] R. Rand, "Mechanical properties of the red cell membrane: II. Viscoelastic breakdown of the membrane," *Journal of biophysics*, vol. 4, no. 4, p. 303, 1964.
- [77] P. Janmey, U. Euteneuer, P. Traub and M. Schliwa, "Viscoelastic properties of vimentin compared with other filamentous biopolymer networks.," *Journal of cell biology*, vol. 113, no. 1, pp. 155- 160, 1991.
- [78] N. Wang and D. Stamenović, "Contribution of intermediate filaments to cell stiffness, stiffening, and growth.," *The American Journal of Physiology-Cell Physiology*, vol. 279, pp. C188-94, 2000.
- [79] H. Kojima, A. Ishijima and T. Yanagida, "Direct measurement of stiffness of single actin filaments with and without tropomyosin by in vitro nanomanipulation.," *Proceedings of the National Academy of Sciences*, vol. 91, no. 26, pp. 12962-6, 1994.
- [80] D. Ingber, "Journal of Cell Science," *Tensegrity I. cell structure and hierarchical systems biology*, vol. 116, no. 7, pp. 1157-1173., 2003.
- [81] F. Gittes, B. Mickey, J. Nettleton and J. Howard, "Flexural rigidity of microtubules and actin filaments measured from thermal fluctuations in shape," *Journal of Cell biology*, vol. 120, pp. 923-934, 1993.



- [82] A. Kiyoumarsioskouei, M. S. Saidi and B. Firoozabadi, "An endothelial cell model containing cytoskeletal components: Suspension and adherent states," *Journal of Biomedical Science and Engineering*, vol. 5, no. 12, p. 737, 2012.
- [83] R. P. Jean, C. S. Chen and A. A. Spector, "Finite-element analysis of the adhesion-cytoskeleton-nucleus mechanotransduction pathway during endothelial cell rounding: axisymmetric model," *Journal of Biomechanical Engineering*, vol. 127, no. 4, pp. 594-600, 2005.
- [84] R. P. Jean, D. S. Gray, A. A. Spector and C. S. Chen, "Characterization of the Nuclear Deformation Caused by Changes in Endothelial Cell Shape," *Journal of biomechanical engineering*, vol. 126, p. 552–558, 2004.
- [85] "Cytoskeleton, Inc," The Proteine experts, Denver, USA, [Online]. Available: [www.cytoskeleton.com](http://www.cytoskeleton.com) .
- [86] J. Stricker, T. Falzone and M. and Gardel., "Mechanics of the F-actin cytoskeleton," *Journal of biomechanics*, Vols. 43., p. 9–14, 2010.
- [87] S. Deguchi, M. Yano, K. Hashimoto, H. Fukamachi, S. Washio and K. Tsujioka, "Assessment of the mechanical properties of the nucleus inside a spherical endothelial cell based on microtensile testing," *Journal of Mechanics of Materials and Structures*, vol. 2, no. 6, pp. 1087-1102, 2007.
- [88] H. Miyazaki, Y. Hasegawa and K. Hayashi, "Tensile properties of contractile and synthetic vascular smooth muscle cells," *JSME International Journal Series C Mechanical Systems*, vol. 45, no. 4, pp. 870-9, 2002.
- [89] H. Pakravan , M. Saidi and B. Firoozabadi , "A multiscale approach for determining the morphology of endothelial cells at a coronary artery.," *Int J Numer Method Biomed Eng*, vol. 33, no. 12, 2017.
- [90] O. Lisicky, A. Mala, Z. Bednarik, T. Novotny and J. Bursa, "Consideration of stiffness of wall layers is decisive for patient-specific analysis of carotid artery with atheroma," *PLOS ONE*, vol. 15, no. 9, pp. 1-18, 2020.
- [91] L. Horný , M. Netušil and T. Voňavková , "Axial prestretch and circumferential distensibility in biomechanics of abdominal aorta," *Biomech Model Mechanobiol*, vol. 13, no. 4, pp. 783-99, 2014.
- [92] G. Sommer, P. Regitnig , L. Költringer and G. Holzapfel , "Biaxial mechanical properties of intact and layer-dissected human carotid arteries at physiological and suprphysiological loadings," *Am J Physiol Heart Circ Physiol*, vol. 298, no. 3, pp. H898-912, 2010.
- [93] P. Prendergast, "Computational Modelling of Cell and Tissue Mechanoresponsiveness," *Gravit. Space Res.*, vol. 20, no. 2, pp. 43-50, 2007.
- [94] A. C. Shieh and K. A. Athanasiou, "Dynamic compression of single cells," *Osteoarthritis and Cartilage*, vol. 15, no. 3, p. 328–334, 2007.
- [95] N. D. Leipzig and K. A. Athanasiou, "Static compression of single chondrocytes catabolically modifies single-cell gene expression," *Biophysical Journal*, vol. 94, no. 6, p. 2412–2422, 2008.
- [96] D. Dugdale, "Yielding of steel sheets containing slits," *J. Mech. Phys. Solids* , vol. 8, p. 100–104, 1960.
- [97] G. Barenblatt, " Mathematical theory of equilibrium cracks in brittle fracture.," *Advances in Applied Mechanics*, , vol. VII, 1962..
- [98] A. Needleman, " A continuum model for void nucleation by inclusion debonding," *J. Appl. Mech.* , vol. 54, 1987.

- [99] V. Tvergaard, "Effect of fibre debonding in a whisker-reinforced metal.," *Mater. Sci. Eng. A* , vol. 125, 1990. .
- [100] X. Xu and A. Needleman, "Void nucleation by inclusion debonding in crystal matrix," *Model. Simul. Mater. Sci. Eng.* , vol. 1, p. 111–132., 1993.
- [101] N. Chandra, H. Li, C. Shet and H. Ghonem, "Some issues in the application of cohesive zone models for metal–ceramic interfaces," *Int. J. Solids Struct.*, vol. 39, p. 2827–2855., 2002.
- [102] H. Wang, W. Ip, R. Boissy and E. Grood, "Cell orientation response to cyclically deformed substrates: experimental validation of a cell model," *J.Biomech.*, vol. 28, p. 1543–1552, 1995.
- [103] M. Moretti, A. Prina-Mello, A. Reid, V. Barron and P. Prendergast, "Endothelial cell alignment on cyclically-stretched silicone surfaces.," *J.Mater.Sci.Mater.Med*, vol. 15, p. 1159–1164., 2004.
- [104] H. Hsu, C. Lee and R. Kaunas, "Adynamics to chastic model of frequency-dependent stress fiber alignment induced by cyclic stretch.," *PloS one* , vol. 4, p. e4853., 2009.
- [105] J. McGarry, B. Murphy and P. Mchugh, "Computational mechanics modelling of cell-substrate contact during cyclic substrate deformation," *J.Mech.Phys.Solids*, vol. 53, p. 2597–2637., 2005.
- [106] B. Chan, V. Bhat, S. Yegnasubramanian, W. Reichert and G. Truskey, "An equilibrium model of endothelial cell adhesion via integrin-dependent ligands," *Biomaterials*, vol. 20, p. 2395–2403, 1999.
- [107] O. Thoumine, P. Kocian, A. Kottelat and J. Meister, "Short-term binding of fibro blasts to fibronectin: optical tweezers experiments and probabilistic analysis," *Eur.Biophy.J.*, vol. 29, p. 398–408, 2000.
- [108] B. D. Hoffman and J. C. Crocker, "Cell mechanics: dissecting the physical responses of cells to force," *Ann Rev Biomed Eng*, vol. 11, pp. 259-88, 2009.

## List of Figures

<b>Figure 1. 1:</b> Successive layers of the arterial wall. Figure adapted from [3]-----	<b>2</b>
<b>Figure 2. 1:</b> Tensegrity FE model of suspended cell by ( [17]; [18]) including nucleoskeleton (purple), cytoplasm (blue) and discrete elements representing cytoskeleton structure.-----	<b>6</b>
<b>Figure 2. 2:</b> Sections of continuous elements (a) and structural arrangement of cytoskeletal components (b) with respect to the nucleus for suspended cell model. From [27]-----	<b>7</b>
<b>Figure 3. 1:</b> Arrangement of endothelial cells lining the luminal surface of arteries and veins (silver nitrate staining), a) Strongly elongated and oriented endothelial cells in human thoracic aorta. The direction of blood flow is indicated by the arrow. Bright field; magnification, ×225. b) Polygonally shaped endothelial cells of human saphenous vein. Sample was obtained after bypass surgery. Bright field; magnification, ×350. This picture is adopted from [35].....	<b>13</b>
<b>Figure 3.2:</b> Laminar fully developed blood flow in a tubular vessel [39].....	<b>14</b>
<b>Figure 3. 3:</b> Shear stress patterns in the asymmetric stenosis model as computed in a numerical Simulation (A) [42].....	<b>15</b>
<b>Figure 3. 4:</b> A single cell's tensile test is depicted in this diagram. The cantilever and the cell are not depicted in precise relative scale, and the cantilever deflection is exaggerated [47]. .....	<b>17</b>
<b>Figure 3. 5:</b> Schematic diagram of the Compression test of a single cell from [50].....	<b>18</b>
<b>Figure 3. 6:</b> Digitized video images of a round cell (a–c), a spread cell (d–f), and an isolated nucleus (g–i) exposed to compression. This picture is taken from the [50] .....	<b>18</b>
<b>Figure 3. 7:</b> Cone and plate viscometer, original (A) [52] and modified with a step (B) [55]	<b>19</b>
<b>Figure 3. 8:</b> Parallel plate chamber, original (A) [57] and modified with a step (B) [59] .....	<b>19</b>
<b>Figure 4. 1:</b> Finite element hybrid model of endothelial cell representing (a) the continuum mesh and the cytoskeletal components of the elongated flat model with AFs (red), IFs (green), and MTs (blue) (b) front view of the domed cell model with supports and varying thickness.....	<b>22</b>
<b>Figure 4. 2:</b> Sectional view of the hybrid model representing nucleus on the centre. ....	<b>22</b>
<b>Figure 4. 3:</b> MTs architecture in the proposed computational model. ....	<b>23</b>

<b>Figure 4. 4:</b> IFs architecture in the proposed computational model.....	<b>23</b>
<b>Figure 4. 5:</b> Stress-strain relationship defining the mechanical behaviour of (a) IFs with applied positive strain and (b) AFs with applied negative strain (pre-strain) in their undeformed configurations. ....	<b>24</b>
<b>Figure 4. 6:</b> AFs architecture in the proposed computational model. ....	<b>24</b>
<b>Figure 4. 7:</b> Spherical model of suspended endothelial cell.....	<b>27</b>
<b>Figure 4. 8:</b> Typical images of: (a) an adherent cell on a rigid microplate [50] and (b) corresponding proposed FE adherent cell model.....	<b>27</b>
<b>Figure 4. 9:</b> Structural arrangement of cytoskeletal components with respect to the nucleus.	<b>28</b>
<b>Figure 4. 10:</b> (a) architecture in the proposed computational model and (b) Microscopic fluorescence image of the architecture of ABs cited from [85].....	<b>28</b>
<b>Figure 5. 1:</b> Suspended cell model during consecutive steps in simulation of Compression test at 50% compression (blue) and unloaded state (wire frame).....	<b>31</b>
<b>Figure 5. 2:</b> Comparison of simulated force-deformation (%) curve with the experimental curves taken from a study by [50] investigating the biomechanical properties of a single endothelial cell using a micromanipulation technique.....	<b>32</b>
<b>Figure 5. 3:</b> Simulation results of 50% cell compression: Stresses in (a) AFs (b) IFs and (c) MTs; (d) distribution of first principal strain in the continuous elements representing nucleus. ....	<b>33</b>
<b>Figure 5. 4:</b> The suspended cell model during consecutive steps in simulation of tensile test: (a) spherical cell, (b) compressing the cell by 20% and (c) stretching the cell 50% .....	<b>34</b>
<b>Figure 5. 5:</b> Comparison of simulated force-deformation (%) curve with the experimental curves taken from a study by [87], measuring the tensile properties of cultured Bovine aortic endothelial cells. ....	<b>35</b>
<b>Figure 5. 6:</b> Simulation results of 50% cell elongation: axial stress distribution in (a) AFs (b) IFs and (c) MTs; (d) distribution of first principal strain representing nucleus.....	<b>36</b>
<b>Figure 5. 7:</b> Contribution of cytoskeletal components in spherical cell model to its stiffness (a) in compression, (b) in tension. The reaction force is normalized to 1 with respect to that from hybrid model. ....	<b>37</b>
<b>Figure 5. 8:</b> FE model of an adherent cell in the Compression test, with constraints and displacement load applied on the top of the cell. (front view).....	<b>39</b>

<b>Figure 5. 9:</b> Adherent cell model in simulation of Compression test: unloaded shape of truncated sphere in wire frame and final shape with 50% compression of the cell in solid blue color. ....	<b>40</b>
<b>Figure 5. 10:</b> Distribution of (a ) first principal strain (b) third principle strain in the nucleus of adherent endothelial cell. ....	<b>40</b>
<b>Figure 5. 11:</b> Comparison of simulated force-deformation curves obtained with the adherent cell and flat cell models with the experimental curves taken from the study by [50]. ....	<b>41</b>
<b>Figure 5. 12:</b> Contribution of cytoskeletal components in adherent cell model to its stiffness (a) in compression. The reaction force is normalized to 1 with respect to that from hybrid model.....	<b>42</b>
<b>Figure 5. 13:</b> FE model of undeformed shape of regular flat hybrid endothelial cell.....	<b>42</b>
<b>Figure 5. 14:</b> Distribution of (a) first principal strain (b) third principle strain in the nucleus of flat endothelial cell in isometric view. ....	<b>43</b>
<b>Figure 5. 15:</b> Contribution of cytoskeletal components in cell models to their stiffness in compression flat model. The reaction force is normalized to 1 with respect to that from hybrid model. ....	<b>44</b>
<b>Figure 5. 16:</b> Boundary conditions of flat endothelial cell for shear.....	<b>45</b>
<b>Figure 5. 17:</b> Shear deformation of regular flat endothelial cell .....	<b>45</b>
<b>Figure 5. 18:</b> Distribution of shear strain in xy direction of flat endothelial cell at 15% shear deformation in isometric view. (a) regular flat (b) regular domed .....	<b>45</b>
<b>Figure 5. 19:</b> Distribution of first principal strain in the nucleus of regular endothelial cell at 15% shear deformation in isometric view (a) regular flat (b) regular domed.....	<b>46</b>
<b>Figure 5. 20:</b> (a) Finite element mesh (in axial view) of the arterial wall model with media (orange) and adventitia (pink) layers. (b) Arrangement of hexagonal endothelial cells on the inner surface of the artery used for transmission of deformation between the artery and cell model.....	<b>48</b>
<b>Figure 5. 21:</b> Examples of the deformed shapes of regular flat endothelial cell model variant Bi under extreme biaxial strains according to Tab. 5.3: (a) 0/20 and (b) 30/10 .....	<b>50</b>
<b>Figure 5. 22:</b> Simulated dependences of biaxial tension forces (variant Bi) on the increasing blood pressure (between 0 and 20 kPa) recalculated into circumferential strain of the cell. (a), 30/20 case, (b) 0/20 case.....	<b>53</b>
<b>Figure 5. 23:</b> Comparison of simulated force-deformation curves for regular flat equibiaxial strain (5/20) models (with and without cytoskeleton) with simulated and typical experimental results in compression [71], [50].....	<b>54</b>

**Figure 5. 24:** Mixed mode separation is computed at bottom of the (a) 1st cycle (b) 30th cycles reaching 5 % strain..... **57**

**Figure 5. 25:** The computed normal tractions (a) at the top of the 1st cycle (b) at the top of the 30<sup>th</sup> cycle (c) at the bottom of 1st cycle (d) at the bottom of 30<sup>th</sup> cycle. (Top View), Due to downwards orientation of the y axis, the normal tractions with maximum magnitude are negative and shown in blue colour..... **58**

**Figure 5. 26:** The computed normal displacements (a) at the top of the 1st cycle (b) at the top of the 30<sup>th</sup> cycle (c) at the bottom of 1st cycle (d) at the bottom of 30<sup>th</sup> cycle. (Top View), Due to downwards orientation of the y axis, the normal displacements with maximum magnitude are negative and shown in blue colour..... **59**

**Figure 5. 27:** The computed tangential tractions (a) at the top of the 1st cycle (b) at the top of the 30<sup>th</sup> cycle (c) at the bottom of 1st cycle (d) at the bottom of 30<sup>th</sup> cycle. (Top View). **60**

**Figure 5. 28:** Full history of normal separation during 30 cycles for both sides of deformation. .... **61**

**Figure 5. 29:** Normal traction during all the 30 cycles. (The dashed line represents the bottom values of each cycle representing residual tractions)..... **61**

**Figure 5. 30:** Contour plot of the strain component in the direction of substrate stretching at the top of the 30th cycles. .... **62**

## List of Tables

<b>Table 4. 1:</b> Elastic properties of discrete components of cell model -----	<b>26</b>
<b>Table 4. 2:</b> Hyper elastic properties of continuous components of cell model-----	<b>26</b>
<b>Table 4. 3:</b> Mesh properties of the adherent cell model in ANSYS -----	<b>29</b>
<b>Table 4. 4:</b> Elastic properties of discrete components of adherent cell model -----	<b>29</b>
<b>Table 4. 5:</b> Hyper elastic properties of continuous components of adherent cell model-----	<b>30</b>
<b>Table 5. 1:</b> Hyper-elastic material properties of arterial layers [90] .....	<b>47</b>
<b>Table 5. 2:</b> Dimensions of different arteries and circumferential strains on their inner surface (endothelium) under zero axial pre-strain and blood pressure of 20 kPa – a combination typical for older individuals .....	<b>49</b>
<b>Table 5. 3:</b> Axial and circumferential strains of endothelium used to formulate boundary conditions of the individual cell model in the circumferential direction .....	<b>49</b>
<b>Table 5. 4:</b> The first principal strains in the nucleus in the calculated cases for regular hexagonal endothelial cell. Pulsations represent the cyclic increase of the first principal strain in nucleus between blood pressures of 10 and 20 kPa. ....	<b>51</b>
<b>Table 5. 5:</b> The first principal strains in the nucleus in the calculated cases for elongated hexagonal endothelial cell. Pulsations represent the cyclic increase of the first principal strain in nucleus between blood pressures of 10 and 20 kPa. ....	<b>52</b>

## Abbreviations

1D	one-dimensional
3D	three-dimensional
a	cross-sectional area of cell, $\mu\text{m}^2$
ABs	actin bundles
AC	actin cortex
AFM	atomic force microscopy
AFs	actin filaments
CM	cell membrane
CZM	cohesive zone model
D	diameter of suspended cell, $\mu\text{m}$
DOFs	degrees of freedom
ECM	extracellular matrix
f	reaction force at stretched edge, $\mu\text{N}$
FAs	focal adhesions
FE	finite element
ID	Inner diameter, $\mu\text{m}$
IFs	intermediate filaments
l	elongated length of cell, $\mu\text{m}$
$l_0$	length of cell at zero reaction force, $\mu\text{m}$
MTC	magnetic twisting cytometry
MTs	microtubules
OD	outer diameter, $\mu\text{m}$
SD	substrate deformation
SFs	stress fibers
SMCs	smooth muscle cells
$\varepsilon$	conventional strain
$\sigma$	conventional stress, $\text{N/m}^2$



## Appendix A

**Title:** "Finite Element Simulations of Mechanical Behaviour of Endothelial Cells"

**Authors:** Veera Venkata Satya Varaprasad Jakka, Jiri Bursa

**Journal Name:** BioMed Research International

**Impact Factor:** 3.411

### **Citation:**

Veera Venkata Satya Varaprasad Jakka, Jiri Bursa, "Finite Element Simulations of Mechanical Behaviour of Endothelial Cells", **BioMed Research International**, vol. 2021, ArticleID 8847372, 17 pages, 2021. <https://doi.org/10.1155/2021/8847372>.

## Research Article

# Finite Element Simulations of Mechanical Behaviour of Endothelial Cells

**Veera Venkata Satya Varaprasad Jakka  and Jiri Bursa**

*Institute of Solid Mechanics, Mechatronics and Biomechanics (ISMMB), Faculty of Mechanical Engineering (FME), Brno University of Technology (BUT), Technicka 2896/2, 61669 Brno, Czech Republic*

Correspondence should be addressed to Veera Venkata Satya Varaprasad Jakka; 207437@vutbr.cz

Received 24 September 2020; Revised 26 January 2021; Accepted 5 February 2021; Published 17 February 2021

Academic Editor: Kazuhisa Nishizawa

Copyright © 2021 Veera Venkata Satya Varaprasad Jakka and Jiri Bursa. This is an open access article distributed under the Creative Commons Attribution License, which permits unrestricted use, distribution, and reproduction in any medium, provided the original work is properly cited.

Biomechanical models based on the finite element method have already shown their potential in the simulation of the mechanical behaviour of cells. For instance, development of atherosclerosis is accelerated by damage of the endothelium, a monolayer of endothelial cells on the inner surface of arteries. Finite element models enable us to investigate mechanical factors not only at the level of the arterial wall but also at the level of individual cells. To achieve this, several finite element models of endothelial cells with different shapes are presented in this paper. Implementing the recently proposed bendotensegrity concept, these models consider the flexural behaviour of microtubules and incorporate also waviness of intermediate filaments. The suspended and adherent cell models are validated by comparison of their simulated force-deformation curves with experiments from the literature. The flat and dome cell models, mimicking natural cell shapes inside the endothelial layer, are then used to simulate their response in compression and shear which represent typical loads in a vascular wall. The models enable us to analyse the role of individual cytoskeletal components in the mechanical responses, as well as to quantify the nucleus deformation which is hypothesized to be the quantity decisive for mechanotransduction.

## 1. Introduction

Atherosclerosis is a leading cause of morbidity and mortality in the developed world. It is characterized by progressive narrowing and hardening of arteries which lead to ischemia of the heart, brain, or extremities and may cause infarction or stroke [1]. To elucidate the atherogenesis, it is important to understand the cellular responses to mechanical stimuli exerted on endothelial cells from their haemodynamic environment or artery deformation.

The endothelium is a monolayer of endothelial cells that line inner walls of arteries, hence providing an interface between the flowing blood and the artery wall [2] and playing a key role in the pathobiology of atherosclerosis [3]. The endothelial cells are of flat hexagonal shape [4, 5] elongated in the blood flow direction [6].

Living cells are highly complex structures consisting of a large number of distinct structural components such as the

cytosol, cell membrane (CM), cytoskeleton, nucleus, and other organelles. The cytoskeletal network is composed of three types of components, namely, actin filaments (AFs), microtubules (MTs), and intermediate filaments (IFs), which are spread throughout the cytoplasm and interlinked to each other, to the nucleus, and to the CM [7]. Their structural arrangement is decisive for the response of the cytoskeleton to mechanical stimuli and for the stiffness of the whole cell. The prestress in AFs is balanced mainly by MTs but partly also by continuum parts and the extracellular matrix, to which the cell is tethered [8].

In the past few decades, the development of microrheological techniques [9] has made quantitative mechanical measurements of single living cells feasible. For our research, the following testing methods are most relevant: microplate stretcher [10], microplate manipulation [11, 12], and atomic force microscopy (AFM) [13]. There are other more recent techniques which can reveal the mechanical characteristics

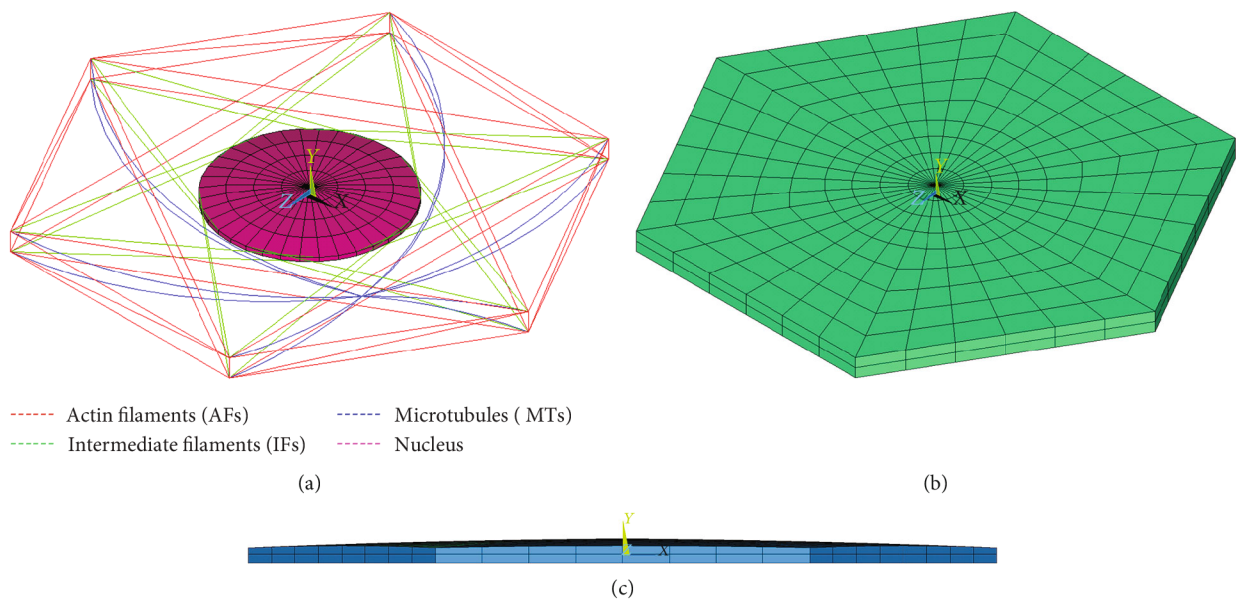


FIGURE 1: Arrangement of cytoskeletal components with respect to the nucleus in the flat and dome models (a); continuous elements of the flat model (b); front view of the dome model (c).

of cells such as a microfluidic device [14], dissipative particle dynamics [15], or micropipette aspiration [16, 17].

Some recent models of cell mechanics consider their structure to include the cytoskeleton, e.g., the multistructural model [18], the spring network cell model [19], and the granular cell model [20]. Other studies of active approaches incorporate the cell's inherent active nature in computational modelling such as the bio-chemo-mechanical model [21], the dynamic stochastic model [22], and the kinematic model [23]. Although these models are equipped with formulations to explain both passive and active responses of cells, they do not elucidate the contribution of cytoskeletal components. This is feasible with tensegrity-based finite element (FE) models consisting of both tension- and compression-bearing elements [24] which show a self-stabilizing effect [25].

In order to interpret the relation between the biological response of living cells and mechanical stresses, tensegrity models are predominantly suitable for cytoskeletal structures of living cells [26]. However, in cytoskeletal tensegrity models presented in the literature, the MTs appear too stiff because they do not account for the flexural behaviour of MTs [27]. In order to overcome this problem, the most sophisticated hybrid model has been recently created using the bendotensegrity concept [28] for modelling smooth muscle cells [29]. This concept was adopted also in this study, and the model was modified to represent specific features of endothelial cells and the role of individual cytoskeletal components in their mechanical response.

## 2. Materials and Methods

For the simulation of mechanical tests of an endothelial cell, FE models with different shapes were created using the commercial software ANSYS (ANSYS Inc., USA). The hybrid modelling approach is similar to the model of the vascular

smooth muscle cell in [30], where the cytoplasm, nucleus, and CM are modelled with continuum elements while the individual cytoskeletal components are modelled as discrete (unidimensional) elements. This approach enables us to study the mechanical role of individual cytoskeletal components in cellular mechanical response as well as the propagation of mechanical stimuli throughout the cell, including quantification of nucleus deformation under different types of loads. Both the cytoplasm and nucleus were modelled with eight-node hexahedral isoparametric elements. A thin flexible layer circumscribing the cytoplasm referred to as CM was modelled with four-node quadrilateral shell elements on the outer surface of the cytoplasm, with no bending stiffness and a thickness of  $0.01 \mu\text{m}$  [31], coupled with the 3D elements through nodal displacements only, thus leaving nodal rotations of the shell free. The cytoskeleton (with the same topology in all the models as described below) was inscribed inside the continuous part thus creating the hybrid model.

Three different mechanical tests were simulated to validate the proposed model: tensile and compression tests of a suspended (spherical) cell with micropipettes and microplates, respectively, and a compression test of the cell adhered to a substrate which thus had the shape of a truncated sphere. The model of the endothelial cell in its typical flat shape in the endothelium layer cannot be validated due to lack of experimental data. Therefore, this flat model was created on the basis of the above validated models, keeping their topology and volume; then, it was used for the simulation of compression and shear of the endothelium cell in its natural shape. Based on its physiological dimensions and shape, the cell was modelled as a very short flat regular hexagonal prism [4, 32] with a thickness of  $0.5 \mu\text{m}$  [4, 33, 34] as shown in Figure 1(b). In order to investigate an even more physiological shape, the flat model was then modified into a dome with the cell being 20% higher at the centre than at the edges; this

TABLE 1: Finite elements used for discrete components of the cell models and their elastic parameters.

Cell component	Elastic modulus, $E$ (Pa)	Poisson's ratio, $\nu$	Diameter (nm)	Finite element specification	Nature
Microtubules (MTs) [45]	$1.2 \times 10^9$	0.3	25/17 (outer/inner)	BEAM188	Curved beams
Actin filaments (AFs) [46]	$2.2 \times 10^9$	0.3	4.5	LINK180	Tension only trusses
Intermediate filaments (IFs) [46]	$2.0 \times 10^9$	0.3	10	LINK180	Tension only trusses
Actin bundles (ABs) [41]	$0.34 \times 10^6$	0.3	250	LINK180	Tension only trusses

TABLE 2: Finite elements used for continuous components of the cell models and their hyperelastic parameters.

Component name	Young's modulus, $E$ (Pa)	Shear modulus, $G$ (Pa)	Bulk modulus, $K$ (Pa)	Finite element specifications
Cytoplasm [47]	$0.5 \times 10^3$	$0.17 \times 10^3$	$2.77 \times 10^3$	Solid 185
Nucleus [47]	$5 \times 10^3$	$1.7 \times 10^3$	$27.77 \times 10^3$	Solid 185
Cell membrane (CM) [31]	$1 \times 10^6$	$0.33 \times 10^6$	Infinity	Shell 181
Actin cortex (AC) [48]	$2 \times 10^3$	$0.67 \times 10^3$	Infinity	Shell 181

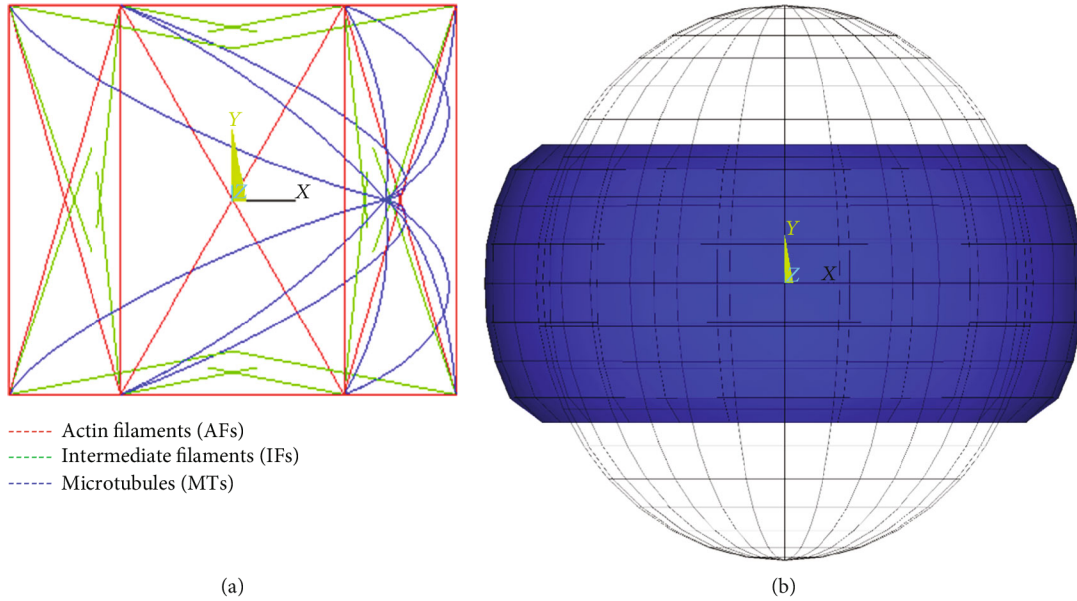


FIGURE 2: Suspended cell model for simulation of the compression test: (a) unloaded cytoskeleton in front view and (b) unloaded model in wire frame and under 50% compression.

nonuniform height corresponds better to the physiological endothelial shape [14, 35].

The cytoskeletal arrangement is decisive for the mechanical and possibly also for the biochemical response of living cells [8, 36, 37]. The cytoskeleton in our model comprises 12 beam elements (representing the MTs which are curved, all connected in the centrosome, and capable of bearing flexion and tension or compression), 36 prestressed truss elements (representing the AFs and bearing tension only), and 24 truss elements representing the IFs. To mimic their waviness, the IFs have a prestrain of 20 percent to resist tensile

loads only under larger elongations [38–40]. In contrast, the experimentally measured prestrain of 24% [41, 42] was always assigned to AFs in the first load step to generate their prestress (initial force without load) essential for the cell shape stability.

The MTs of unequal lengths originate from the centrosome, represented by a node located near the nucleus. They emanate outward through the cytoplasm till the cortex where they interact with other cytoskeletal filaments at focal adhesions (FAs). Due to the different nature of truss and beam elements, the rotational degrees of freedom of beams remain

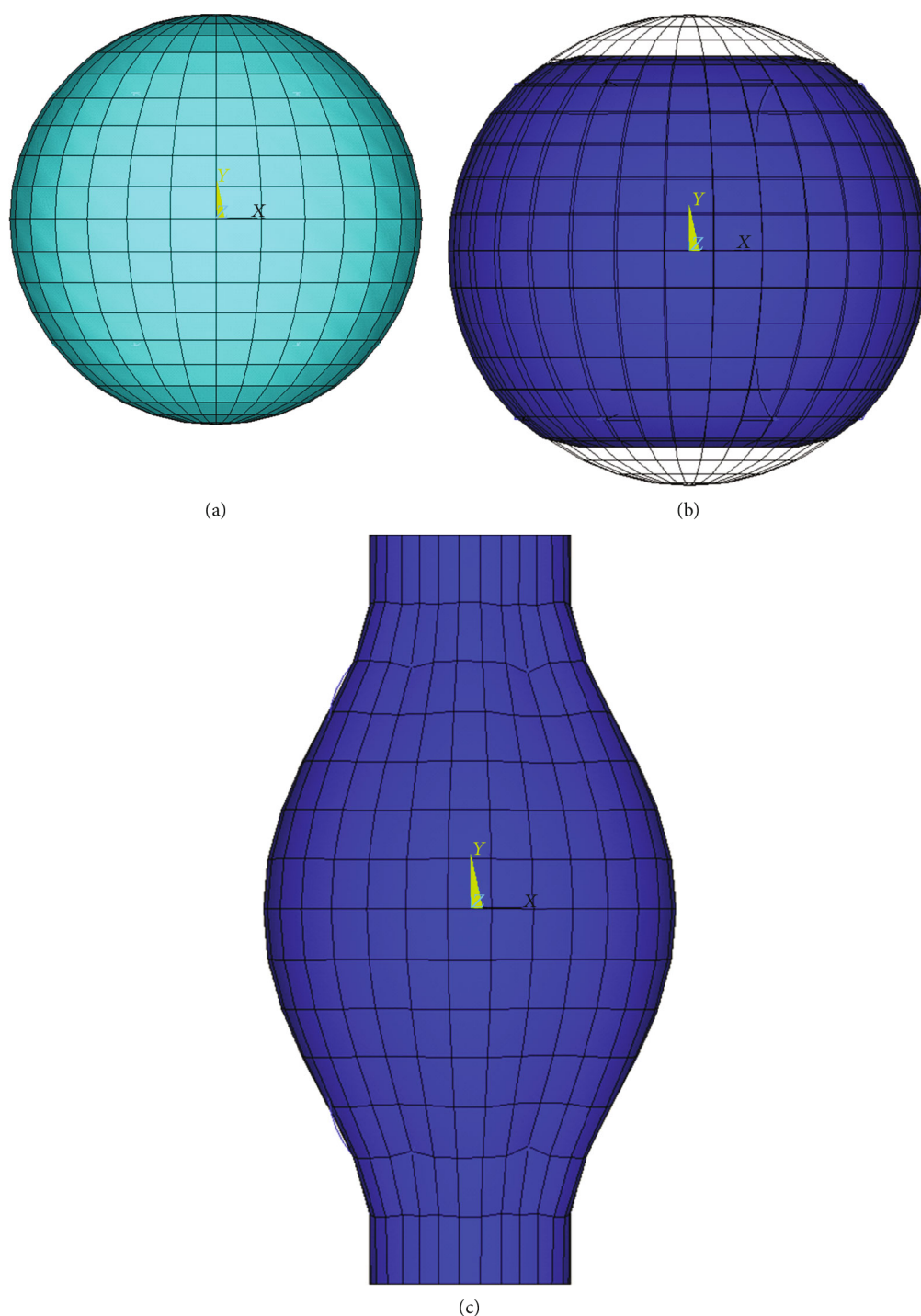


FIGURE 3: Suspended cell model for consecutive steps in simulation of tensile test: (a) unloaded spherical cell, (b) compressing the cell by 20%, and (c) stretching the cell by 50%.

free here, and no other contacts (and consequently no friction) are assumed between the MTs and the continuum elements representing the cytoplasm. The authors believe that this behaviour of MTs (but also of AFs and IFs) corresponds to the fluid nature of the cytosol and to the character of the FAs. Every FA is connected to the centrosome with only one MT, and it is ensured that they do not penetrate the nucleus.

IFs are scattered throughout the intracellular space, connecting the FAs to the nucleus and creating a dense network in the perinuclear region that stabilizes the nucleus at the cell centre [39]. For better transmission of mechanical stimuli to the nucleus and its stabilization at the centre of the cell, each FA was connected to the nucleus via at least two IFs. To mimic their real structural arrangement, they were modelled

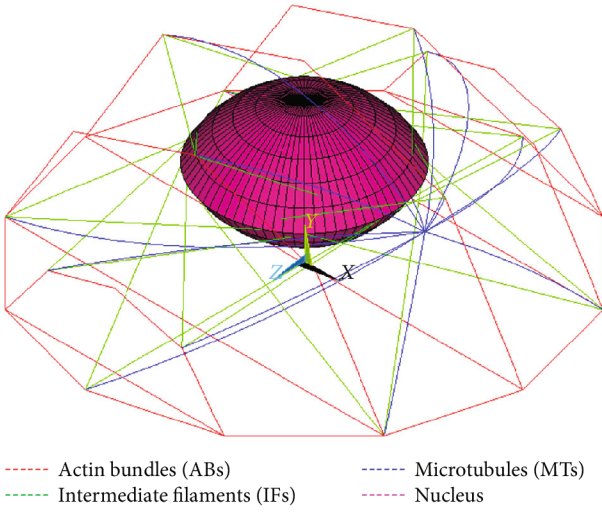


FIGURE 4: Structural arrangement of cytoskeletal components with respect to the nucleus in the adherent cell model.

tangentially to the nucleus, thus creating a dense network in the perinuclear region.

For the flat cell model, thin AFs were stretched between each pair of 12 nodes of the hexagonal prism, except for those which would penetrate the nucleus. The same arrangement was used in the dome and spherical model. In the adherent cell, actin is arranged in thick longitudinal bundles (ABs), the arrangement of which is described in detail in Section 2.3.

**2.1. Material Properties.** Although the cytoplasm behaves as a liquid rather than as a solid, the shear stresses induced in it during (static, i.e. relatively slow) mechanical tests are negligible. Thus, a very low compressibility represents its basic feature, which can be modelled using the Neo-Hookean model given by the following formula for its strain energy density  $W$ :

$$W = \frac{G}{2} (\bar{I}_1 - 3) + \frac{1}{d} (J - 1)^2, \quad (1)$$

where  $G(\text{Pa})$  is the initial shear modulus,  $d(\text{Pa}^{-1})$  is the compressibility parameter,  $J$  is the 3rd determinant of the deformation gradient tensor, and  $\bar{I}_1$  is the 1st invariant of the isovolumic part of the right Cauchy-Green deformation tensor. To keep the negligible shear stresses, the shear modulus was set very low (170 Pa). For the cell membrane, the material parameters were calculated from the known elastic constants as follows:

$$\begin{aligned} G &= \frac{E}{2(1 + \nu)}, \\ K &= \frac{E}{3(1 - 2\nu)} = \frac{2}{d}, \end{aligned} \quad (2)$$

where  $E(\text{Pa})$  is Young's modulus,  $\nu(-)$  is Poisson's ratio, and  $K(\text{Pa})$  is initial bulk modulus.

For the cytoskeleton, we use the following linear elastic model:

$$\varepsilon = \frac{\sigma}{E} + \varepsilon_0, \quad (3)$$

where  $\sigma(\text{Pa})$  is engineering stress,  $\varepsilon(-)$  is engineering strain, and  $\varepsilon_0(-)$  is applied prestrain which is negative for AFs and positive for IFs. All the parameters are summarized in Table 1 and Table 2 with the literature they are based on. The nonrealistic values of Poisson's ratio for cytoskeletal elements (0.3) are taken from the literature [18, 30, 43, 44] and have no impact on the results because they are represented as a 1D element.

**2.2. FE Model for Suspended (Spherical) Endothelial Cell.** In order to validate the simulated mechanical response of the endothelial cell, we rearranged the flat endothelial cell model into a spherical shape occurring in experiments [47]. For this purpose, we assumed the same volume of the cell, which gave us two concentric spheres representing the cytoplasm and the nucleus with diameters of  $7.4 \mu\text{m}$  and  $3.0 \mu\text{m}$ , respectively. The cytoskeletal arrangement of the spherical cell is shown in Figure 2(a).

**2.2.1. Boundary Conditions for Compression.** Compression of the cell was simulated for comparison with the experimental cell response in a compression test done with microplates [47]. To avoid difficulties related to the contact between the cell and the microplates (which are supposedly rigid), the cell model was fixed in its central node in all directions and vertical displacements were prescribed on both top and bottom sides to flatten the area being in contact with the microplates, and to achieve 50% shortening of the cell vertical dimension (see Figure 2(b)).

**2.2.2. Boundary Conditions for Tension.** The tensile test of a suspended cell was simulated in several steps for comparison with the cell response during stretching with rigid micropipettes [49]. With AFs being prestressed in the first load step, a bonded contact between the spherical cell and the faces of both micropipettes was established in the second load step by compressing the cell by approximately 20% (see Figure 3(b)). In the third load step, the cell was elongated to achieve zero reaction forces in the micropipettes; this unloaded state defines the initial length of the cell for calculation of its global relative deformation (strain) evaluated in percentage similarly to the experiments. In the final load step, uniform displacement was applied to the nodes of the top and bottom surfaces to achieve 50% elongation of the model (see Figure 3(c)).

**2.3. FE Model of Adherent Endothelial Cell.** The model with an axisymmetric truncated spherical geometry possessed a maximum diameter of 20 microns and a maximum height of 8 microns, with the nucleus having a flat ellipsoidal shape, and the centre placed in half height of the model; its major and minor (height) axes are 8 microns and 4 microns, respectively, based on experimental observations [47, 50].

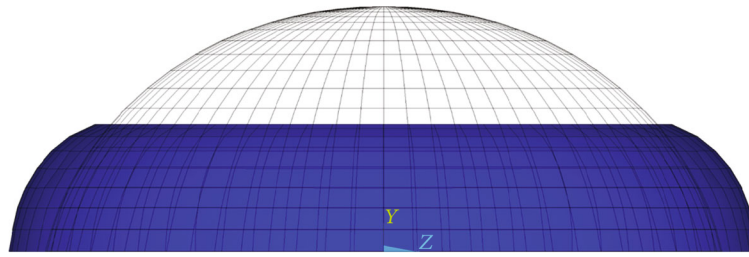


FIGURE 5: Adherent cell model in simulation of compression test at its initial shape and under 50% compression (blue).

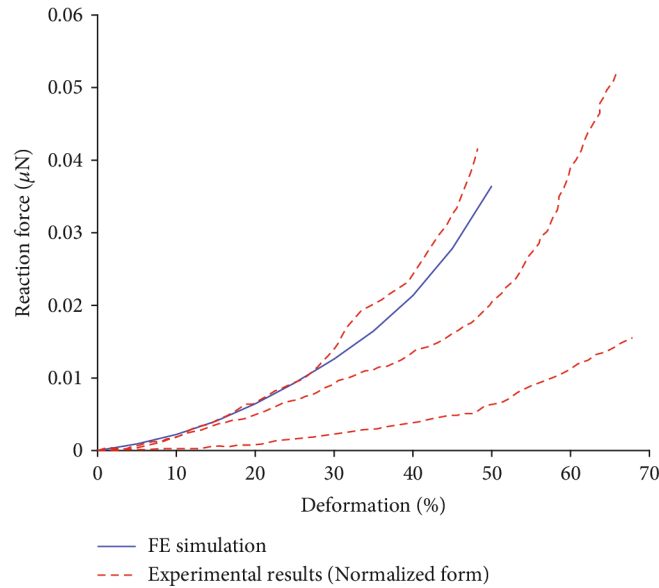


FIGURE 6: Comparison of simulations of suspended cell compression with force-deformation curves from the corresponding experiments in [47, 53]. The highest, medium, and lowest stiffness curves are taken from the experimental results.

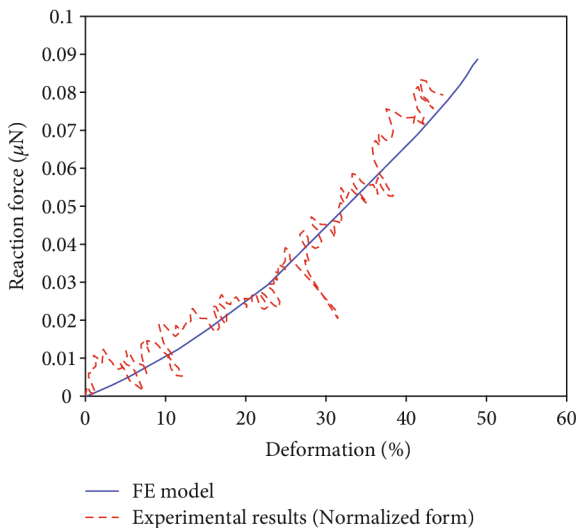


FIGURE 7: Comparison of the simulated force-deformation curve in tension with the experimental response obtained with cultured bovine aortic endothelial cells [49].

To consider a different structural arrangement of the adherent cell [30], thick actin bundles (ABs) were incorporated in the model instead of AFs (with the same prestrain); they were observed at the cell periphery running almost uniformly in the longitudinal direction [18, 41]. Moreover, a thin layer of actin-gel referred to as actin cortex (AC) was added to the shell elements on the cell model surface to represent both CM and the subcortical network of AFs. The experimentally measured thickness of the cortical layer of  $0.2 \mu\text{m}$  was chosen for our model [51, 52], being 20 times higher than the cell membrane itself; this value is consistent with another study on endothelial cells [50]. The arrangement of the cytoskeletal components of the adherent cell model (ABs, MTs, and IFs) is shown in Figure 4.

**2.3.1. Boundary Conditions of Adherent Cell in Compression.** To validate a model with a modified geometry and structure, simulation of a compression test of an adherent endothelial cell done with microplates was performed with boundary conditions mimicking the experimental approach [47]. After application of the prestress to the ABs, the cell was fixed at the bottom surface to mimic the (rigid) substrate and compressed vertically on the top side by application of vertical displacements to the nodes coming gradually into contact with the upper rigid microplate; these displacements were

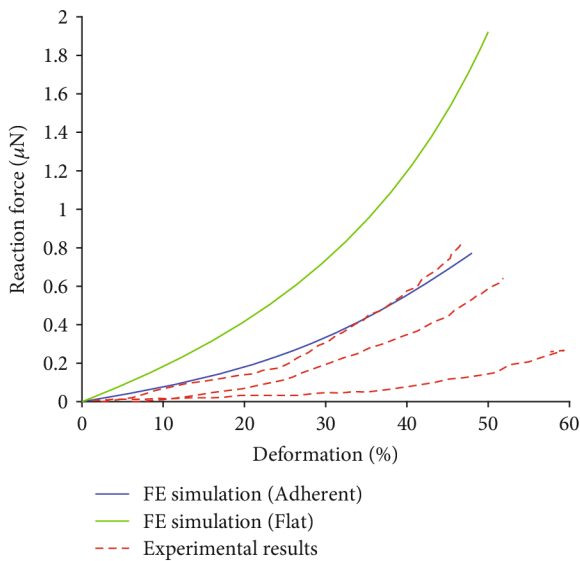


FIGURE 8: Comparison of simulated force-deformation curves obtained with the adherent cell and flat cell models with the experimental curves from [47]. The highest, medium, and lowest stiffness curves are taken from the experimental results.

calculated in order to flatten the contact area and to achieve the total 50% deformation of the cell (see Figure 5). The reaction force was evaluated as the sum of forces at nodes of the top side of the cell.

**2.4. Flat and Dome FE Models for Endothelial Cell.** The hexagonal shape of the flat cell model (with an edge length of 12.5 microns and a thickness of 0.5 microns) is typical for cells creating an endothelial layer. The nucleus is ellipsoidal with a major (horizontal) axis of 9 microns and a minor axis (height) of 0.4 microns, located again symmetrically on top view and with a spacing of 0.05 microns between the bottom surfaces of the cell and nucleus. The arrangement of its individual cytoskeleton components is shown in Figures 1(a) and 1(b). With this model, two typical types of physiological load were simulated, namely, compression (being equivalent to biaxial tension in the arterial wall) and shear, induced by viscous forces from the blood flow. The dome model was then created by increasing the height by 20% in the central region of the cell to mimic better the real shape in the vascular endothelium (see Figure 1(c)). Then, it was used to investigate the shear response and to assess the impact of nonuniform cell thickness on shear response in the physiological hexagonal cell shape.

**2.4.1. Boundary Conditions.** To mimic the compression experiment [47], the endothelial cell model was compressed in the thickness direction (symmetrically on top and on the bottom side) to achieve a 50% reduction of the cell height. The resulting reaction force was evaluated as a sum of the reaction forces in nodes either on top or on the bottom surface.

The shear load of the flat endothelial cell model was simulated in two steps. In the first step, all the nodes of the bottom hexagonal face were fixed in all directions and the cell was loaded in all the surface nodes on the top side by pre-

scribed displacements reaching 15% of the cell height in  $x$ -direction. The resulting reaction forces were then applied in a new simulation at all the nodes on the top side of the cell model, and the same load was applied also on the dome model. In this way, the force-controlled load was applied, corresponding to real shear forces induced by the blood flow and being the same at both models for their direct comparison.

**2.5. FE Mesh Density.** For all the solved models, the meshes counted between 5 and 18 k elements; their sufficient density was confirmed as follows. When the mesh size was reduced to a half, the number of elements increased by a factor of approximately 8. With this denser mesh, the calculated maximum strains in the nucleus as well as the other quantities related to the continuum part increased by 3-4% while the stresses in beam elements (MTs) changed even less and the link elements (AFs, ABs, and IFs) were insensitive to the number of elements.

### 3. Results

With the exception of the shear load, the symmetric geometrical shape of the model and the arrangement of the cytoskeleton resulted in a nearly isotropic behaviour of the model without a preferred orientation.

**3.1. Results for Suspended Cell Compression.** The force-deformation curve calculated from the compression test simulation is in good agreement with the experimental curves in normalized form obtained from the compression tests of cultured endothelial cells [47, 53] and also shows a similar strain stiffening (see Figure 6). This strain stiffening occurring with all the investigated shapes of the cell (see also Figures 7 and 8) is reached by mimicking the cytoskeleton with tensegrity structures; they show strain stiffening as their basic feature even if made of linear elastic materials. The cell diameter in the experiments differs from our model; thus, for comparison, the experimental reaction force  $F$  was transformed into  $F_N$  by normalization to the same diameter.

$$F_N = F \left[ \frac{D}{D_{\text{exp}}} \right]^2, \quad (4)$$

where  $D$  is the diameter of the model, and  $D_{\text{exp}}$  is the cell diameter in the experiment.

The logic of normalization is based on proportionality between the cell cross-section area and the resulting force under the same stress.

The MTs in the central region being perpendicular to the direction of loading are straightened and bear much higher tensile forces while the others remain bended (see Figure 9(c)). Also, the AFs reoriented perpendicularly to the loading direction resist high tensile stresses as shown in Figure 9(a), and their number increased with cell compression. In contrast, the IFs reoriented perpendicularly to the direction of compression are only slightly uncoiled from their initial waviness, and exhibit very lower positive stresses presented in Figure 9(b).



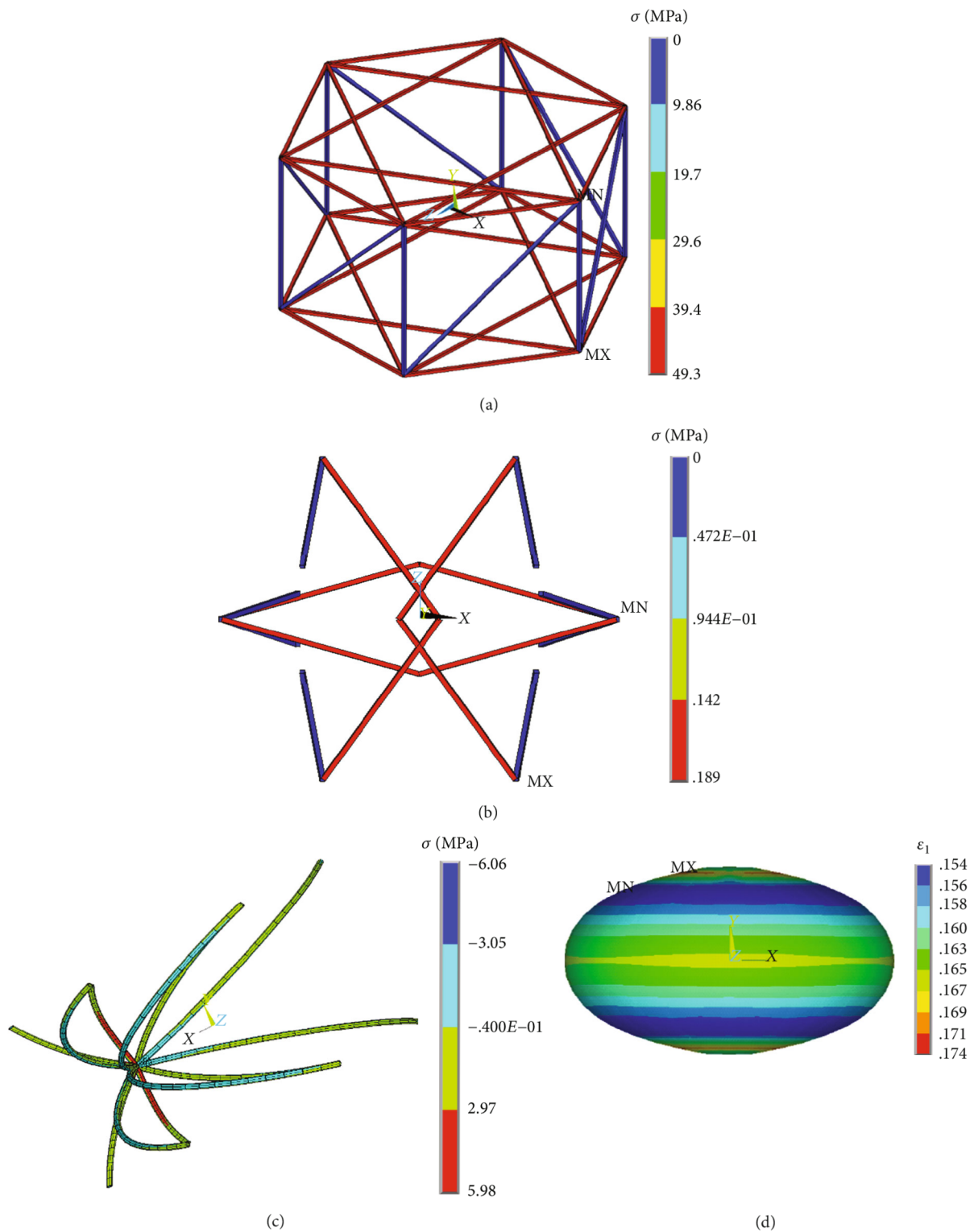


FIGURE 9: Simulation results of 50% cell compression: stresses in (a) AFs (isometric view), (b) IFs (top view), and (c) MTs (isometric view); (d) distribution of first principal (logarithmic) strain in the nucleus.

The nucleus appears elongated in the transversal plane perpendicular to the loading direction, analogous to that observed in experiments [47]. The maximum first principal strain in the nucleus (see Figure 9(d)) was chosen as the quantitative characterization of nucleus deformation which

is hypothesized to be decisive for transducing mechanical signals into changes in gene expression [54, 55].

**3.2. Results for Suspended Cell Tension.** The force-elongation curve calculated from the tensile test simulation is in good

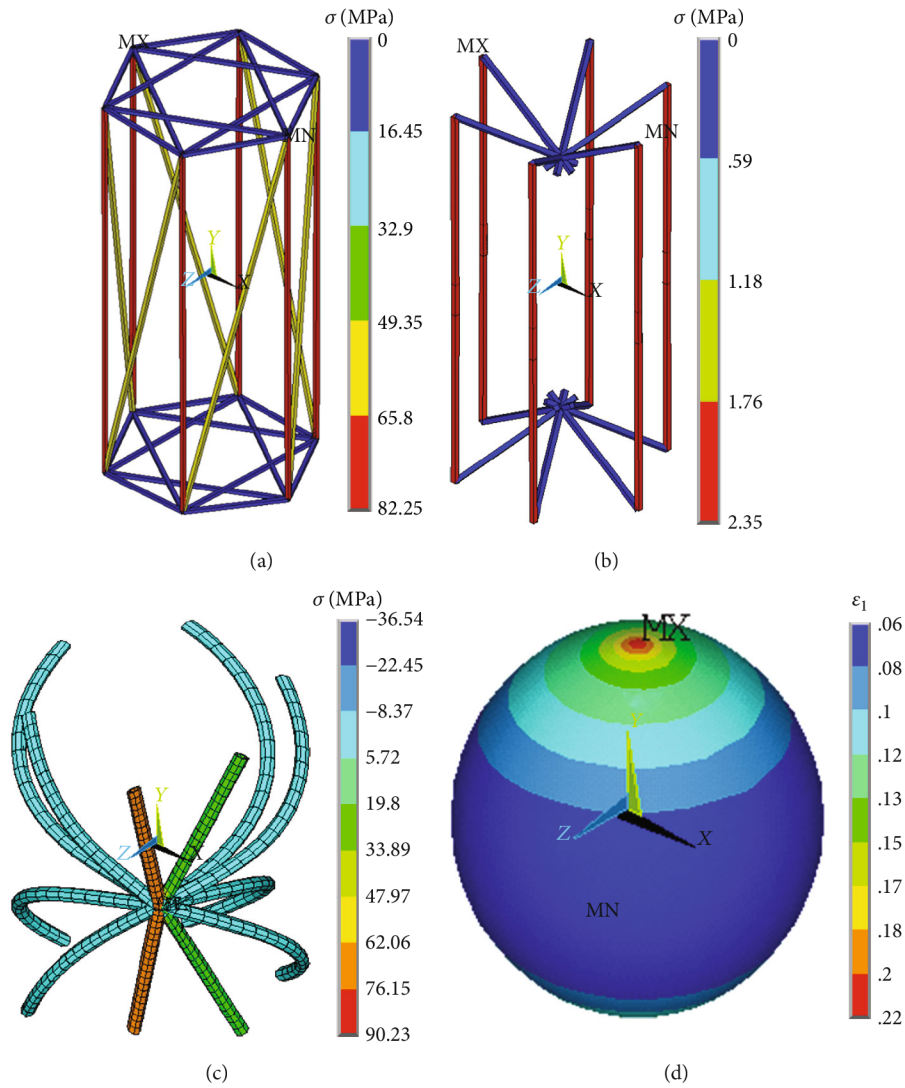


FIGURE 10: Simulation results of 50% elongation of a suspended cell: axial stress distribution in (a) AFs, (b) IFs, and (c) MTs; (d) distribution of first principal (logarithmic) strain in the nucleus.

agreement with the experimental response, as illustrated in Figure 7 where the experimental results are also in their normalized form as described in Section 3.1.

The stiffness of the hybrid model of a suspended cell in tension was evaluated as secant modulus  $\sigma/\epsilon$  of the resulting curve recalculated into conventional stress ( $\sigma$ ) and conventional strain ( $\epsilon$ ). The conventional stress is given as:

$$\sigma = \frac{f}{a}, \quad (5)$$

where  $f = 0.0765 \mu\text{N}$  is the reaction force at maximum deformation of the cell, and  $a = 42.9866 \mu\text{m}^2$  is the (maximal undeformed) cross-sectional area of the cell. With reference to Figure 7, the modulus of 3.17 kPa calculated for the FE model ( $D = 7.4 \mu\text{m}$ ) is in concordance with the modulus of  $2.6 \pm 0.7 \text{ kPa}$  calculated for the experiments [49]. The cell stiffness increases with load in accordance with [19, 56], and the proposed model can predict the contribution of spe-

cific cytoskeletal components to the cell stiffness. The randomly oriented AFs tend to be aligned in the loading direction and to show high stresses as represented in Figure 10(a), which increases the overall reaction force of the cell. Also some MTs are merely straightened out while some others remain bended as shown in Figure 10(c). IFs aligned in the direction of the load are straightened and exhibit significant stresses while zero stress occurs in the others which remain wavy (see Figure 10(b)). The maximum first principal strain in the nucleus (see Figure 10(d)) is also presented as the quantitative characterization of nucleus deformation.

**3.3. Results for Adherent Cell Compression.** The simulated force-deformation curve is in good agreement with the experimental responses obtained from the compression test of endothelial cells cultured on a rigid substrate [47], including their strain stiffening, as represented in Figure 8. The distribution of the first and third principal strains in the nucleus

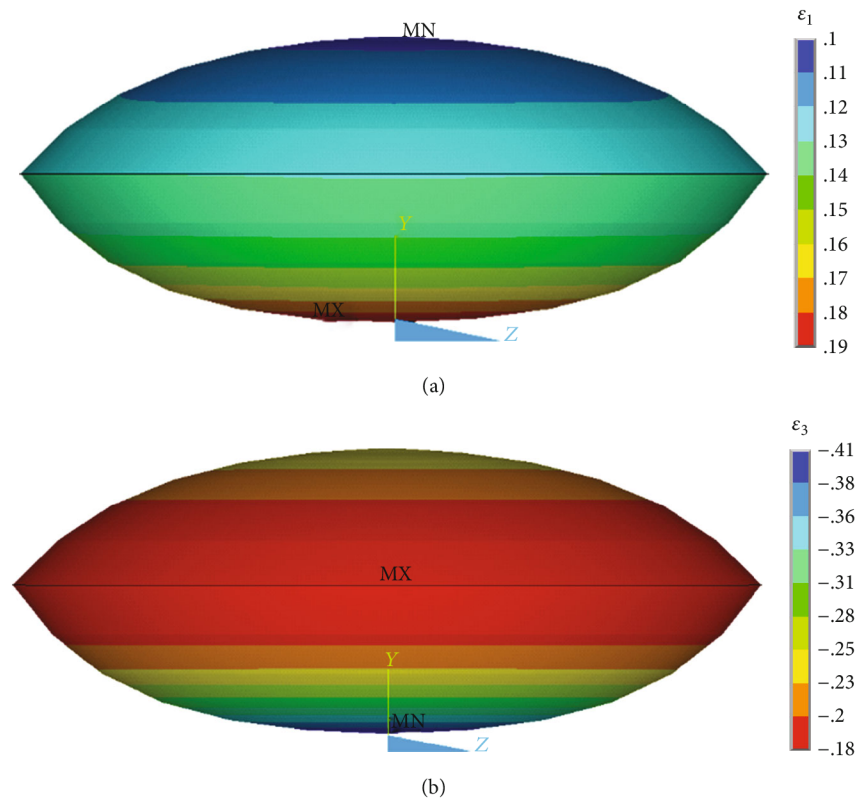


FIGURE 11: Distribution of (a) the first and (b) third (maximal negative) principal (logarithmic) strains in the nucleus of an adherent endothelial cell under 50% compression.

is represented in Figure 11. The reason for showing also the third principal strain is that in compression its absolute value is higher than that of the first principal strain, and thus it might be decisive for mechanotransduction under these conditions.

**3.4. Results for Compression of Flat Cell Model.** The stiffness of the flat model (see Figure 8) is several times higher than that of the adherent model or of the spread cells obtained experimentally [47]. The reason is the different shape of the model (very short hexagonal prism) when the shape cannot change so much and the impact of volume incompressibility is much higher. Distribution of the first and third principal strains in the nucleus of the flat endothelial cell model under compression is shown in Figure 12.

**3.5. Results for Shear of Flat Cell Model.** Total reaction force calculated as the sum of reactions in nodes of the top hexagonal plane was  $F_S = 759$  pN. As the area of the regular hexagon is  $A_H = 405.95 \mu\text{m}^2$  (with a side length of  $12.5 \mu\text{m}$ ), the resultant shear stress is  $\tau = F_S/A_H = 1.87$  Pa, which is within the physiological range of wall shear stress in arteries. The same results were obtained with the corresponding force-controlled load of the model. The maximum first principal strain in the nucleus was about 0.039, and its distribution is presented in Figure 13(a). When the same forces were applied in the nodes of the top surface of the dome model, the maximum first principal strain in the nucleus was about 0.029 (see Figure 13(b)), i.e., some 26% lower. This difference

shows that the local differences in thickness [14, 35] captured by the dome model may be significant, and the dome shape of the endothelial cell model should be preferred to its flat shape.

The maximum shear strain (in  $xy$  plane in which the shear stress is acting) within the whole cell occurs in the cytoplasm above the nucleus; it is 0.50 for the flat model and 0.40 for the dome model (see Figure 14). In contrast, the nucleus undergoes much lower strains as it is 10 times stiffer than the cytoplasm and the shear deformation is concentrated in the cytoplasm above and below the nucleus. Evidently, the transmission of strain to the nucleus is much lower in shear than under the other loading conditions, probably due to a lower role of cytoplasm incompressibility in shear.

**3.6. Contribution of Cytoskeleton to Cell Stiffness.** The role of each cytoskeletal component in cell stiffness was investigated via removal of this component from the hybrid model as illustrated in Figures 15 and 16 comparing the stiffness of the modified models, i.e., the total reaction force under the same (maximum) deformation. The results in Figure 15(a) show that the stiffness of the spherical model in compression decreases by some 32% when all the cytoskeleton components are removed; the contribution of AFs to the stiffness appears to be the highest: compared to the reaction force of the hybrid model, removal of AFs reduced the reaction force of the cell model by 20%. This rather counterintuitive result relates to volume incompressibility of the cytoplasm and a

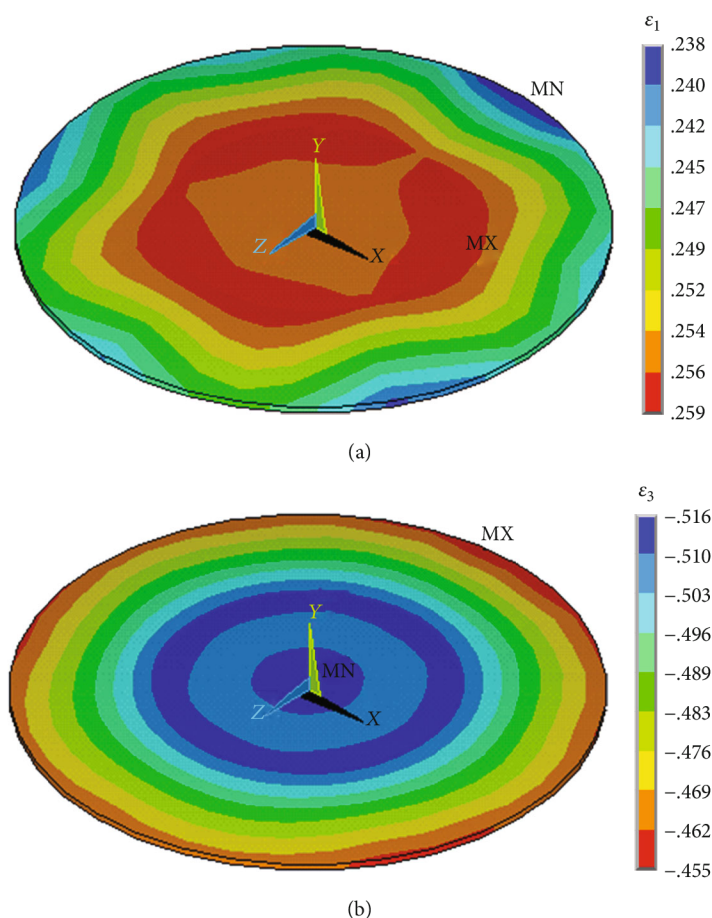


FIGURE 12: Distribution of (a) the first and (b) third (maximal negative) principal (logarithmic) strains in the nucleus of the flat endothelial cell model under 50% compression (isometric view).

consequent increase in lateral dimensions of the cell under compression.

In simulations of the tensile test of the spherical model, the maximum reaction force of the cell model without a cytoskeleton was 66% lower than that for the hybrid model (see Figure 15(b)), and both AFs and MTs played a vital role in this decrease.

Investigation done with adherent and flat cell models under compression brought results qualitatively similar to those with the spherical model under compression, as illustrated in Figure 16.

#### 4. Discussion

A new hybrid FE model of endothelial cells was exploited for simulations of mechanical responses of cells with different shapes and under different types of loads. It was validated by comparison of the calculated responses with experiments done with suspended endothelial cells in tension and compression, and with a compression test of an adherent cell. The same concept, topology, structure arrangement, and material properties were used in the flat and dome models of the hexagonal endothelial cell, which correspond more or less to its common shape within the vascular endothelium layer. These models were used to simulate the cell response

under compression and shear, representing types of loads typical for “*in vivo*” endothelial cells. While shear load is induced directly by the blood flow as captured by the presented models, compression (in radial direction) represents an approximate equivalent of biaxial tension. However, this holds accurately only for homogeneous, isotropic, and incompressible materials; thus, biaxial tension (in circumferential and axial directions) should be preferred in the future, corresponding to the real load of the endothelial cells in the arterial wall.

In addition to the realistic simulation of experiments, the proposed model can predict stress/strain distribution within the specific cell components under different types of loads, as well as the impact of individual cytoskeletal components on the cell response. Thus, it surpasses not only all continuum models of cells [18–23] but also the tensegrity models envisioning the AFs as tension supporting cables and MTs as compression supporting struts [8]. Although these models explain successfully several observations in cell mechanics [43], they neither take into account the influence of flexural behaviour of MTs nor predict the impact of individual cytoskeletal components nor mimic the load transmission onto the nucleus. Moreover, the excessive compression stiffness of the struts introduces nonrealistic artefacts in mechanical responses, as shown in [27, 57]. The cell model based on

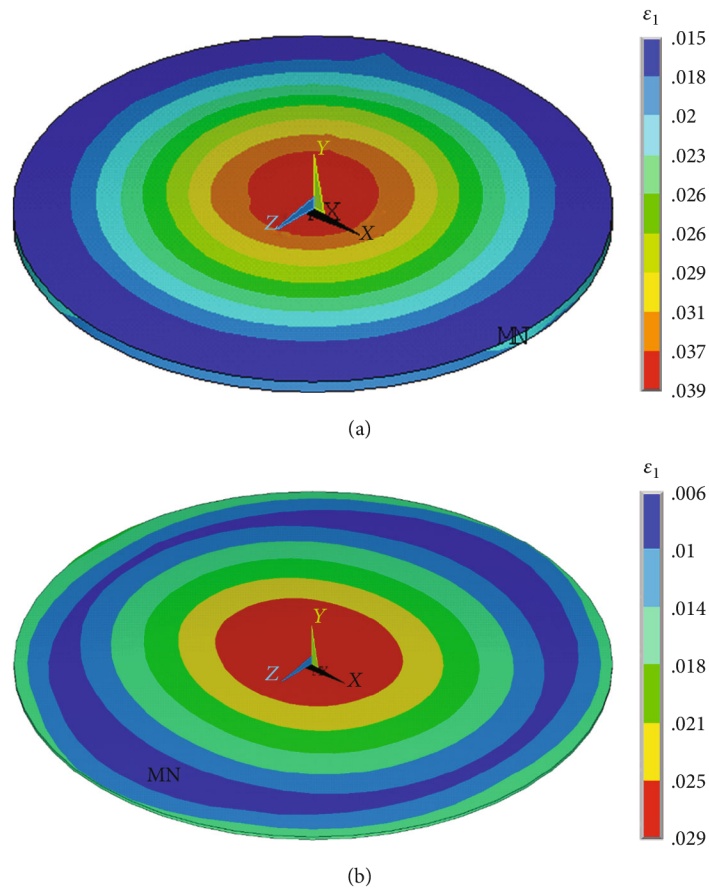


FIGURE 13: Distribution of first principal strain in the nucleus of flat- (a) and dome-shaped (b) endothelial cell models under 1.87 Pa shear stress.

the bendotensegrity concept was proposed in [30] for smooth vascular cells, but to the best knowledge of the authors, such models have not been used for endothelial cells till now. The published models of endothelial cells are mostly much simpler [4], and the role of the cytoskeleton is seldom investigated in existing literature. The recent study in cell mechanics simulated the mechanical behaviour of a cell with an oversimplified tensegrity structure, and the role of individual filaments was not accessed [44, 58]. However, there are studies analysing the role of the cytoskeleton in cell mechanics [30, 59]. Moreover, some published FE models on cell mechanics deal with the degradation of the cytoskeleton using more simplified cytoskeletal arrangements [60].

Among the cell components, the nucleus plays a vital role in mechanotransduction; thus, its deformation, described locally by strain tensor, may be decisive in the initiation of the cell's biochemical response to mechanical load. Within the strain tensor, we hypothesize that the component with the highest absolute value (either first principal strain  $\epsilon_1$  or third principal strain  $\epsilon_3$  if its absolute value exceeds  $\epsilon_1$ ) is decisive. Therefore, these strain components are preferentially evaluated. Naturally, for confirmation of this hypothesis, challenging comprehensive mechanical-biological studies are needed.

In contrast to stress, more frequently used in mechanics, the advantage of our choice of strain as the decisive quantity

is its much lower dependence on material properties. Constitutive models of materials represent an important limitation of any computational cell model due to lack and large dispersion of experimental data concerning individual cell components, and the consequent simplification of their responses via Hookean (linear elastic) or neo-Hookean (simplest hyperelastic) models.

Our model gave maximal  $\epsilon_1$  values of 0.18 and 0.22 under 50% global deformation in compression and tension of a suspended cell, respectively, 0.19 in an adherent endothelial cell under 50% compression, 0.25 in a flat endothelial cell under 50% compression, and 0.039 and 0.029 in flat and domed endothelial cells under a physiological magnitude shear load, respectively. All these values are logarithmic (natural) strains. It is well established that cells respond to mechanical stimuli in a variety of ways that range from changes in cell morphology to activation of biochemical responses [61], which may affect the cell phenotype. Based on the proposed model, the amount of nucleus deformation could enable the researcher to compare mechanobiological responses under different mechanical stimuli.

The simulations realized with the created models give mechanical responses in accordance with experiments under different types of loads and enable a deeper analysis of the role of individual cytoskeletal components in cell stiffness.

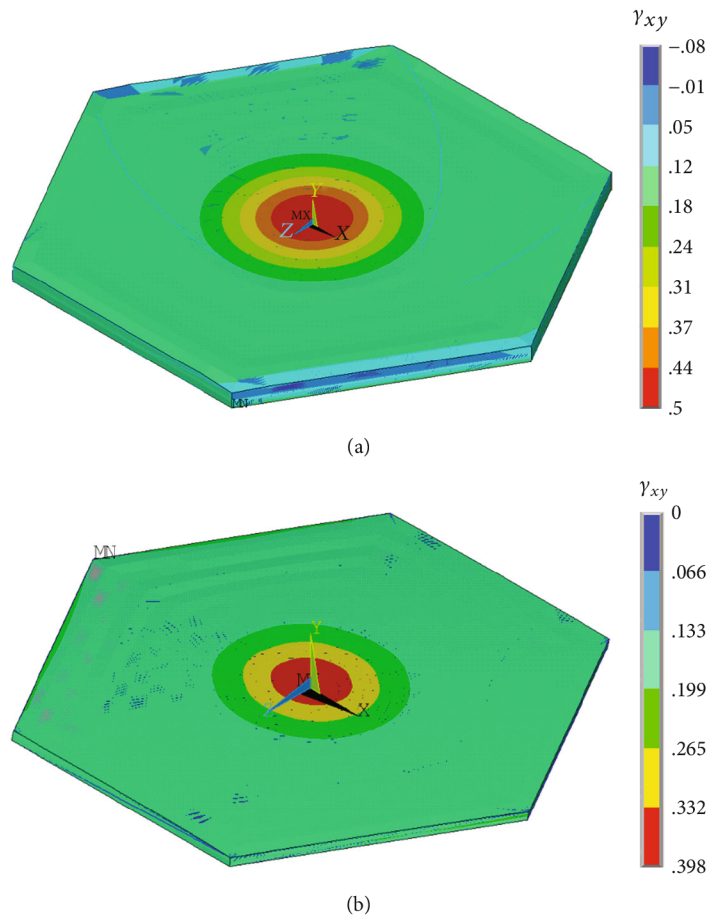


FIGURE 14: Distribution of shear strain in the cytoplasm of the flat- (a) and dome-shaped (b) models of endothelial cells under 1.87 Pa shear stress.

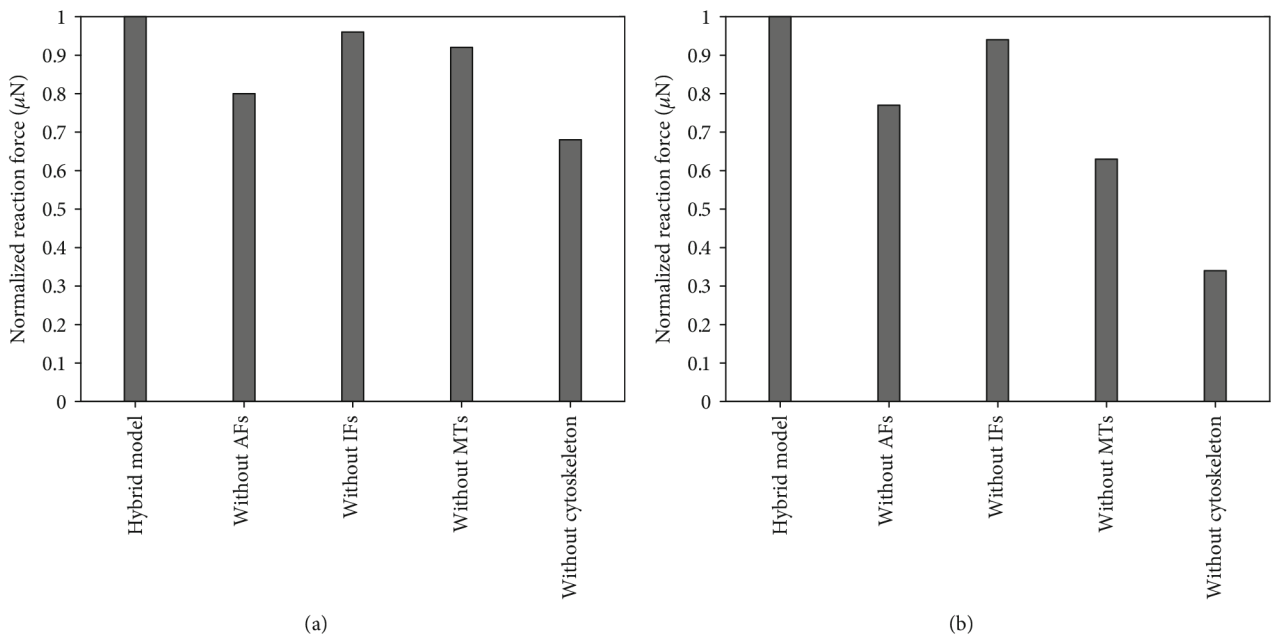


FIGURE 15: Contribution of cytoskeletal components in a spherical cell model to its stiffness (a) in compression and (b) in tension. The reaction force is normalized to 1 with respect to that from the hybrid model.

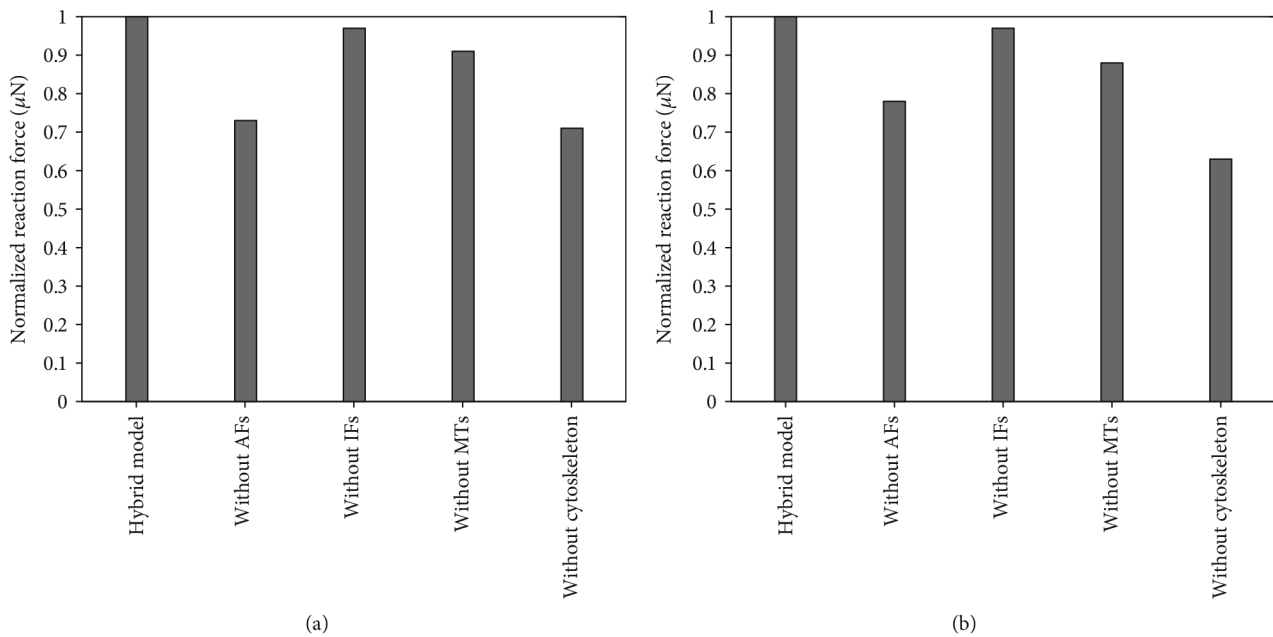


FIGURE 16: Contribution of cytoskeletal components in cell models to their stiffness in compression: (a) adherent model; (b) flat model. The reaction force is normalized to 1 with respect to that from hybrid model.

It was shown that, in any shape of the cell and under any type of load, the prestressed AFs are most significant for the cell stiffness; for instance, simulations of tension and compression tests with a spherical (suspended) cell model demonstrated that removal of AFs reduced the cell stiffness by approximately 23% and 20%, respectively. This modification of the model corresponds to cell treatment with cytochalasin D that results in disruption of not only the deep actin fibres but also of the actin meshwork beneath the CM [11]. The role of the other components is less pronounced; the initially wavy IFs contribute to cell stiffening with increasing load due to their reorientation and straightening, thus contributing to the nonlinear cell response. A similar effect occurs with the bended MTs when some of them become straight under load. This is the case specifically under high tension (see Figure 15(b)). Although the proposed models have advantages over the previous models, they have more limitations than those mentioned above. The structural arrangement of cytoskeletal components does not capture their true complexity and dynamic behaviour as observed in living cells. These models also do not take into consideration the viscoelastic nature of cells. Thus, they cannot predict very fast responses of the cell in which the viscoelastic nature of the cytoplasm (and possibly also of other components) becomes significant. Due to their passive nature, none of these models can capture active responses of the cell such as remodelling of AFs and MTs exhibited with respect to mechanical loading when the cytoskeletal fibres undergo polymerisation and depolymerisation. However, this remodelling occurs in time periods much longer than the duration of the considered experiments; thus, they cannot be captured either by the experimental responses.

As concerns the cell shape, within the arterial wall the endothelial cells are elongated in the direction of blood flow

while we have considered a regular hexagon for idealization. However, the differences cannot be pronounced and the shape can be easily changed if the presented flat and dome models are applied in the future for investigation of adhesion between the cells and of possible disruption of the endothelial monolayer.

**4.1. Limitations of the Model.** Although our model considers the basic nonlinear feature of filaments, i.e., prestress in AFs and prestrain (waviness) of IFs, it cannot consider their strain stiffening [62] due to software limitations. However, within the range of some 10% strain occurring in the simulations, this nonlinearity is not significant, and the linear elastic models of the cytoskeletal components are fully acceptable. Neither a possible rearrangement of the cytoskeleton as a consequence of the load acting on the cell during its testing was considered because the time needed for it is longer than the typical time of an experiment (e.g., 5 up to 10 minutes for rearrangement of microtubules); therefore, these processes cannot manifest during this time. Also, the nonlinear behaviour of integrin in focal adhesions [63] is not considered because focal adhesions are represented only by the nodes of the bendotensegrity structure in our model. Although the number of cytoskeletal elements is significantly lower than in a real cell, it was shown that this number is not decisive for the quality of the model [27, 30, 43, 57], and the authors do not know of any discrete model having the number of elements comparable with reality.

## 5. Conclusion

The FE bendotensegrity models of endothelial cells with different shapes were used for simulations of different mechanical loading conditions. Some of them were validated using

experimental results in the literature. The model with the shape corresponding to real cell geometry within an arterial wall was loaded by loads corresponding to those induced by a physiological blood flow. In the investigated models, the impact of different loads on individual cell components was evaluated and the role of individual cytoskeleton components was assessed. It was shown that in cell stiffness, the AFs play the dominating role, with a significant contribution of MTs under high tensile loads. Principal strains in the nucleus are hypothesized as quantities decisive for mechanotransduction, and the presented models enable comparing them under different loading conditions. In the future, the model can be expanded to a cell population in the endothelium layer and combined with corresponding biological experiments quantifying the biological response of the cells. Thus, we could investigate the impact of different loading conditions in the arterial wall on remodelling or disruption of the endothelium layer which is decisive in the initial phase of atherosclerosis.

### Data Availability

The data sets generated and analysed during the current study are available from the corresponding author upon request.

### Conflicts of Interest

The authors declare that there is no conflict of interests regarding the publication of this paper.

### Acknowledgments

This work was supported by Czech Science Foundation, project No. 18-13663S.

### References

- [1] R. Ross, "Atherosclerosis: an inflammatory disease," *The New England Journal of Medicine*, vol. 340, no. 2, pp. 115–126, 1999.
- [2] A. Comerford, *Computational models of endothelial and nucleotide function*, Doctoral thesis, University of Canterbury, New Zealand, 2007.
- [3] B. Sumpio, J. Timothy Riley, and A. Dardik, "Cells in focus: endothelial cell," *The International Journal of Biochemistry & Cell Biology*, vol. 34, no. 12, pp. 1508–1512, 2002.
- [4] A. Nieto, J. Escribano, F. Spill, J. M. Garcia-Aznar, M. J. Gomez-Benito, and M. J. Gomez-Benito, "Finite element simulation of the structural integrity of endothelial cell monolayers: a step for tumor cell extravasation," *Engineering Fracture Mechanics*, vol. 224, article 106718, 2020.
- [5] R. D. Oea and J. R. King, "Continuum limits of pattern formation in hexagonal-cell monolayers," *Journal of Mathematical Biology*, vol. 64, no. 3, pp. 579–610, 2012.
- [6] M. Ye, H. M. Sanchez, M. Hultz et al., "Brain microvascular endothelial cells resist elongation due to curvature and shear stress," *Scientific Reports*, vol. 4, p. 4681, 2015.
- [7] R. Lebiš, "Computational modelling of mechanical behaviour of the cell," PhD thesis, Mechanical Engineering, Brno University of Technology, Faculty of Mechanical Engineering, Czech Republic, Brno, 2007.
- [8] D. Ingber, "Cellular tensegrity: defining new rules of biological design that govern the cytoskeleton," *Journal of Cell Science*, vol. 104, pp. 613–627, 1993.
- [9] H. Huang, C. Dai, H. Shen et al., "Recent advances on the model, measurement technique, and application of single cell mechanics," *International Journal of Molecular Sciences*, vol. 21, no. 17, p. 6248, 2020.
- [10] K. Nagayama, Y. Nagano, M. Sato, and T. Matsumoto, "Effect of actin filament distribution on tensile properties of smooth muscle cells obtained from rat thoracic aortas," *Journal of Biomechanics*, vol. 39, no. 2, pp. 293–301, 2006.
- [11] Y. Ujihara, M. Nakamura, H. Miyazaki, and S. Wada, "Contribution of actin filaments to the global compressive properties of fibroblasts," *Journal of the Mechanical Behaviour of Biomedical Materials*, vol. 14, pp. 192–198, 2012.
- [12] B. V. Nguyen, Q. Wang, N. J. Kuiper, A. J. HajEl, C. R. Thomas, and Z. Zhang, "Strain-dependent viscoelastic behaviour and rupture force of single chondrocytes and chondrons under compression," *Biotechnology Letters*, vol. 31, no. 6, pp. 803–809, 2009.
- [13] A. Pillarisetti, J. Desai, H. Ladjal, A. Schiffmacher, A. Ferreira, and C. Keefer, "Mechanical phenotyping of mouse embryonic stem cells: increase in stiffness with differentiation," *Cellular Reprogramming*, vol. 13, no. 4, pp. 371–380, 2011.
- [14] M. Kelsey and M. K. G. Stroka, "Vascular endothelial cell mechanosensing: new insights gained from biomimetic microfluidic models," *Seminars in Cell & Developmental Biology*, vol. 71, pp. 106–117, 2017.
- [15] L. Kirill, N. Yasaman, and S. Menglin, "Probing eukaryotic cell mechanics via mesoscopic simulations," *PLoS Computational Biology*, vol. 13, pp. 1–22, 2017.
- [16] R. Daza, B. González-Bermúdez, J. Cruces et al., "Comparison of cell mechanical measurements provided by Atomic Force Microscopy (AFM) and Micropipette Aspiration (MPA)," *Journal of the mechanical behavior of biomedical materials*, vol. 95, pp. 103–115, 2019.
- [17] A. Mohammadkarim, M. Mokhtari-Dizaji, A. Kazemian et al., "The mechanical characteristics of human endothelial cells in response to single ionizing radiation doses by using micropipette aspiration technique," *Molecular & Cellular Biomechanics*, vol. 16, no. 4, pp. 275–287, 2019.
- [18] S. Barreto, C. Clausen, C. Perrault, D. Fletcher, and D. Lacroix, "A multi-structural single cell model of force-induced interactions of cytoskeletal components," *Biomaterials*, vol. 34, no. 26, pp. 6119–6126, 2013.
- [19] Y. Ujihara, M. Nakamura, H. Miyazaki, and S. Wada, "Proposed spring network cell model based on a minimum energy concept," *Annals of Biomedical Engineering*, vol. 38, no. 4, pp. 1530–1538, 2010.
- [20] B. Maurin, P. Canadas, H. Baudriller, P. Montcourrier, and N. Bettache, "Mechanical model of cytoskeleton structuration during cell adhesion and spreading," *Journal of Biomechanics*, vol. 41, no. 9, pp. 2036–2041, 2008.
- [21] V. S. Deshpande, R. M. McMeeking, and A. G. Evans, "A biochemo-mechanical model for cell contractility," *Proceedings of national academy of science of the U.S.A.*, vol. 3, no. 38, pp. 14015–14020, 2006.
- [22] R. de, A. Zemel, and S. Safran, "Dynamics of cell orientation," *Nature Physics*, vol. 3, no. 9, pp. 655–659, 2007.



- [23] R. Kaunas and H. J. Hsu, "A kinematic model of stretch-induced stress fiber turnover and reorientation," *Journal of Theoretical Biology*, vol. 257, no. 2, pp. 320–330, 2009.
- [24] T. Shen, B. Shirinzadeh, Y. Zhong, J. Smith, J. Pinski, and M. Ghafarian, "Sensing and modelling mechanical response in large deformation indentation of adherent cell using atomic force microscopy," *Sensors*, vol. 20, no. 6, p. 1764, 2020.
- [25] D. Kardas, U. Nackenhorst, and D. Balzani, "Computational model for the cell-mechanical response of the osteocyte cytoskeleton based on self-stabilizing tensegrity structures," *Bio-mechanics and Modelling in Mechanobiology*, vol. 12, no. 1, pp. 167–183, 2013.
- [26] A. Alippi, A. Bettucci, and A. Biagioni, "Nonlinear behaviour of cell tensegrity models," *AIP Conference Proceedings*, vol. 1433, pp. 329–332, 2012.
- [27] J. Bursa, R. Lebis, and J. Holata, "Tensegrity finite element models of mechanical tests of individual cells," *Technology and Health Care*, vol. 20, no. 2, pp. 135–150, 2012.
- [28] M. Mehrbod and R. Mofrad, "On the significance of microtubule flexural behavior in cytoskeletal mechanics," *PLoS One*, vol. 6, no. 10, article e25627, 2011.
- [29] Y. D. Bansod, *Computational simulation of mechanical tests of isolated animal cells*, Doctoral Thesis, Brno University of Technology, 2016, available from:.
- [30] Y. D. Bansod, T. Matsumoto, K. Nagayama, and J. Bursa, "A finite element bendo-tensegrity model of eukaryotic cell," *Journal of Biomechanical Engineering*, vol. 140, no. 10, 2018.
- [31] R. Rand, "Mechanical properties of the red cell membrane: II. Viscoelastic breakdown of the membrane," *Biophysical Journal*, vol. 4, no. 4, pp. 303–316, 1964.
- [32] B. J. Bachmann, C. Giampietro, A. Bayram et al., "Honeycomb-structured metasurfaces for the adaptive nesting of endothelial cells under hemodynamic loads," *Biomaterials science*, vol. 6, no. 10, pp. 2726–2737, 2018.
- [33] A. Pries, T. Secomb, and P. Gaehtgens, "The endothelial surface layer," *Pflügers Archiv-European Journal of Physiology*, vol. 440, no. 5, pp. 653–666, 2000.
- [34] M. Feletou, *The Endothelium: Part 1: Multiple Functions of the Endothelial Cells-Focus on Endothelium-Derived Vasoactive Mediators*, Morgan & Claypool Life Sciences, San Rafael, 2011.
- [35] M. Carine, "Endothelial cell functions," *Journal of Cellular Physiology*, vol. 196, pp. 430–443, 2003.
- [36] D. Ingber, "Tensegrity I. cell structure and hierarchical systems biology," *Journal of cell science*, vol. 116, no. 7, pp. 1157–1173, 2003.
- [37] D. Ingber, S. Heidemann, P. Lamoureux, and R. Buxbaum, "Opposing views on tensegrity as a structural framework for understanding cell mechanics," *The American Physiological Society*, vol. 89, pp. 1663–1678, 2000.
- [38] P. Janmey, U. Euteneuer, P. Traub, and M. Schliwa, "Viscoelastic properties of vimentin compared with other filamentous biopolymer networks," *The Journal of Cell Biology*, vol. 113, no. 1, pp. 155–160, 1991.
- [39] N. Wang and D. Stamenović, "Contribution of intermediate filaments to cell stiffness, stiffening, and growth," *American Journal of Physiology-Cell Physiology*, vol. 279, no. 1, pp. C188–C194, 2000.
- [40] D. Stamenovic and N. Wang, "Invited review. Engineering approaches to cytoskeletal mechanics," *Journal of Applied Physiology*, vol. 89, no. 5, pp. 2085–2090, 2000.
- [41] S. Deguchi, T. Ohashi, and M. Sato, "Evaluation of tension in actin bundle of endothelial cells based on preexisting strain and tensile properties measurements," *Molecular & Cellular Biomechanics*, vol. 2, no. 3, pp. 125–133, 2005.
- [42] H. Kojima, A. Ishijima, and T. Yanagida, "Direct measurement of stiffness of single actin filaments with and without tropomyosin by in vitro nanomanipulation," *Proceedings of the National Academy of Sciences*, vol. 91, no. 26, pp. 12962–12966, 1994.
- [43] Centre for Bioengineering, Department of Mechanical Engineering, Trinity College Dublin, Ireland, J. McGarry, and P. J. Prendergast, "A three-dimensional finite element model of an adherent eukaryotic cell," *eCM*, vol. 7, pp. 27–34, 2004.
- [44] F. Xue, A. B. Lennon, and K. K. Mckayed, "Effect of membrane stiffness and cytoskeletal element density on mechanical stimuli within cells: an analysis of the consequences of ageing in cells," *Computer Methods in Biomechanics and Biomedical Engineering*, vol. 18, pp. 468–476, 2013.
- [45] F. Gittes, B. Mickey, J. Nettleton, and J. Howard, "Flexural rigidity of microtubules and actin filaments measured from thermal fluctuations in shape," *Journal of Cell biology*, vol. 120, no. 4, pp. 923–934, 1993.
- [46] A. Kiyomarsioskouei, M. S. Saidi, and B. Firoozabadi, "An endothelial cell model containing cytoskeletal components: suspension and adherent states," *Journal of Biomedical Science and Engineering*, vol. 5, no. 12, pp. 737–742, 2012.
- [47] N. Caille, O. Thoumine, Y. Tardy, and J. Meister, "Contribution of the nucleus to the mechanical properties of endothelial cells," *Journal of Biomechanics*, vol. 35, no. 2, pp. 177–187, 2002.
- [48] J. Stricker, T. Falzone, and M. Gardel, "Mechanics of the F-actin cytoskeleton," *Journal of Biomechanics*, vol. 43, no. 1, pp. 9–14, 2010.
- [49] S. Deguchi, N. Yano, K. Hashimoto, H. Fukamachi, S. Washio, and K. Tsujioka, "Assessment of the mechanical properties of the nucleus inside a spherical endothelial cell based on micro-tensile testing," *Journal of Mechanics of Materials and Structures*, vol. 2, no. 6, pp. 1087–1102, 2007.
- [50] R. P. Jean, D. S. Gray, A. A. Spector, and C. S. Chen, "Characterization of the nuclear deformation caused by changes in endothelial cell shape," *Journal of Biomechanical Engineering*, vol. 126, no. 5, pp. 552–558, 2004.
- [51] G. Unnikrishnan, U. Unnikrishnan, and J. Reddy, "Constitutive material Modeling of cell: a micromechanics approach," *Journal of Biomechanical Engineering*, vol. 129, no. 3, pp. 315–323, 2007.
- [52] R. P. Jean, C. S. Chen, and A. A. Spector, "Finite-element analysis of the adhesion-cytoskeleton-nucleus mechanotransduction pathway during endothelial cell rounding: axisymmetric model," *Journal of Biomechanical Engineering*, vol. 127, no. 4, pp. 594–600, 2005.
- [53] H. Ghaffari, M. S. Saidi, and B. Firoozabadi, "Biomechanical analysis of actin cytoskeleton function based on a spring network cell model," *Proceedings of the Institution of Mechanical Engineers, Part C: Journal of Mechanical Engineering Science*, vol. 231, 2017.
- [54] N. D. Leipzig and K. A. Athanasiou, "Static compression of single chondrocytes catabolically modifies single-cell gene expression," *Biophysical Journal*, vol. 94, no. 6, pp. 2412–2422, 2008.

- [55] A. C. Shieh and K. A. Athanasiou, "Dynamic compression of single cells," *Osteoarthritis and Cartilage.*, vol. 15, no. 3, pp. 328–334, 2007.
- [56] H. Miyazaki, Y. Hasegawa, and K. Hayashi, "Tensile properties of contractile and synthetic vascular smooth muscle cells," *JSME International Journal Series C*, vol. 45, no. 4, pp. 870–879, 2002.
- [57] J. Bursa, R. Lebis, and P. Janicek, "FE models of stress-strain states in vascular smooth muscle cell," *Technology and Health Care*, vol. 14, no. 4–5, pp. 311–320, 2006.
- [58] W. Lili and C. Weiyi, "Modelling cell origami via a tensegrity model of the cytoskeleton in adherent cells," *Applied Bionics and biomechanics*, vol. 2019, Article ID 8541303, 2019.
- [59] L. Wang, L. Wang, L. Xu, and C. Weiyi, "Finite element modeling of single-cell based on atomic force microscope indentation method," *Computational and Mathematical Methods in Medicine*, vol. 2019, Article ID 7895061, 2019.
- [60] D. Katti and K. Katti, "Cancer cell mechanics with altered cytoskeletal behavior and substrate effects: a 3D finite element modeling study," *Journal of the Mechanical Behavior of Biomedical Materials*, vol. 76, pp. 125–134, 2017.
- [61] M. R. K. Mofrad and R. D. Kamm, *Cytoskeletal mechanics: models and measurements*, Cambridge University Press, 2009.
- [62] J.-F. Nolting, W. Möbius, and S. Köster, "Mechanics of individual keratin bundles in living cells," *Biophysical Journal*, vol. 107, no. 11, pp. 2693–2699, 2014.
- [63] H. Huang, R. D. Kamm, P. T. So, and R. T. Lee, "Receptor-based differences in human aortic smooth muscle cell membrane stiffness," *Hypertension*, vol. 38, no. 5, pp. 1158–1161, 2001.

## Appendix B

**Title:** “Impact of physiological loads of arterial wall on nucleus deformation in endothelial cells: A computational study”

**Authors:** Veera Venkata Satya Varaprasad Jakka, Jiri Bursa

**Journal Name:** Computers in Biology and Medicine

**Impact Factor:** 4.589

### **Citation:**

Veera Venkata Satya Varaprasad Jakka, Jiri Bursa, “Impact of physiological loads of arterial wall on nucleus deformation in endothelial cells: A computational study”, Computers in Biology and Medicine, Volume 143, 2022, 105266, ISSN 0010-4825, <https://doi.org/10.1016/j.combiomed.2022.105266>.



Contents lists available at ScienceDirect

## Computers in Biology and Medicine

journal homepage: [www.elsevier.com/locate/combiomed](http://www.elsevier.com/locate/combiomed)

## Impact of physiological loads of arterial wall on nucleus deformation in endothelial cells: A computational study

Veera Venkata Satya Varaprasad Jakka<sup>\*</sup>, Jiri Bursa

Institute of Solid Mechanics, Mechatronics and Biomechanics (ISMMB), Faculty of Mechanical Engineering (FME), Brno University of Technology (BUT), Technicka 2896/2, 61669, Brno, Czech Republic

## ARTICLE INFO

## Keywords:

Cell mechanics  
Biaxial load  
Finite element model  
Bendo-tensegrity  
Shear load

## ABSTRACT

**Introduction:** Computational modeling can enhance the understanding of cell mechanics. To achieve this, finite element models of endothelial cells were proposed with shapes mimicking their natural state inside the endothelium within the cardiovascular system. Implementing the recently proposed bendo-tensegrity concept, these models consider flexural (buckling) as well as tensional/compressional behavior of microtubules and also incorporate the waviness of intermediate filaments.

**Materials and methods:** Four different models were created (flat and domed hexagons, both regular and elongated in the direction of blood flow) and loaded by biaxial deformation, blood pressure, and shear load from blood flow – natural physiological conditions of the arterial endothelium – aiming to investigate the “in situ” mechanical response of the cell.

**Results:** The impact of individual components of loads on the nucleus deformation (more specifically on the first principal strain) potentially influencing mechanotransduction was investigated and the role of the cytoskeleton and its constituents in the mechanical response of the endothelial cell was assessed. The results show (i) the impact of pulsating blood pressure on cyclic deformations of the nucleus, which increase substantially with decreasing axial pre-stretch of the cell, (ii) the importance of relatively low shear stresses in the cell response and nucleus deformation.

**Conclusion:** Not only the pulsatile blood pressure but also the wall shear stress may induce significant deformation of the nucleus and thus trigger remodeling processes in endothelial cells.

## 1. Introduction

Atherosclerosis-related clinical events are the leading cause of morbidity and mortality worldwide [1]. The inner surface of arteries is covered with a monolayer of flat endothelial cells that play a decisive role in early atherogenesis [2]. It separates the wall tissue from the blood, enabling an exchange of some substances between the two. Infiltration of low-density lipoproteins and inflammatory cells into the wall, which occurs as such substance exchange, is one of the decisive effects in the inception of atheroma, also known as an intimal thickening, and consequent reduction of the blood flow [3]. Mechanical damage of the endothelium is considered to accelerate this infiltration significantly due to pulsating shear stresses induced by the blood flow

and due to stress increase in the arterial wall [4]. At the individual cell level, the biochemical processes related to mechanotransduction are controlled by the cell nucleus which is the reason for studying the mechanical response of endothelial cells with respect to their structural arrangement.

In addition to experimental approaches, recent microstructural computational models help us to evaluate the mechanical response of individual cells, especially the quantities which cannot be measured directly. They enable us to evaluate stresses and strains in individual cell components such as the nucleus or cytoskeletal fibers and can be used to deduce the mechanisms underlying cell responses to various mechanical stimuli [5–13]. To reflect the cell structural arrangement (organelles), multiscale approaches combining the continuum models with

**Abbreviations:** AFs, actin filaments; IFs, intermediate filaments; MTs, microtubules; Bi, biaxial; BiP, biaxial with blood pressure; BiPS, biaxial with blood pressure and shear load; AA, abdominal aorta.

<sup>\*</sup> Corresponding author. Brno University of Technology, Institute of Solid Mechanics, Mechatronics and Biomechanics (ISMMB), Faculty of Mechanical Engineering (FME), Technicka 2896/2, 61669, Brno, Czech Republic.

E-mail address: [207437@vutbr.cz](mailto:207437@vutbr.cz) (V.V.S.V. Jakka).

<https://doi.org/10.1016/j.combiomed.2022.105266>

Received 24 November 2021; Received in revised form 17 January 2022; Accepted 22 January 2022

Available online 24 January 2022

0010-4825/© 2022 Elsevier Ltd. All rights reserved.

microstructural models of cells are needed instead of purely continuum approaches [14].

In microstructural approaches, the cytoskeleton is identified to be a vital component of cell dynamics. The cellular tensegrity model, which mimics the physiological arrangement of the cytoskeleton by an interconnected network of cables in tension representing actin filaments (AFs) and struts in compression representing microtubules (MTs) [15], is one of the most frequently used models in this class. This model has successfully predicted the time-dependent response [16–18] as well as some experimentally observed cell mechanical features like strain hardening [19] or “action at a distance” effect [20].

In contrast to the tensegrity models, which cannot include continuous cell components, the hybrid modeling approach [10] combines discrete and continuous elements in the finite element analysis for a more reliable description of cell mechanical behavior. A cell model including the nucleus, cytoplasm, and cell membrane in its continuous part together with a 210-membered tensegrity structure predicted successfully the cell behavior during tensile and indentation tests [21,22]. However, to reduce the excessive stiffness of straight MTs in the tensegrity model, the model was modified using the bendo-tensegrity concept to capture the curved shape of MTs and their flexural behavior [23]. Additional cables were also included to represent wavy intermediate filaments (IFs) and their role in the stabilization of the nucleus position.

Recently, this hybrid bendo-tensegrity model was used in simulations of endothelial cell response to different loads; the spherical and paraboloidal shapes used for simulations of mechanical “in vitro” tests of individual cells have been validated by experimental results [24]. Referring to the physiological shape of endothelial cells within the arterial endothelium [25,26], structurally and topologically analogical computational models were created as hexagonal prisms with the thickness being either constant (flat model) or higher in the central region (domed model). These models were used in Ref. [24] to simulate the mechanical response of endothelial cells in compression and shear and to investigate the impact of individual components on the overall cell stiffness. In this paper, we use a multilevel approach to simulate the

mechanical response of an endothelial cell that undergoes physiological conditions within the arterial wall and the impact of its individual components on the deformation of the nucleus.

## 2. Materials and Methods

Two types of computational models were created in commercial ANSYS software based on the finite element method. Models of different human arteries with a two-layer wall were created to evaluate biaxial physiological deformations of the endothelium; displacements calculated for a carotid artery were then applied to the hybrid model of a single endothelial cell [24] to simulate its physiological loading conditions. All the simulations are quasi-static, i.e. without any inertial or transient effects, because they are negligible due to the relatively low strain rates in endothelial cells. Also, no remodeling processes commonly observed in cells were considered because they take much more time than the duration of experiments.

### 2.1. Endothelial cell model

Two different geometries of endothelial cell models within an arterial wall were introduced in Ref. [24] based on a flat (with constant cell thickness equal to  $0.5\ \mu\text{m}$  [27]) and domed (with non-constant thickness, tapered from the center to the edges) regular hexagons. However, while the ratio of longitudinal to circumferential dimension of a regular hexagonal cell [27] (see Fig. 2(b)) is 0.87, the “in situ” endothelial cells are irregular, elongated in the direction of blood flow [25]. Therefore, we modified the model geometry to capture the natural shape of endothelial cells in arteries and used the ratio 0.96 in our simulations [28,29].

The model is created by finite elements with quadratic base functions. For all the solved models, the meshes counted between 5 and 18 k elements. When the number of elements increased by a factor of 8, the calculated results changed by 0–4% only. The mesh is kept consistent across all of the four created geometry variants. An automatic load increment estimation minimizes the computation time while ensuring

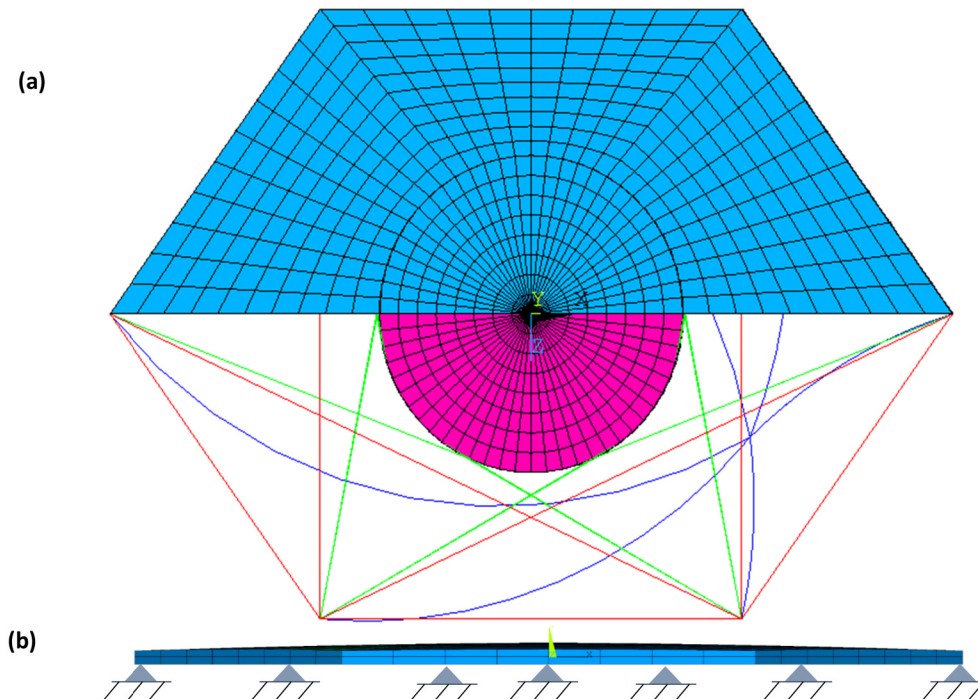


**Fig. 1.** Finite element hybrid model of endothelial cell representing (a) the continuum mesh and the cytoskeletal components of the elongated flat model with AFs (red), IFs (green), and MTs (blue) and (b) the front view of the domed cell model with supports and varying thickness. (For interpretation of the references to colour in this figure legend, the reader is referred to the Web version of this article.)

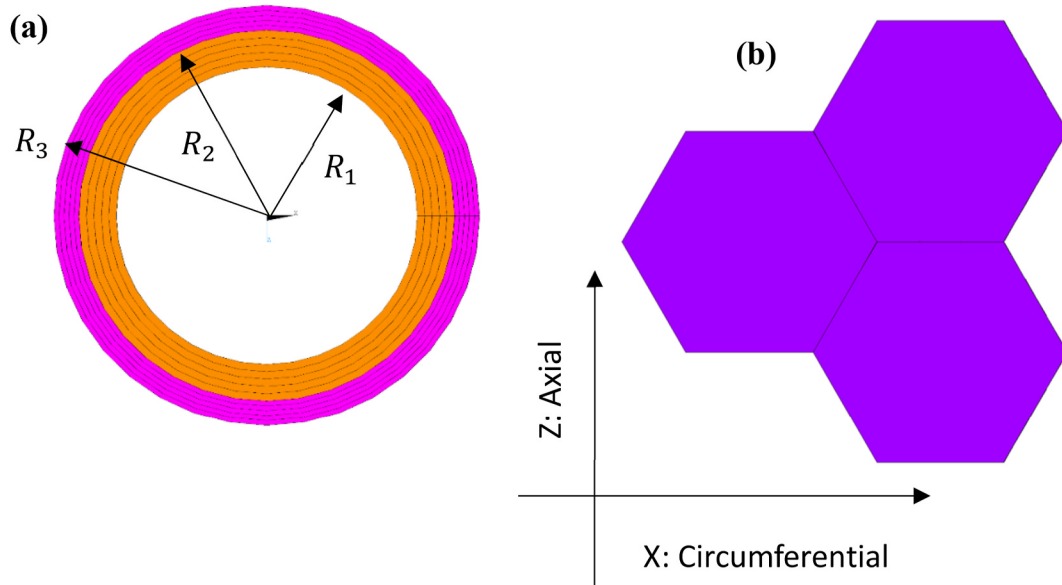


**Fig. 2.** (a) Finite element mesh (in axial view) of the arterial wall model with media (orange) and adventitia (pink) layers. (b) Arrangement of hexagonal endothelial cells on the inner surface of the artery used for transmission of deformation between the artery and cell model. (For interpretation of the references to colour in this figure legend, the reader is referred to the Web version of this article.)

sufficient accuracy of the results. The structure is composed of a continuum part comprising solid elements (nucleus and cytoplasm) and shell elements (cell membrane including actin cortex), and a discrete cytoskeletal part consisting of link elements representing AFs and IFs and beam elements (with additional bending) representing MTs, as shown in Fig. 1. The continuum part is connected to the bend-tensegrity structure by coupled displacements (rotations are not constrained) of each end node of the AFs representing focal adhesions with the closest node of the shell elements (representing the cell membrane). IFs are tangent connections of focal adhesions to the nucleus surface, while the inner ends of all MTs are oriented to a single point in the proximity of the nucleus representing the centrosome (see Fig. 1), which is not fixed to the solid elements of the cytosol. This arrangement mimics the non-affine deformation between cytoskeletal fibers and the cytosol, which corresponds to the rather liquid character of cytosol. We used a neo-Hookean hyper-elastic incompressible constitutive model for the continuum parts, while the discrete elements were linear elastic. All specifications of the discrete and continuous components of the endothelial cell model are summarized in Table 1 and Table 2, respectively.

2.2. Finite element model of the arterial wall

The “in situ” physiological load of an arterial endothelial cell

**Table 1**  
Finite elements used for discrete components of the cell models and their elastic parameters.

Cell component	Parameter				
	Elastic modulus, E (Pa)	Poisson’s ratio, $\nu$	Diameter (nm)	Finite element specification	Nature
Microtubules (MTs) [30]	$1.2 \times 10^9$	0.3	25/17 (outer/inner)	BEAM188	Curved Beams
Actin filaments (AFs) [31]	$2.2 \times 10^9$	0.3	4.5	LINK180	Tension only trusses
Intermediate filaments (IFs) [31]	$2.0 \times 10^9$	0.3	10	LINK180	Tension only trusses

**Table 2**  
Finite elements used for continuous components of the cell models and their hyper-elastic parameters recalculated from literature.

Cell component	Parameter			Finite element specification
	Shear Modulus G (Pa)	Bulk Modulus K (Pa)		
Cytoplasm [32]	$0.17 \times 10^3$	$2.77 \times 10^3$		SOLID 185
Nucleus [32]	$1.7 \times 10^3$	$27.77 \times 10^3$		SOLID 185
Cell membrane [33]	$0.33 \times 10^6$	Infinity		SHELL 181

comprises blood pressure and the corresponding circumferential strain, axial pre-stretch intrinsic for arteries, and shear load from the blood flow [14]. While all the other physiological conditions can be found in literature, the circumferential strain depends, apart from the blood pressure magnitude, on the dimensions and material properties of the arterial wall and its layers. As intima is very thin and mechanically irrelevant in healthy arteries [34], we used only two layers representing media and adventitia of different arteries to calculate circumferential deformations of the endothelium.

The dimensions of media and adventitia (inner  $R_1$ , interface  $R_2$  and outer  $R_3$  radiuses, see Fig. 2(a)) of the chosen arteries are specified in Table 4.

The arterial wall was modeled as axisymmetric with material properties described by a 3rd order ( $N = 3$ ) hyper-elastic incompressible Yeoh model with strain energy potential given as:

$$W = \sum_{i=1}^N C_{i0} (\bar{I}_1 - 3)^i$$

**Table 3**  
Hyper-elastic material properties of arterial layers [34].

Tissue	Material Constants [kPa]		
	$C_{10}$	$C_{20}$	$C_{30}$
Media	122.3	0	337.7
Adventitia	88.7	0	45301.4

**Table 4**

Dimensions of different arteries and circumferential strains on their inner surface (endothelium) under zero axial pre-strain and blood pressure of 20 kPa – a condition typical for older individuals.

Dimension	Artery (location)				
	Middle of the thoracic aorta	Distal AA	Renal artery	Iliac artery	Carotid artery
Inner radius [mm]	11.20	8.25	2.3	4.8	2.83
Wall thickness [mm]	2.05	2.3	1.05	2.00	1.17
Strains [%]	11.9	11.3	7.5	10.28	9.2

where  $\bar{I}_1$  is the 1st invariant of right Cauchy-Green deformation tensor and  $C_{i0}$  are stress-like material parameters. Note that the neo-Hookean model used for continuous cell components is a specific case of a Yeoh model for  $N = 1$ . The material parameters of media and adventitia (according to Ref. [34]) are specified in Table 3.

Boundary conditions in the following simulations are given by blood pressures of 10, 16, 20 kPa corresponding to the diastolic, systolic, and hypertensive values, respectively. Axial pre-strains equal to 0, 0.05, 0.1, 0.2, 0.3 are applied as boundary conditions since they are the typical values for the aorta and are reportedly decreasing with age [35]. In this model, no shear load is applied because its mechanical impact on the rather stiff arterial layers is negligible.

The resulting circumferential strains present at the arterial inner surface (endothelium) for different dimensions of arteries under the combination of loads typical for older individuals (0% axial pre-strain, 20 kPa blood pressure) are presented in Table 4. For an application at the cell level, typical dimensions of common or internal carotid arteries were selected with their values of 2.83 mm, 3.53 mm and 4 mm [36]. The solved combinations of boundary conditions and the resulting circumferential strains present at the inner surface after deformation revealing the whole range of physiological biaxial loads of the endothelial cell are summarized in Table 5.

### 2.3. Boundary conditions of the cell model

The biaxial strains in the endothelium obtained using the artery model (combination of the chosen axial pre-strain and the circumferential strains calculated for the specific blood pressure, see Table 5) were recalculated into axial and circumferential displacements and prescribed in the corners of all the cell models; these boundary conditions are denoted as a variant Bi below. In most of the analyses, where only the final state was investigated, these two strain components were

**Table 5**

Axial and circumferential strains of endothelium used in the formulation of boundary conditions for the individual cell model in the circumferential direction.

Axial pre-strain (%) / Pressure (kPa)	Circumferential strain (%) at a given pressure and axial pre-strain
0/10	4.6
0/16	7.5
0/20	9.2
5/10	2
5/16	5
5/20	6.6
10/10	-0.1
10/16	1.1
10/20	2.49
20/10	-8
20/16	-7.4
20/20	-6.8
30/10	-13
30/16	-12.6
30/20	-12.5

introduced simultaneously. On the contrary, while investigating the dependence of reaction force on the pulsating blood pressure (shown in Fig. 5), the model was initially loaded by axial pre-strain and subsequently by an increasing circumferential strain corresponding to blood pressure between 0 and 20 kPa. The models were gradually loaded on the luminal cell surface with the blood pressure (variant BiP), and with shear load (variant BiPS) corresponding to the physiological shear stress of 1.87 Pa [24,37–39] to be in better accordance with the physiological conditions. The opposite surface was fixed to mimic the “in situ” conditions of the cell attachment to the artery wall by means of the basal membrane (see Fig. 1(b)). This fixation is enabled by a much higher stiffness of the other arterial layers in comparison with the endothelium.

A comprehensive mesh sensitivity analysis was performed in Ref. [24] with the same model geometry and the resulting mesh density was maintained through all the investigated variants.

### 3. Results

All of the four model geometries (flat and domed, regular and elongated hexagons) were analyzed under a variety of biaxial deformations, i.e., with fifteen different combinations of axial and circumferential strains, and in three consecutive load steps: under biaxial extension (Bi), biaxial extension with the addition of blood pressure (BiP), and biaxial extension with blood pressure and shear load (BiPS) acting on the luminal surface thus obtaining 180 solutions in total (for more details refer to Table 6). It is worth mentioning, that the biaxial extension is an application of the circumferential strain calculated using the carotid artery model under the selected blood pressure, thus the addition of the blood pressure on the inner surface itself represents a minor modification only.

Illustrative examples of deformed shapes of the regular flat model in the variant Bi under minimum and maximum distortion are shown in Fig. 3.

Since the nucleus deformation is considered to be the decisive quantity for mechanotransduction [23,40–42], the first principal strain distributions of the nucleus are presented as examples in Fig. 4 and their maximum values for all the solved cell models are summarized in Tables 6 and 7.

The entire force-displacement curves for models loaded with the highest and lowest axial pre-strain (cases 30/20 and 0/20) are shown in Fig. 5. As the circumferential strain calculated based on blood pressure in the artery is applied, the curves represent dependences of reaction forces on blood pressure from 0 up to 20 kPa at a constant axial pre-strain. Therefore, they enable us to evaluate the force pulsations in the endothelial layer.

As there are no experimental measurements for biaxial loading conditions available in the literature for validation of the results, we compared our results for approximately equibiaxial loading conditions with our compression test simulations for flat and adherent endothelial cells published in Ref. [24] and with experimental results for cell compression published in Ref. [32]. It is known that for incompressible materials (product of all the three stretches equals 1), the deformations under equibiaxial tension and uniaxial compression are the same. The out-of-plane engineering strain of the 5/20 model (5% axial and 6.6% circumferential strains, which is nearly equibiaxial deformation) is approximately 11%. This way it was possible to recalculate the simulated curves and plot them as functions of strain in radial (out-of-plane) direction (as shown in Fig. 6). The stiffness in equibiaxial tension is similar to that in uniaxial compression but the behavior is noticeably more non-linear due to higher cell distortion (curved edges occur, see Fig. 3(b)).

Stresses generated in the cytoskeletal components of the most distorted model 30/10 are presented in Fig. 7. It proves that all the stresses in AFs are positive, i.e., the AFs have sufficient pre-strain to keep their loadbearing capacity. In contrast, only a few IFs reach their strain limit to become straight and show non-zero stresses (see Fig. 7(b)), while the

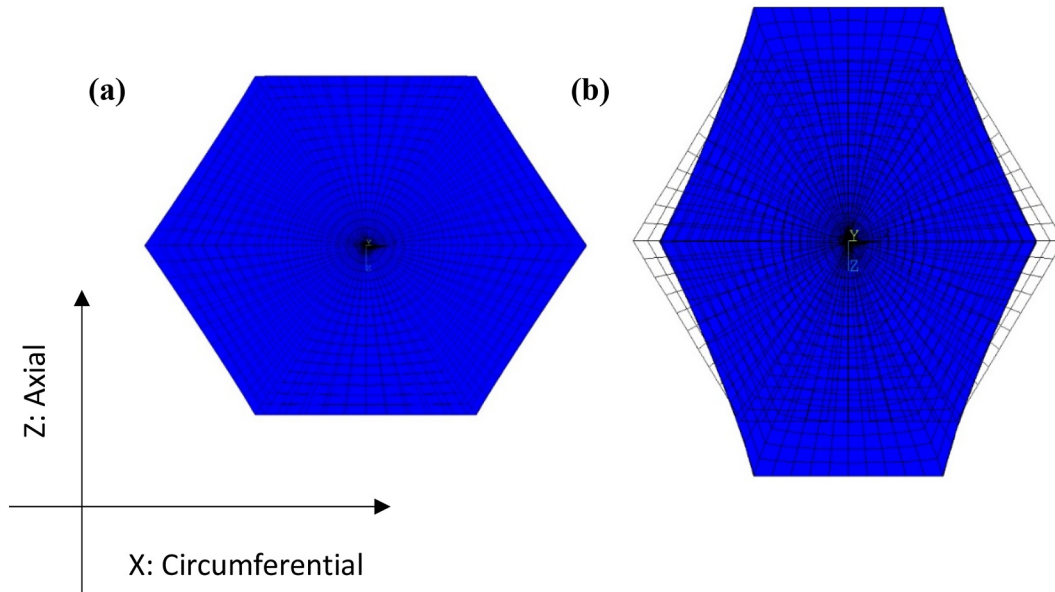


Fig. 3. Examples of the deformed shapes of regular flat endothelial cell model variant Bi under extreme biaxial strains according to Table 5: (a) 0/20 case and (b) 30/10 case.

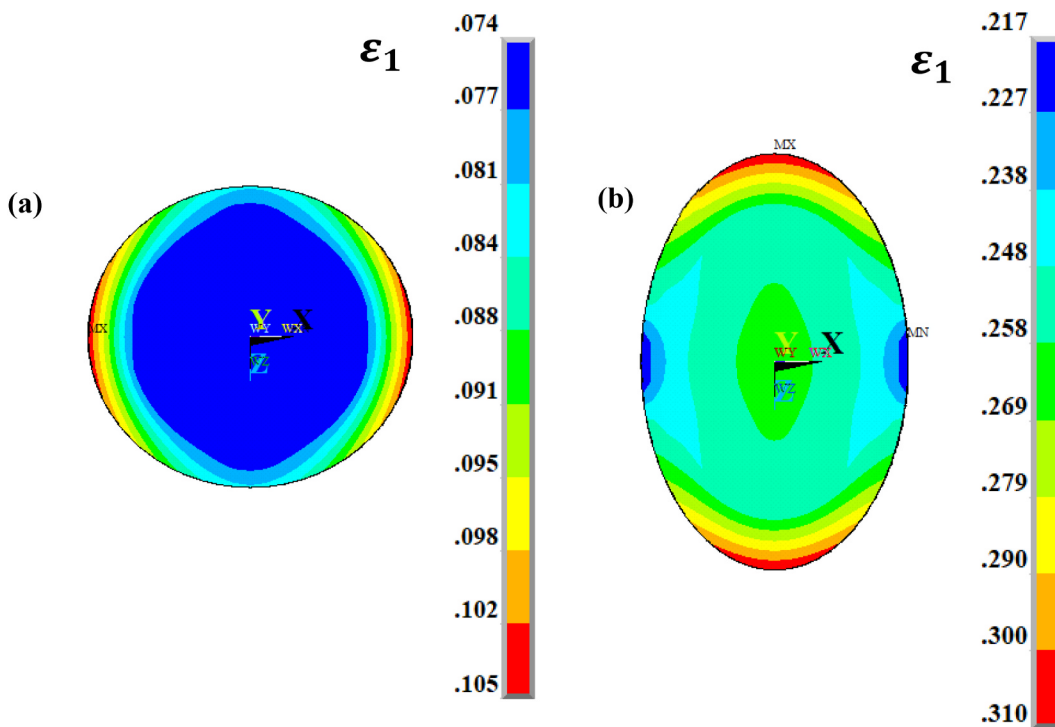


Fig. 4. Examples of the first principal strain distribution ( $\epsilon_1$ ) in the nucleus of a regular flat endothelial cell model variant Bi under minimum and maximum distortion: (a) 0/20 case and (b) 30/10 case.

most elongated MTs become straight (see Fig. 7(c)), which enhances their stiffness and consequently stress by order and they may contribute significantly to the non-linear cell response.

### 3.1. Impact of individual cytoskeletal components

The role of cytoskeletal components is analyzed for the 30/10 (most distorted) and 0/20 loading cases. The normalized axial reaction force under 30/10 and the circumferential reaction force under 0/20 loading conditions (for the full hybrid model and its modifications with some

cytoskeletal components being removed) are displayed in Figs. 8 and 9 respectively.

## 4. Discussion

The bendo-tensegrity-based hybrid model of an endothelial cell proposed and validated in Ref. [24] has been used to simulate the mechanical behavior of an endothelial cell under physiological loading conditions in an artery. The model provides new insights into the cellular mechanical responses, the role of the cytoskeletal components in



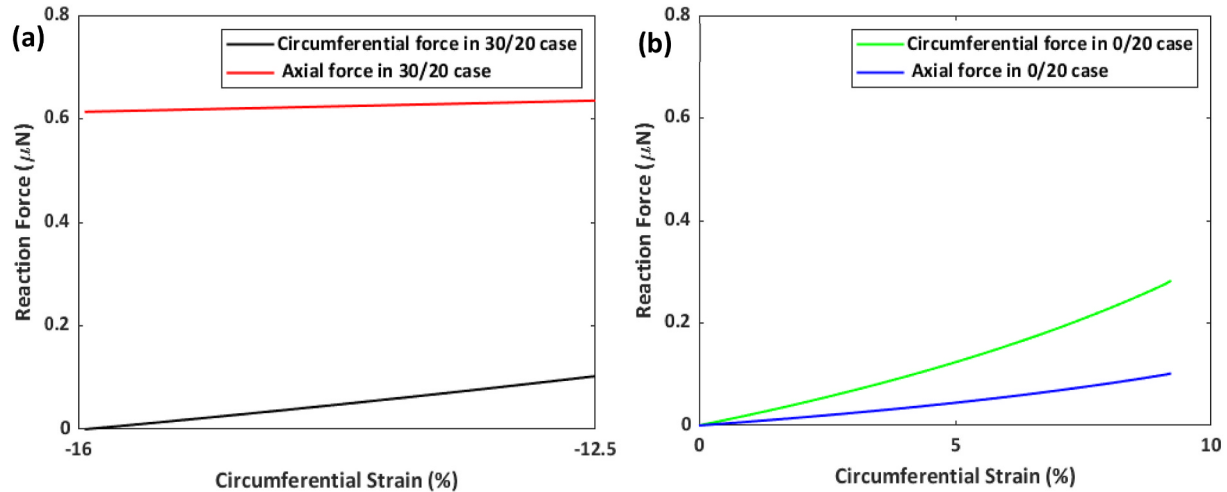


Fig. 5. Simulated dependences of biaxial tension forces (variant Bi) on the increasing blood pressure (between 0 and 20 kPa) recalculated into the circumferential strain of the cell: (a) 30/20 case and (b) 0/20 case.

Table 6

The first principal strains of the nucleus in the calculated cases for regular hexagonal endothelial cell. Pulsations represent the cyclic increase of the first principal strain of the nucleus while the cell undergoes pulsating blood pressure between 10 and 20 kPa.

Model variant	Axial pre-strain [%]	Pressure [kPa]	First principal strain of the nucleus for the regular model variant					
			Flat model			Domed model		
			Bi	BiP	BiPS	Bi	BiP	BiPS
0/10	0	10	0.055	0.060	0.160	0.052	0.048	0.138
0/16	0	16	0.088	0.090	0.175	0.083	0.071	0.148
0/20	0	20	0.107	0.110	0.193	0.101	0.083	0.155
		Pulsations	+0.052	+0.050	+0.033	+0.049	+0.035	+0.017
5/10	5	10	0.067	0.070	0.140	0.064	0.058	0.119
5/16	5	16	0.071	0.070	0.155	0.067	0.057	0.129
5/20	5	20	0.075	0.080	0.167	0.070	0.057	0.129
		Pulsations	+0.008	+0.010	+0.027	+0.006	-0.001	+0.010
10/10	10	10	0.122	0.112	0.136	0.119	0.107	0.130
10/16	10	16	0.121	0.120	0.140	0.121	0.111	0.133
10/20	10	20	0.119	0.124	0.144	0.118	0.111	0.137
		Pulsations	-0.003	+0.012	+0.008	-0.001	+0.004	+0.007
20/10	20	10	0.220	0.197	0.231	0.218	0.187	0.225
20/16	20	16	0.220	0.204	0.230	0.218	0.188	0.225
20/20	20	20	0.221	0.201	0.230	0.218	0.191	0.225
		Pulsations	+0.001	+0.004	-0.001	+0.000	+0.004	+0.000
30/10	30	10	0.31	0.277	0.326	0.308	0.263	0.317
30/16	30	16	0.31	0.279	0.326	0.308	0.264	0.317
30/20	30	20	0.31	0.280	0.326	0.308	0.264	0.317
		Pulsations	+0.000	+0.003	+0.000	+0.000	+0.001	+0.000

cell stiffness, and the nucleus deformation under different loading conditions.

It is well established that cells respond to mechanical stimuli in a variety of ways that range from changes in cell morphology to activation of biochemical responses. The nucleus plays a central role in governing cell responses and it was hypothesized in Refs. [24,40–42] that mechanotransduction might be controlled through the first principal strain ( $\epsilon_1$ ) of the nucleus. Therefore, this quantity was observed in all the 180 investigated cases based on four different geometries of the cell model under different loading configurations (biaxial deformation, biaxial deformation with pressure, and biaxial deformation with pressure and shear load).

Not surprisingly, only small changes in the first principal strain of the nucleus were observed when the model was loaded, apart from the biaxial deformation, with blood pressure on the luminal surface of the endothelial cell. This low impact of blood pressure can be explained by the very thin shape of the endothelial cell due to which the blood pressure acts on one of the cell faces (with both the axial and

circumferential displacements being fixed) and thus induces a nearly hydrostatic stress state, which cannot contribute significantly to the deformation due to the incompressibility of the cytoplasm. Also, the differences in nucleus strains for different loading conditions are rather small for axially pre-strained cells, but a significant increase (up to three times the original value) occurs with the addition of the shear load for low axial pre-strains.

As the deviations across different cell model geometries are minor (below 20%), it appears reasonable to analyze the most realistic elongated domed shape in detail. While the shear load (corresponding to shear stress of  $<2$  Pa) is capable to double or even triple (as in the 0/10 case) the first principal strains of the nucleus under low axial pre-strains, these changes did not exceed 10% under higher axial pre-strains and become negligible under axial pre-strain equal to 30%. Also, the impact of cell shape on deformation under shear load decreases with increasing axial pre-strain from 20% to only a few percent difference between the elongated and regular domed endothelial cell model. These results anticipate a significant impact of axial pre-strain on nucleus deformation

**Table 7**

The first principal strains of the nucleus in the calculated cases for elongated hexagonal endothelial cell. Pulsations represent the cyclic increase of the first principal strain of the nucleus while the cell undergoes pulsating blood pressure between 10 and 20 kPa.

Model variant	Axial pre-strain [%]	Pressure [kPa]	First principal strain of the nucleus for the elongated model variant					
			Flat model			Domed model		
			Bi	BiP	BiPS	Bi	BiP	BiPS
0/10	0	10	0.052	0.055	0.115	0.052	0.049	0.164
0/16	0	16	0.085	0.085	0.123	0.085	0.073	0.172
0/20	0	20	0.104	0.092	0.144	0.104	0.087	0.178
		Pulsations	+0.052	+0.037	+0.039	+0.052	+0.038	+0.014
5/10	5	10	0.066	0.066	0.095	0.066	0.062	0.145
5/16	5	16	0.071	0.072	0.112	0.069	0.067	0.154
5/20	5	20	0.075	0.075	0.120	0.072	0.067	0.160
		Pulsations	+0.009	+0.009	+0.025	+0.006	+0.005	+0.015
10/10	10	10	0.122	0.113	0.126	0.122	0.107	0.141
10/16	10	16	0.124	0.12	0.128	0.124	0.113	0.145
10/20	10	20	0.126	0.119	0.130	0.125	0.111	0.150
		Pulsations	+0.004	+0.006	+0.004	+0.003	+0.004	+0.009
20/10	20	10	0.220	0.202	0.237	0.224	0.194	0.228
20/16	20	16	0.22	0.203	0.237	0.224	0.193	0.229
20/20	20	20	0.22	0.204	0.238	0.224	0.193	0.229
		Pulsations	+0.000	+0.001	+0.001	+0.000	-0.001	+0.001
30/10	30	10	0.312	0.279	0.338	0.316	0.272	0.322
30/16	30	16	0.313	0.28	0.337	0.316	0.275	0.322
30/20	30	20	0.313	0.282	0.337	0.316	0.276	0.322
		Pulsations	+0.001	+0.003	-0.001	0.000	+0.004	0.000

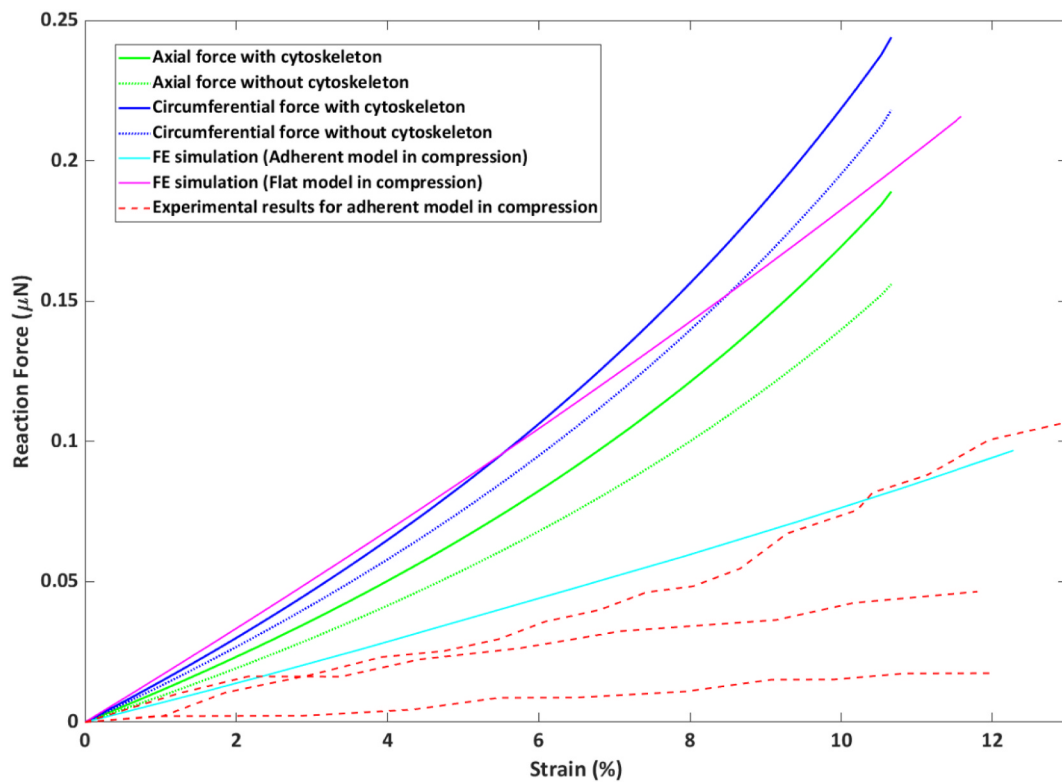


**Fig. 6.** Comparison of simulated force-deformation curves for regular flat models under equibiaxial strain (5/20) (with and without cytoskeleton) with simulated and experimental results in compression [24,32].

as discussed below in detail.

We assume a decisive impact of the first principal strains of the nucleus on the cell biological response, but the question is about the role of their steady and pulsatile components. It is well known that pulsatile load contributes significantly to the remodeling and healing of tissues [43]. The magnitude of the pulsatile component of the strain (difference between its values under systolic and diastolic pressure) also increases significantly with decreasing axial pre-strain in the artery.

The role of the cytoskeleton in the mechanical response of the cell was investigated in the cases with maximum axial (30/10) and maximum circumferential (0/20) elongation. As expected, no contribution of IFs was found in the latter case under circumferential stretch being lower than the limit stretch of the IFs. In agreement with similar analyses performed in Refs. [23,24,44], AFs and MTs have a vital role in cell stiffness. The MTs seem to dominate the cell stiffness under shear loads in contrast to AFs prevailing in the stiffness of the flat model in

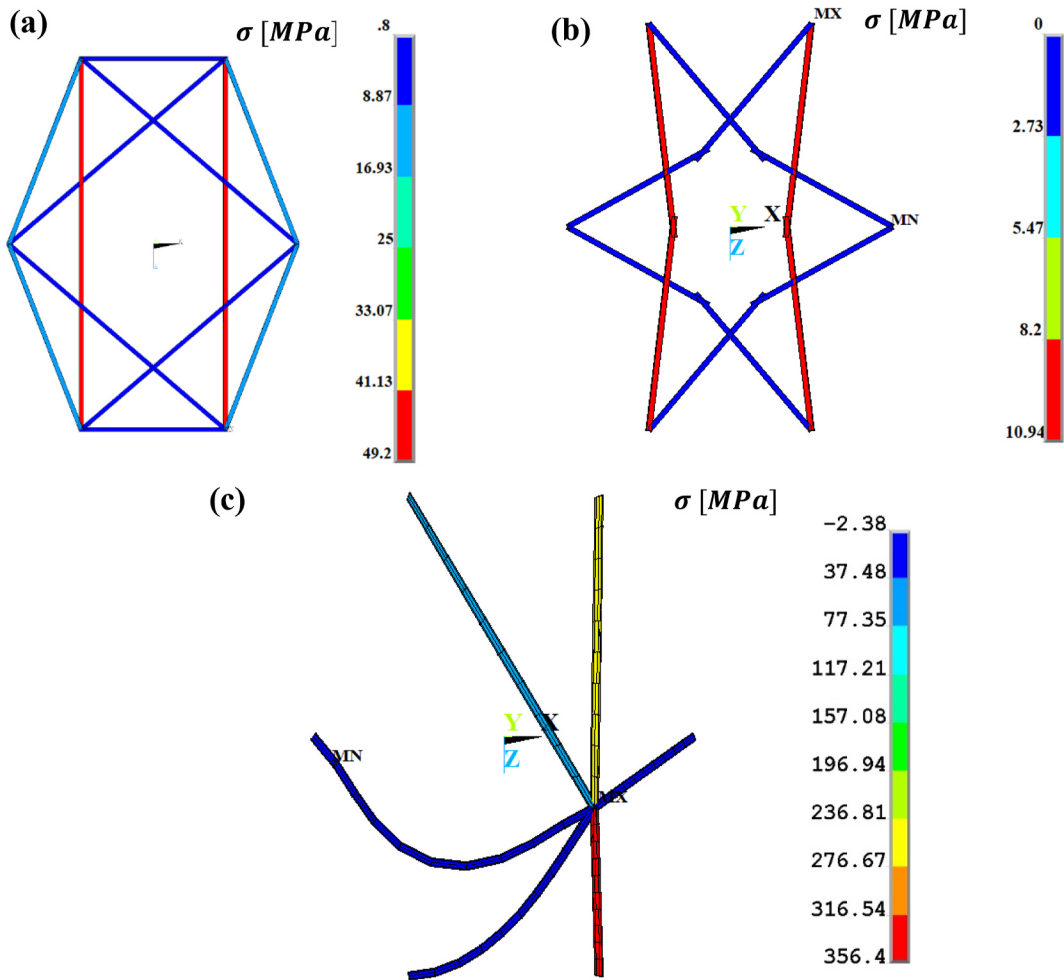


**Fig. 7.** Examples of stresses in the cytoskeletal components of a regular flat endothelial cell in the 30/10 model in (a) actin filaments, (b) intermediate filaments, and (c) microtubules.

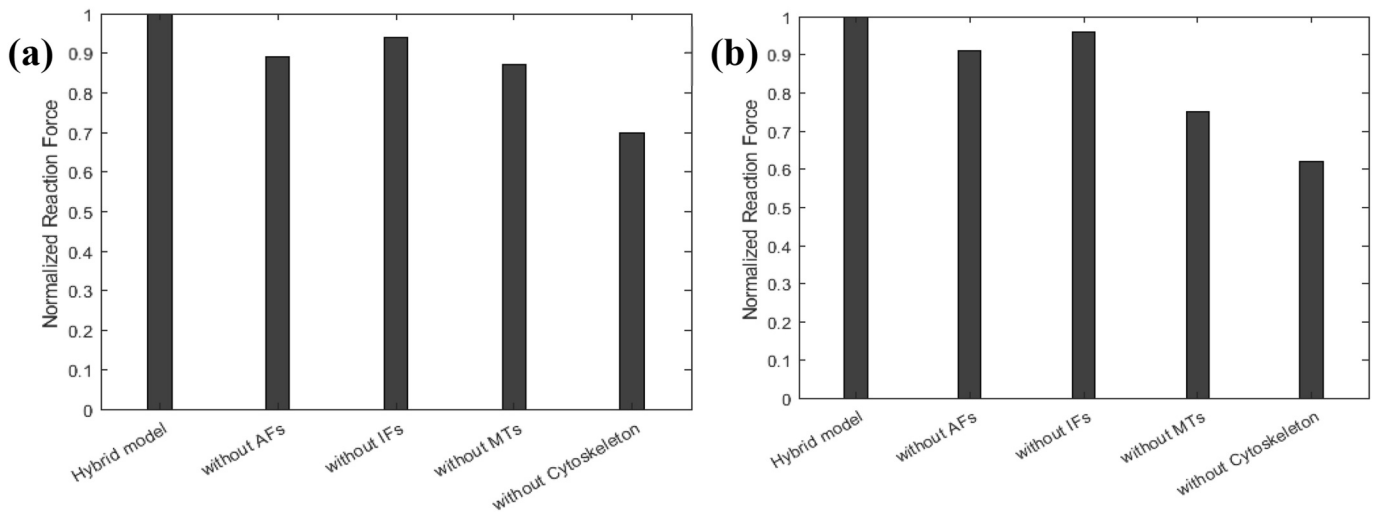


**Fig. 8.** Contribution of cytoskeletal components of the regular hexagonal cell model to its stiffness under 30/10 loading condition for (a) the flat model and (b) the domed model. The axial reaction force is normalized to 1 with respect to the force from the corresponding hybrid model.

compression [24].

Although the realized simulations of the cell mechanical behavior are static, the results are obtained for various levels of loads which enables us to assess the cyclic deformations of the cell caused by the

pulsatile nature of blood pressure in arteries as well. The first principal strains of the nucleus (see Tables 6 and 7) under systolic and diastolic pressure show that highest pulsations occur in the cases with the lowest axial pre-strain as typical for arterial conditions in older individuals

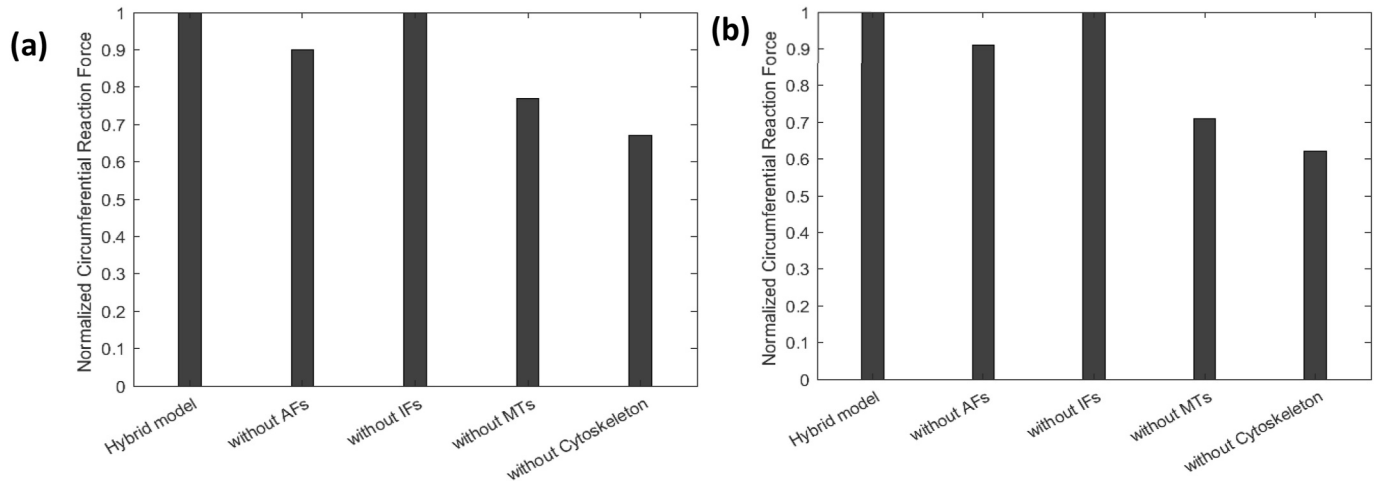


**Fig. 9.** Contribution of cytoskeletal components of the regular hexagonal cell model to its stiffness under 0/20 loading condition for (a) the flat model and (b) the domed model. The reaction force is normalized to 1 with respect to the force from the corresponding hybrid model.

[35].

All the recent research in the field of cell mechanics as well as the limitations they bear are summarized in Table 8. Priority of the presented model consists generally in considering the physiological loading conditions of the cell and several different shapes which mimic the realistic cell geometry in the endothelium.

Aside from the aforementioned advantages, the proposed models have certain limitations. First, they do not consider the dynamic and time-dependent behavior of living cells because we have no applicable viscoelastic experimental data for the cytoskeletal components as available for whole cells, e.g. in Ref. [47]. If available, they could be introduced in the model together with a non-linear elastic behavior of

the cytoskeletal fibers.

Also, active responses of the cell (cell lifetime and cytoskeletal remodeling related to the rearrangement of AFs and MTs under persisting mechanical load) are not considered. Although the remodeling occurs after longer time scales than typical for cell mechanical testing, it may have a significant influence on our results.

In our biaxial loading conditions, axial deformation is steady and represents axial pre-stretch of the artery, however, it is disputable whether the high values generally valid for the aortic wall are realistic in this case. First, atherosclerosis as a basic motivation of these simulations is typical for older people showing low axial pre-stretch [35]. Second, the lifetime of endothelial cells does not exceed one year [48]; in between, they remodel themselves [49] and grow on a pre-stretched basal membrane within the arterial wall, but without being necessarily pre-stretched. Consequently, the high axial pre-stretch of the endothelium may be also questionable for young individuals and these models might be out of reality. Therefore we consider the models with low or even zero axial pre-stretch to be more clinically relevant. However, this issue is worth researching further, preferably combining suitably tailored experiments with corresponding modifications of the computational modeling introduced herein. The presented model could also be used advantageously in simulations of mechanical behavior of cell population (endothelial monolayer) and detachment of the individual cells from each other and from the basal membrane, which might bring new insight into the inception of atherosclerosis.

Even though there is no indication in the literature on other mechanically-relevant cell organelles and the model is believed to comprehend all of them, the structural arrangement of cytoskeletal components does not capture their true complexity. The number of cytoskeletal elements is significantly lower than in a real cell but it was shown that this number is not decisive for the quality of the model [10, 22–24], and the authors do not know any discrete model having the number of elements comparable with reality.

However, when we created a more complex tensegrity model with 862 members [50], it brought no advantages against the previous tensegrity models with lower numbers of elements [10,21,22] while the basic disadvantages were preserved: the stiffness of MTs being too high, the absence of centrosome in the model, and, consequently, the non-realistic transmission of loads by the individual cytoskeletal elements.

Finally, endothelial cell dysfunction has been linked to atherosclerosis through its response to hemodynamic forces [39]. The model points towards a significant role of wall shear stress in the deformation of arterial endothelium cells and their nuclei. However, further studies

**Table 8**

Comparison of the published results with recent works in the field.

References	Content of the article	Limitations
[6,45]	A 3D FE model of a single cell with a cytoskeletal network was created for simulations of the indentation tests.	These studies simulated the mechanical behavior of a cell with an oversimplified tensegrity structure without considering the flexural behavior of MTs. Also, the role of individual cytoskeletal filaments was not investigated.
[46]	A 3D finite element model of a cell is constructed and includes discrete cytoskeletal architecture and continuum parts (nucleus, cell membrane, cytoplasm)	The role of individual cytoskeletal filaments was investigated including the degradation of the cytoskeleton but the study used simpler cytoskeletal arrangements without considering the flexural behavior of MTs. Only an indentation test was simulated.
[27]	A hybrid model of 3D endothelial monolayers with a regular hexagonal pattern was proposed for an investigation of a crack generated in an endothelial monolayer.	The study addressed the structural integrity of endothelial monolayer without a detailed description of the cytoskeletal arrangement and thus missing an investigation of the role of individual components. The cell model geometry is a flat regular hexagon only.
[5]	An investigation of the time-dependent behavior of the actin cytoskeleton was performed. A 3D FE model was created and the model was validated with compression test simulations for this purpose.	Only the suspended (spherical) endothelial cell was simulated instead of realistic physiological shapes.

are needed to investigate the perception of these loads by a cell monolayer.

## 5. Conclusion

The 3D hybrid finite element model of a single endothelial cell with its realistic geometry is applied in simulations of cell mechanical response within the vascular endothelium layer. The simulations are performed with four different cell geometries under different loading conditions (combinations of biaxial deformation, blood pressure, and shear load from the blood flow). As a decisive parameter for mechano-transduction, the first principal strain of the nucleus is evaluated and compared throughout all the investigated cases with different geometrical configurations and loading conditions. The results indicate that the pulsatile blood pressure may induce significant cyclic deformation on the nucleus and thus trigger the remodeling processes in the endothelium as well as in the whole intima layer. Also, the wall shear stress, however small in absolute values, can significantly change the nucleus deformation and thus contribute to the remodeling of the endothelial cells. Both effects are pronounced specifically for low axial pre-stretch in arteries which is a typical condition in older people. In the future, the model should be expanded to investigate the perception of loads by a monolayer of cells within the vascular endothelium.

## Declaration of competing interest

None.

## Acknowledgments

This work was supported by Czech Science Foundation project 21-21935S.

We acknowledge Jaromír Gumulec and the core facility CELLIM supported by MEYS CR (LM2018129 Czech-BioImaging) for providing images from confocal microscopy.

## Appendix A. Supplementary data

Supplementary data to this article can be found online at <https://doi.org/10.1016/j.compbiomed.2022.105266>.

## References

- [1] M. Judith, *The Atlas of Heart Disease and Stroke*, WHO, 2004.
- [2] R. Seeley, T.D. Stephens, P. Tate, *Anatomy and Physiology*, 6th, McGraw Hill, Boston, MA, 2003.
- [3] A. Lusis, *Atherosclerosis*, *Nature* 407 (2000) 233–241.
- [4] K. Urschel, M. Tauchi, S. Achenbach, B. Diemel, Investigation of wall shear stress in cardiovascular research and in clinical practice—from bench to bedside, *Int. J. Mol. Sci.* 22 (11) (2021).
- [5] H. Ghaffari, M.S. Saidi, B. Firoozabadi, Biomechanical analysis of actin cytoskeleton function based on a spring network cell model, *J. Mech. Eng. Sci.* 231 (7) (2016) 1308–1323.
- [6] P. F. Xue, A. Lennon, K. McKay, V. Campbell, Effect of membrane stiffness and cytoskeletal element density on mechanical stimuli within cells: an analysis of the consequences of ageing in cells *Comput. Methods Biomech. Biomed. Eng.* 18 (5) (2015) 468–476.
- [7] E.P. Dowling, J.P. McGarry, Influence of spreading and contractility on cell detachment, *Ann. Biomed. Eng.* 42 (2014) 1037–1048.
- [8] S. Barreto, C. Clausen, C. Perrault, D. Fletcher, A multi-structural single cell model of force-induced interactions of cytoskeletal components, *Biomaterials* 34 (26) (2013) 6119–6126.
- [9] D. Kardas, U. Nackenhorst, D. Balzani, Computational model for the cell-mechanical response of the osteocyte cytoskeleton based on self-stabilizing tensegrity structures, *Biomech. Model. Mechanobiol.* 12 (2013) 167–183.
- [10] J. McGarry, P. Prendergast, A three-dimensional finite element model of an adherent eukaryotic cell, *Eur. Cell. Mater.* 7 (2004) 27–33.
- [11] G. Unnikrishnan, U. Unnikrishnan, J. Reddy, Constitutive material modeling of cell: a micromechanics approach, *J. Biomech. Eng.* 129 (3) (2007) 315–323.
- [12] B. Maurin, P. Cañadas, H. Baudriller, P. Montcour, Mechanical model of cytoskeleton structuration during cell adhesion and spreading, *J. Biomech.* 41 (9) (2008) 2036–2041.
- [13] C. Wang, S. Li, A. Ademiloye, P. Nithiarasu, Biomechanics of cells and subcellular components: a comprehensive review of computational models and applications, *Int. J. Numer. Meth. Biomed. Engng.* 37 (12) (2021) e3520, <https://doi.org/10.1002/cnm.3520>.
- [14] H. Pakravan, M. Saidi, B. Firoozabadi, A multiscale approach for determining the morphology of endothelial cells at a coronary artery, *Int. J. Numer. Meth. Biomed. Eng.* 33 (12) (2017).
- [15] D. I. Cellular tensegrity: defining new rules of biological design that govern the cytoskeleton, *J. Cell Sci.* 104 (1993) 613–627.
- [16] P. Cañadas, V. Laurent, C. Oddou, D. Isabey, S. Wendling, A cellular tensegrity model to analyse the structural viscoelasticity of the cytoskeleton, *J. Theor. Biol.* 218 (2002) 155–173.
- [17] P. Cañadas, V. Laurent, P. Chabrand, D. Isabey, S. Wendling-Mansuy, Mechanisms governing the visco-elastic responses of living cells assessed by foam and tensegrity models, *Med. Biol. Eng. Comput.* 41 (6) (2003) 733–739.
- [18] P. Cañadas, S. Wendling Mansuy, D. Isabey, Frequency response of a viscoelastic tensegrity model: structural rearrangement contribution to cell dynamics, *J. Biomech. Eng.* 128 (4) (2006) 487–495.
- [19] D. Stamenović, M. Coughlin, The role of prestress and architecture of the cytoskeleton and deformability of cytoskeletal filaments in mechanics of adherent cells: a quantitative analysis, *J. Theor. Biol.* 201 (1) (1999) 63–74.
- [20] H. Shaohua, J. Chen, B. Fabry, Y. Numaguchi, A. Gouldstone, D. Ingber, J. Fredberg, J. Butler, N. Wang, Intracellular stress tomography reveals stress focusing and structural anisotropy in cytoskeleton of living cells, *Am. J. Physiol. Cell.* 285 (2003) 1082–1090.
- [21] J. Bursa, R. Lebis, P. Janicek, FE models of stress-strain states in vascular smooth muscle cell, *Technol. Health Care* 14 (2006) 311–320.
- [22] J. Bursa, J. Holata, R. Lebis, Tensegrity finite element models of mechanical tests of individual cells, *Technol. Health Care* 20 (2) (2012) 135–150.
- [23] Y. Bansod, T. Matsumoto, K. Nagayama, J. Bursa, A finite element bendo-tensegrity model of eukaryotic cell, *J. Biomech. Eng./ASME.* 140 (10) (2018).
- [24] V. Jakka, J. Bursa, Finite element simulations of mechanical behaviour of endothelial cells, *BioMed Res. Int.* (2021) 1–17.
- [25] J. Uzarski, E. Scott, P. McFetridge, Adaptation of endothelial cells to physiologically-modeled, variable shear stress, *PLoS One* 8 (2) (2013).
- [26] Y.M. Shin, H.J. Shin, Y. Heo, I. Jun, Y.-W. Chung, K. Kim, Y.M. Lim, H. Jeon, H. Shin, Engineering aligned endothelial monolayer on a topologically modified nanofibrous platform with a micropatterned structure produced by femtosecond laser ablation, *J. Mater. Chem. B* 5 (2) (2016), <https://doi.org/10.1039/C6TB02258H>.
- [27] A. Nieto, J. Escribano, F. Spill, M. Garcia-Aznar, M.J. Gomez-Benito, Finite element simulation of the structural integrity of endothelial cell monolayers: a step for tumor cell extravasation, *Eng. Fract. Mech.* 224 (2020).
- [28] M. Sato, T. Ohashi, Biorheological views of endothelial cell responses to mechanical stimuli, *Biorheology* 42 (6) (2005) 421–441.
- [29] A. Remuzzi, C. Dewey, P. Davies, M. Gimbrone, Orientation of endothelial cells in shear fields in vitro, *Biorheology* 21 (4) (1984).
- [30] F. Gittes, B. Mickey, J. Nettleton, J. Howard, Flexural rigidity of microtubules and actin filaments measured from thermal fluctuations in shape, *J. Cell Biol.* 120 (4) (1993) 923–934.
- [31] A. Kiyomarsioskouei, M. Saidi, B. Firoozabadi, An endothelial cell model containing cytoskeletal components: suspension and adherent states, *J. Biomed. Sci. Eng.* 5 (12) (2012) 737–742.
- [32] N. Caille, O. Thoumine, Y. Tardy, J. Meister, Contribution of the nucleus to the mechanical properties of endothelial cells, *J. Biomech.* 35 (2) (2002) 177–187.
- [33] R. Rand, Mechanical properties of the red cell membrane: II. Viscoelastic breakdown of the membrane, *Biophys. J.* 4 (4) (1964) 303–316.
- [34] O. Lisicky, A. Mala, Z. Bednarik, T. Novotny, J. Bursa, Consideration of stiffness of wall layers is decisive for patient-specific analysis of carotid artery with atheroma, *PLoS One* 15 (9) (2020) 1–18.
- [35] L. Horný, M. Netušil, T. Voňavková, Axial prestretch and circumferential distensibility in biomechanics of abdominal aorta, *Biomech. Model. Mechanobiol.* 13 (4) (2014) 783–799.
- [36] G. Sommer, P. Regitnig, L. Kölringer, G. Holzapfel, Biaxial mechanical properties of intact and layer-dissected human carotid arteries at physiological and supraphysiological loadings, *Am. J. Physiol. Heart Circ. Physiol.* 298 (3) (2010) H898–H912.
- [37] R. Etienne, P. Bougaran, P. Dufourcq, T. Couffignal, Fluid shear stress sensing by the endothelial layer, *Front. Physiol.* 11 (2020) 861.
- [38] P. Cahill, E.M. Redmond, Vascular endothelium - gatekeeper of vessel health, *Atherosclerosis* 248 (2016) 97–109.
- [39] K.S. Cunningham, A.I. Gotlieb, The role of shear stress in the pathogenesis of atherosclerosis, *Lab. Invest.* 85 (1) (2005) 9–23.
- [40] P. Prendergast, Computational modelling of cell and tissue mechanoresponsiveness, *Gravit. Space Res.* 20 (2) (2007) 43–50.
- [41] A.C. Shieh, K.A. Athanasiou, Dynamic compression of single cells, *Osteoarthritis Cartilage* 15 (3) (2007) 328–334.
- [42] N.D. Leipzig, K.A. Athanasiou, Static compression of single chondrocytes catabolically modifies single-cell gene expression, *Biophys. J.* 94 (6) (2008) 2412–2422.
- [43] C.H.G. Neutel, C. Giulia, P. Puylaert, G.R.Y. De Meyer, W. Martinet, P.-J. Gans, High pulsatile load decreases arterial stiffness: an ex vivo study, *Front. Physiol.* 12 (2021) 1804.
- [44] L. Wang, L. Wang, L. Xu, C. Weiyei, Finite element modeling of single-cell based on atomic force microscope indentation method, *Comput. Math. Methods. Med.* 2019 (7895061) (2019), <https://doi.org/10.1155/2019/7895061>.

- [45] W. Lili, C. Weiyi, Modelling cell origami via a tensegrity model of the cytoskeleton in adherent cells, *Appl. Bionics Biomechanics* 2019 (8541303) (2019), <https://doi.org/10.1155/2019/8541303>.
- [46] D. Katti, K. Katti, Cancer cell mechanics with altered cytoskeletal behaviour and substrate effects: a 3D finite element modeling study, *J. Mech. Behav. Biomed. Mater.* 76 (2017) 125–134.
- [47] B. Hoffman, J. Crocker, Cell mechanics: dissecting the physical responses of cells to force, *Annu. Rev. Biomed. Eng.* 11 (2009) 259–288.
- [48] K. Kliche, P. Jeggle, H. Pavenstädt, H. Oberleithner, Role of cellular mechanics in the function and life span of vascular endothelium, *Pflügers Archiv* 462 (2) (2011).
- [49] T. Girão-Silva, M. Fonseca-Alaniz, J. Ribeiro-Silva, J. Lee, N. Patil, L. Dallan, A. Baker, M. Harmsen, High stretch induces endothelial dysfunction accompanied by oxidative stress and actin remodeling in human saphenous vein endothelial cells, *Sci. Rep.* 11 (1) (2021).
- [50] J. Bursa, Y. Bansod, Design and applications of prestressed tensegrity structures, in: 20th International Conference, Engineering Mechanics 2014, Svratka, Czech Republic, 2014.

## Appendix C

**Title:** “Bendo-tensegrity model simulates compression test of animal cell”

**Authors:** Y.D. Bansod, Veera V.S.V.P. Jakka and J. Bursa.

**Conference Name:** 24th International Conference, Engineering Mechanics, Svratka, Czech Republic, May14–17, 2018.

**Citation:**

Y.D. Bansod, Veera V.S.V.P. Jakka and J. Bursa. (2018). “Bendo-tensegrity model simulates compression test of animal cell”. Engineering Mechanics. DOI: [10.21495/91-8-45](https://doi.org/10.21495/91-8-45)

## BENDO-TENSEGRITY MODEL SIMULATES COMPRESSION TEST OF ANIMAL CELL

Y. D. Bansod<sup>\*</sup>, Veera V. S. V. P. Jakka<sup>\*\*</sup>, J. Burša<sup>\*\*\*</sup>

**Abstract:** *A hybrid model of suspended animal cell proposed earlier, with a bendo-tensegrity structure mimicking cytoskeleton, is applied to simulate the global response of the cell under compression and to describe mechanical behaviour of its components. The Finite Element model incorporates Microtubules, Actin Filaments, Intermediate Filaments, nucleus, cytoplasm, and Cell Membrane, all of them with realistic geometrical and material parameters. The unique features of this structural model keep fundamental principles governing cell behaviour, such as interaction between the cytoskeletal components redistributing the prestress of actin filaments throughout all the structure. The force-deformation curve from the simulated compression test with microplates is validated by comparison with the experimental response from literature. The model enables us to investigate the mechanical role of individual cellular and cytoskeletal components in intracellular force propagation by means of changing their numbers or parameters. As quantitative characterization of nucleus deformation may be hypothetically decisive for mechanotransduction, the model aims at better understanding of how cellular processes are mechanically controlled.*

**Key words:** cell mechanics, cytoskeleton, bendo-tensegrity model, compression test simulation

### 1. Introduction

Mechanical testing of individual cells represents an important source of input data for modelling of their mechanical behaviour. Simulations of these tests enable identification of the models and aim at explaining cellular processes such as mechanotransduction. They represent also a step needed in multilevel modelling of tissues. Different types of cell models have been created using continuum and discrete approaches, or combination of both in hybrid models. Tensegrity models represent one of the most promising concepts, showing however some limitations (see Bursa et al., 2012) which have been overcome using bendotensegrity concept. Such hybride model was created in (Bansod, 2016) using finite element program system ANSYS (ANSYS Inc. PA, US); it encompasses the cell nucleus and cytoplasm surrounded by the Cell Membrane (CM), as well as cytoskeletal components like Actin Filaments (AFs), Micro Tubules (MTs), and Intermediate Filaments (IFs). Microscopic observations of the cell shape in suspended state as well as images of distributions of cytoskeletal proteins were referred to create the 3D suspended cell model and the architecture of its cytoskeletal components. In contrast to the tensegrity models published earlier, MTs are modelled here more realistically as bended (buckled) beams reducing thus their stiffness under compression and making their response under tension more non-linear (Mehrbod et al., 2011). This paper presents results of simulations of compression test with microplates of an isolated suspended cell using this hybrid model.

### 2. Methodology

The proposed model implemented the hybrid modelling approach, i.e. the continuum parts (nucleus, cytoplasm) were modelled using continuous (volume) finite elements circumscribed by a thin layer of shell elements representing CM, while the cytoskeletal components were modelled using discrete (beam

---

\* Ing. Yogesh Deepak Bansod, PhD.: Brno University of Technology, Brno; CZ, yogeshbansod@gmail.com

\*\* Ing. Veera Venkata Satya Varaprasad Jakka, MSc.: Brno University of Technology, CZ, veeravenkata.jakka@mail.polimi.it

\*\*\* Prof. Ing. Jiří Burša, PhD.: Brno University of Technology, Brno; CZ, bursa@fme.vutbr.cz



or truss) elements. The shape of the suspended cell model was defined as spherical with diameter ( $D$ ) of  $32.2\ \mu\text{m}$ , taken from one of the experimental measurements in (Nagayama et al., 2006). The nucleus was also modelled as spherical and positioned at the center of the cell. Similarly to a real cell, its position was stabilized by a network of IFs. Both cytoplasm and nucleus were modelled with eight-node hexahedral isoparametric elements; the flexible CM on the outer surface of cytoplasm was modelled by shell elements, with the thickness of  $0.01\ \mu\text{m}$  (Rand, 1964) and no bending stiffness. The wavy IFs were modelled with negligible stiffness until being sufficiently (by 20% in the presented model) extended, while AFs created a network beneath the CM prestressed by means of their -24% prestrain; both of them were modelled as tension-only truss elements. In contrast, MTs were modelled as bended beam structures, all of them originating from one point near the nucleus representing the centrosome. Geometrical as well as material parameters of all these components were set according to literature sources (see Bansod (2016) for more details). The contact between the cell and the rigid microplates was set as frictionless.

During the simulation, the cell model was compressed against the fixed (bottom) microplate by applying vertical displacements to the nodes of the movable (top) microplate to achieve 50% deformation of the cell. The reaction force was evaluated as the sum of forces at nodes of the contact surface between the cell and the movable microplate.

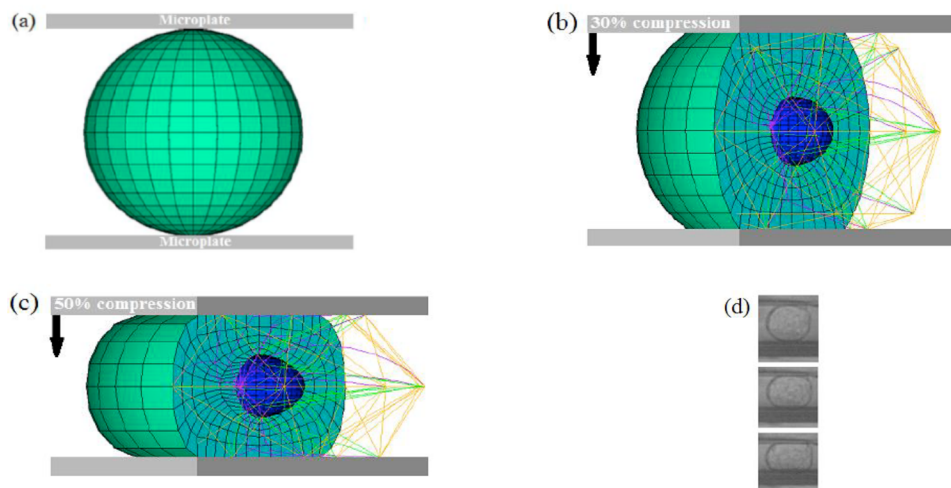


Fig. 1: Sectional views of the suspended cell model during consecutive steps in simulation of compression test: (a) spherical cell and microplates, compressing the cell with the movable microplate to (b) 30% and (c) 50% deformation against the fixed microplate. (d) Snapshots of a cell under compression in the corresponding phases of the experiment (Ujihara et al., 2012).

### 3. Results and discussion

The undeformed model and sectional views of some deformed shapes are presented in Fig. 1 in comparison with the snapshots from experiments. As depicted in Fig. 2, the force-deformation curve calculated from simulation is in good agreement with the non-linear response of the experimental results and validates thus partially the proposed bendo-tensegrity model. The slope of the simulated force-deformation curve increases with increase in cell compression, similar to the effect observed in the experiments (Nguyen et al., 2009; Ujihara et al., 2012).

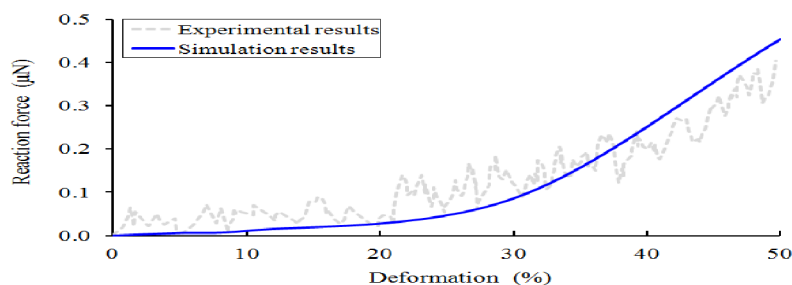


Fig. 2: Comparison of simulated force-deformation curve with the experimental dependence taken from a study by (Nguyen et al., 2009), investigating the biomechanical properties of a single chondrocyte using a micromanipulation technique.

The compression stiffness of the model was calculated as the ratio of conventional stress to conventional strain. Here the reaction force of the cell at the compressed edge was  $0.454 \mu\text{N}$  and its (maximal undeformed) cross-sectional area  $817 \mu\text{m}^2$ . The undeformed and deformed lengths of the cell corresponded to its full and half diameter, respectively, resulting thus in 50% compression and the respective stiffness of the model of 1.11 kPa.

### 3.1. Response of individual cell components

In addition to the global deformation presented in the above figures, the model enables to analyze also responses of the individual cell components under compression. Fig. 3(a) shows the deformed shape of the cell and nucleus; although they seem to be rather similar at the first glance, their aspect ratio (transversal to longitudinal dimension of the originally spherical shape) is very different: 2.1 for the cell against 1.3 for its nucleus. For the IFs the axial strain is chosen instead of stress as representative quantity because stress is zero up to the strain value set in the model to represent the waviness of IFs. The approximately ellipsoidal deformed shape of the nucleus appears analogous to that observed in experiments (Ujihara et al., 2012; Caille et al., 2002). During cell compression, the randomly oriented AFs and IFs were likely to be oriented perpendicularly to the loading direction; the filaments aligned in the loading direction were compressed whereas the perpendicular ones were stretched. The first principle strain in the nucleus is hypothesized to be the decisive quantity of mechanotransduction (Bursa et al., 2012).

The MTs localized in the central region perpendicularly to the direction of loading were straightened and became thus much stiffer than the bended ones. This effect, together with the AFs reoriented perpendicularly to the loading direction and resisting high tensile forces, contributes to the gradually increasing cell stiffness which corresponds to experimental observations (Ujihara et al., 2012). Low contribution of IFs to the cell response was detected because their negative as well as positive strains remained below their applied prestrain keeping thus their waviness and consecutively zero stresses.

### 3.2. Analysis of mechanical contribution of the cell components

The role of each cytoskeletal component in resisting cell compression (to 50 % length) was investigated in greater detail via removal of each cytoskeletal component (individually as well as in all mutual combinations) from the above model which is denoted as control model in Fig. 4 and below. The maximum reaction force decreased by 26% without cytoskeleton with 20 % attributed to AFs being thus the mechanically most significant cytoskeletal component.

Fig. 5 shows the influence of changes in the number of individual cytoskeletal components and in the CM thickness on the cell response under compression. Again, additional AFs created in the cell interior (together with additional nodes on the cell surface representing focal adhesions) increased the global cell reaction force, whereas increase in the density of either MTs or IFs did not show much variation. The

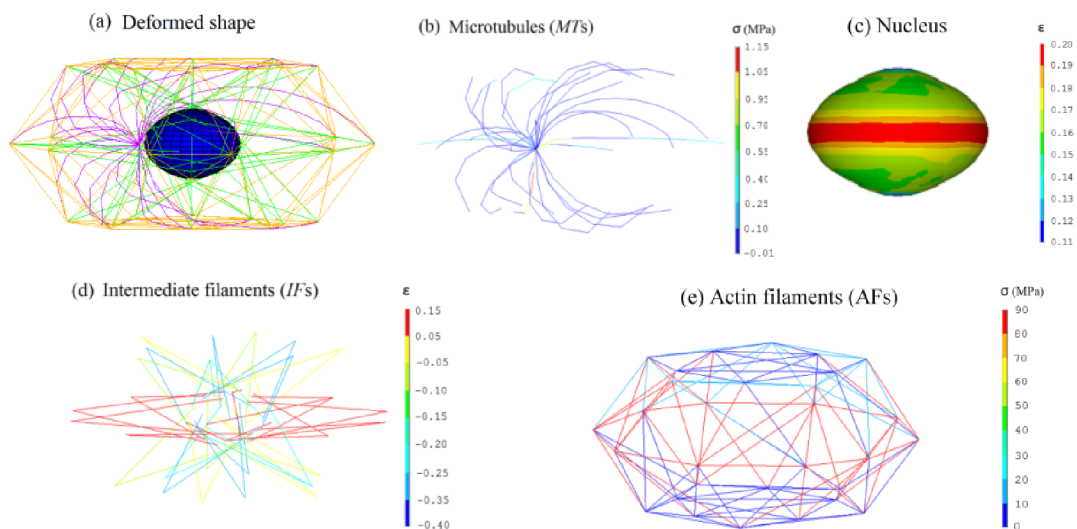


Fig. 3: Simulation results at 50% cell compression: (a) deformed shape of the cell, cytoskeletal components and nucleus; distribution of axial stress in the (b) MTs (c) distribution of first principal strain in the nucleus; (d) distribution of axial strain in the discrete elements representing IFs; and (e) AFs;

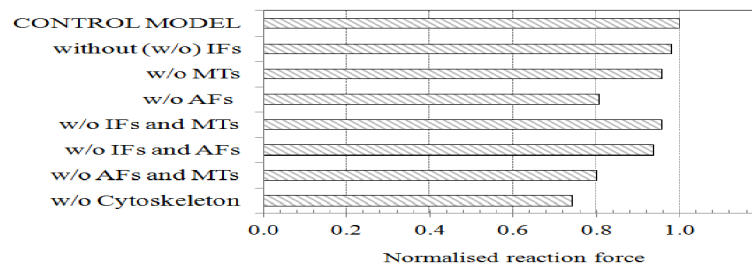


Fig. 4: Contribution of the cytoskeletal components individually and in mutual combinations to the cell stiffness at 50% compression. The reaction force is normalized with respect to that of the control model

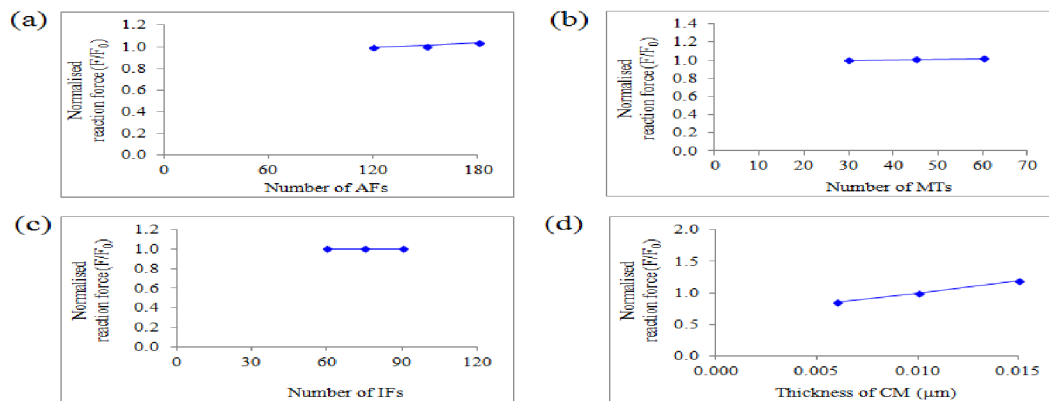


Fig. 5: Effect of increase in the density of cytoskeletal components (a) AFs, (b) MTs, and (c) IFs on the cell reaction force under 50% compression; (d) similar effect of variation of CM thickness.

variations of CM thickness affected the overall cell reaction force most substantially. For the cytoskeletal components a similar effect could be achieved by a proportional increase of their elastic modulus or cross section area.

#### 4. Conclusion

The proposed bendo-tensegrity model of a cell is capable to identify the influence of individual components on its global mechanical response, as well as the nucleus deformation, offering thus new insights into the interdependence of cellular mechanical properties and the mechanical role of cytoskeletal components. The compression test simulations revealed that although being tension-bearing components, actin filaments and cell membrane contributed most significantly to the cell response under compression.

#### Acknowledgement

This work was supported through NETME CENTRE PLUS (LO 1202) under the National Sustainability Programme I and by the Czech Science Foundation project no.18-13663S.

#### References

- Bansod Y.D., (2016), Computational Simulations of Mechanical Tests of Isolated Animal Cells. Doctoral thesis, Brno University of Technology.
- Bursa, J., Lebis, R., Holata, J., (2012), Tensegrity finite element models of mechanical tests of individual cells. *Technology and Health Care*, 20(2) (2012) 135-150.
- Mehrbod, M., and Mofrad, R. K., (2011), On the significance of microtubule flexural behavior in cytoskeletal mechanics. *PloS one*, 6(10), e25627.
- Nagayama, K., Nagano, Y., Sato, M., and Matsumoto, T., (2006). Effect of actin filament distribution on tensile properties of smooth muscle cells obtained from rat thoracic aortas. *J Biomech*, 39(2), 293-301.
- Nguyen, B. V., Wang, Q., Kuiper, N. J., El Haj, A. J., Thomas, C. R., and Zhang, Z., (2009), Strain-dependent viscoelastic behaviour and rupture force of single chondrocytes and chondrons under compression. *Biotechnology letters*, 31(6), 803-9.
- Rand, R., (1964), Mechanical properties of the red cell membrane: II. Viscoelastic breakdown of the membrane. *Biophys J*, 4(4), 303.
- Ujihara, Y., Nakamura, M., Miyazaki, H., and Wada, S., (2012), Contribution of actin filaments to the global compressive properties of fibroblasts. *Journal of the Mechanical Behavior of Biomedical Materials*, 14, 192-8.

## Appendix D

**Title:** “Finite element models of mechanical behaviour of endothelial cells”

**Authors:** Veera Venkata Satya Varaprasad Jakka, Jiří Burša.

**Conference Name:** 26th International Conference, Engineering Mechanics, Svratka, Czech Republic, Nov 24–25, 2020.

**Citation:**

Veera Venkata Satya Varaprasad Jakka, Jiří Burša. (2020). “Finite element models of mechanical behaviour of endothelial cells”. Engineering Mechanics. p. 222-225. ISBN: 978-80-214-5896-3.

## FINITE ELEMENT MODELS OF MECHANICAL BEHAVIOUR OF ENDOTHELIAL CELLS

Jakka Veera V. S. V. P. \*, Burša J. \*\*

**Abstract:** Recently hybrid models of the endothelial cell were created by using the bendo-tensegrity concept to complete the continuum parts of the cell with an adequate cytoskeleton model. The proposed model of endothelial cell includes a network of actin filaments (AFs) as tension supporting cables and microtubules (MTs) as bended beams supporting primarily compression. It is created by adopting the geometrical shape of a short hexagonal prism with its 12 vertices that results in a nearly isotropic behaviour of the model without a preferred orientation. To achieve the synergistic effect of cytoskeletal components, the elements representing AFs, MTs, and Intermediate filaments (IFs) are sharing the same end nodes (representing focal adhesions) with the cell membrane (CM). The AFs are prestressed (i.e. stressed without application of external load), which is essential for the cell shape stability, while the IFs are wavy, thus not bearing load until straightened. The objective is to create different FE models of endothelial cells which will be used to simulate mechanical responses of the cell under different loading conditions. Endothelial cell dysfunction has been linked to atherosclerosis through their response to mechanical loads, especially hemodynamic forces.

**Keywords:** Endothelial cell, Finite element model, Cytoskeleton, Tensegrity, Mechanical behavior.

### 1. Introduction

Endothelium is a continuous, single cell-thick layer lining blood vessels and forming part of their tunica intima. Its cells rest on a connective tissue basement membrane that connects them to the tunica media (mainly composed of elastin, collagen, and smooth muscle cells). The outermost layer of the vessel wall, the tunica adventitia, is largely composed of connective tissue strengthened by collagen fibres.

Continuous lining of endothelial cells protects the luminal surface of mammalian vessels. In vivo, blood flow pulsations in the arteries produce periodic oscillations in vessel diameter, resulting in a cyclic increase and decrease of stretch of the vessel wall. Additionally, the blood flow causes also oscillating fluid shear stresses upon the endothelial lining. Endothelial cells in arteries are elongated and oriented in the direction of the blood flow (Langille et al., 1981) (Levesque et al., 1986) whereas endothelial cells of large veins are polygonally shaped.

Atherosclerosis can cause narrowing of lumen of blood vessels, commonly known as stenosis, creating pro-thrombotic regions. The shear stress in stenotic regions can stimulate vascular cells as well as blood components. Cellular interactions play a key role in diverse biological processes within the cardiovascular system (Konstantinos et al., 1998) such as development of atheroma or thrombosis. They are highly specific and regulated by different factors, such as hemodynamic forces. The attachment of blood components to the vessel wall depends on the balance between dynamic forces (forces acting on the cells) and adhesive forces (interactions of receptors and ligands from one cell to another). Understanding the interactions between hemodynamic forces and vascular cell biology is crucial to understanding cardiovascular diseases. The created models enable us to investigate the impact of mechanical stimuli on the endothelial cells; such stimuli, to which the vessel wall is exposed in healthy and stenotic arteries, may be circumferential and axial stretch, blood pressure, or shear stress from the blood flow.

---

\* Ing. Veera Venkata Satya Varaprasad Jakka, MSc.: Brno University of Technology, CZ, 207437@vutbr.cz

\*\* Prof. Ing. Jiří Burša, PhD.: Brno University of Technology, CZ, bursa@fme.vutbr.cz

## 2. Methodology of the model proposal and discussion

The concept of “bendo-tensegrity” was proposed by (Mehrbood et al., 2011) suggesting a modification of contemporary cytoskeletal tensegrity models to consider the flexural response of MTs. This concept was applied recently, in combination with continuum model of cytoplasm, nucleus and cell membrane, for modelling of mechanical behaviour of smooth muscle cells (Bansod et al., 2018); as the first finite element model it enabled one to mimic the transmission of external mechanical stimuli onto the nucleus, where they may stimulate a biochemical response of the cell.

In this paper, three created bendo-tensegrity models of endothelial cell are presented, i.e. flat, spherical, (suspended) and adherent cell models. The endothelial cell model encompasses the nucleus and cytoplasm surrounded by the CM and cytoskeletal components like AFs, MTs, and IFs (see Fig. 1). For the proposed model implementing hybrid modelling approach, the continuum parts (nucleus, cytoplasm) are modelled using continuous (volume) elements circumscribed by a thin layer of shell elements (representing CM) while the cytoskeletal components are modelled using discrete (beam or truss) elements

### 2.1. FE model of flat endothelial cell

The physiological dimensions of endothelial cells are  $0.5\ \mu\text{m}$  thick,  $15\ \mu\text{m}$  wide and upto  $50\ \mu\text{m}$  long and have a centrally located oval or round nucleus slightly raised compared to the rest of the cell. Endothelial cells are usually flat and elongated in the direction of blood flow (Sumpio et al., 2002). Based on the physiological dimensions and shape, the cell was modelled as a very short ( $0.5\ \mu\text{m}$ ) regular hexagonal prism with the edge length of  $12.5\ \mu\text{m}$  as shown in Fig. 1d. Both cytoplasm and nucleus (Fig. 1e) were modelled with eight-node hexahedral isoparametric elements. A thin flexible layer circumscribing the cytoplasm referred to as CM was modelled with four-node quadrilateral shell elements on the outer surface of the cytoplasm, with thickness of  $0.01\ \mu\text{m}$  (Rand, 1964) and no bending stiffness. The cytoskeleton is inscribed inside this continuous part as follows: AFs are modelled as truss elements connecting all the corners of the prism representing focal adhesions (FAs) as shown in Fig. 1c. The resist only tensile loads and are internally prestressed (i.e. stressed even without application of an external load); to achieve this in the proposed models, the experimentally measured prestrain of 24 % (equal throughout all the model) (Deguchi et al., 2005) (Kojima et al., 1994) was assigned to them, generating thus an initial force (prestress) essential for the cell shape stability. The elements representing AFs, MTs, and IFs were connected by sharing the same end nodes at the CM representing FAs.

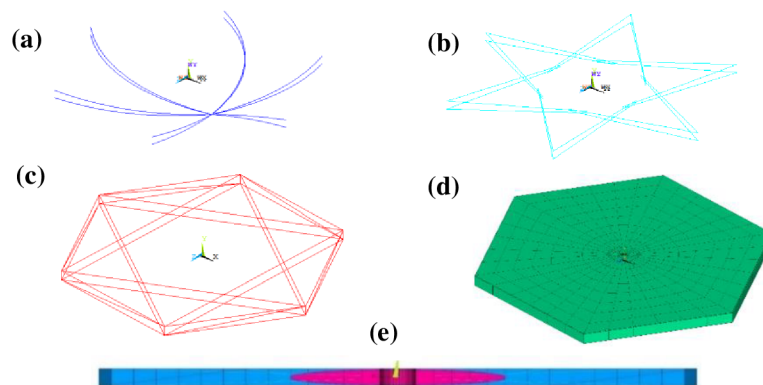


*Fig. 1: Computational model of a flat endothelial cell comprising: (a) Microtubules; (b) Intermediate filaments; (c) Actin filaments; (d) Cytoplasm surrounded by cell membrane (CM); (e) Nucleus (pink) in the cytoplasm (sectional view).*

In a real cell, MTs (see Fig. 1a) originate from the centrosome located near the nucleus and emanate outward through the cytoplasm till the cortex where they interact with other cytoskeletal filaments at focal adhesions (FAs). It is now evident that MTs do not have compression-only behaviour but they appear highly curved (buckled) in living cells under no external load. This shape reduces highly their stiffness under compressive load, therefore previous tensegrity models gave non-realistic results (see Burša et al., 2012).

IFs are scattered throughout the intracellular space and circumscribe the nucleus to stabilize its position within the cell. The proposed model omits their parts adherent to the nucleus and introduces the IFs only as straight fibres being tangential to the nucleus surface and connecting it with the FAs. When stretched, these filaments become straight and behave stiffer, thus contributing to the cell mechanics only at large

strains (above 20 %) (Janmey et al., 1991) (Wang et al., 2000). To incorporate their waviness, the IFs (their arrangement is shown in Fig. 1b) were modelled as truss elements resisting only tensile loads under elongations higher than 20 %, with this limit strain value being equal for all of them.

## 2.2. FE model of spherical endothelial cell

The experiments (Caille et al., 2002) show a spherical shape of cells suspended in a liquid medium as used in most mechanical tests. In order to enable us validation of some mechanical responses of our endothelial cell model, we rearranged the shape of flat endothelial cell model into the spherical cell model as shown in Fig. 2.

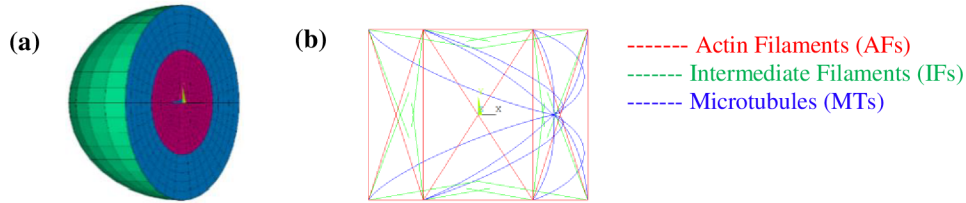


Fig. 2: Spherical model of suspended endothelial cell: (a) sectional view of cytoplasm (blue) with CM (light green) and nucleus (pink); (b) cytoskeleton.

We assumed the same volume of the cell, thus the dimensions are recalculated by equating the volume of regular hexagonal prism to the volume of a sphere. From this, the diameter of cytoplasm is 7.4  $\mu\text{m}$  and diameter of nucleus is 3.0  $\mu\text{m}$ . The topology and arrangement of cytoskeletal elements remains the same as in the flat model (see Fig. 2b).

## 2.3. FE model of adherent endothelial cell

To enable us simulations of mechanical tests done experimentally with cells adhered to a substrate, such as e.g. indentation test or magnetic tweezer test, the FE model of adherent cell was created (see Fig. 3c) on the basis of the model used in (Bansod, et al., 2018) and applying the rules described by (McGarry et al., 2004). Again it was modified from the suspended cell model by creating an axisymmetric cell model with the shape of a truncated sphere. On the basis of experimental observations in (Jean et al., 2004) and (Caille et al., 2002), we used the cell model with a maximum diameter of 20 microns and a maximum height of 8 microns; the nucleus was modelled as a flat ellipsoid with maximum diameter of 8 microns and height of 4 microns. In contrast to the above endothelial cell models, the adherent cell possesses a thin layer of actin-gel at the cell surface referred to as actin cortex (AC). We used an analogous approach as presented by (Barreto et al., 2013) and modelled the AC (i.e. the CM together with the dense acting network below it) with four-node quadrilateral shell elements having no bending stiffness. The experimentally measured thickness of this cortical layer is 0.2  $\mu\text{m}$ , i.e. 20 times thicker than the cell membrane itself (Unnikrishnan et al., 2007), (Jean et al., 2005); this value is consistent with another study on endothelial cells. Another difference within a cell adhered to a rigid substrate is in arrangement of actin, which is, in contrast to the other cell shapes, arranged in a form of thicker Actin Bundles (ABs) localized at the cell periphery and aligned in the longitudinal direction. These bundles, requiring a different topology and geometry of the model (see Fig. 3a), were modelled using truss elements that resist only tensile loads and are arranged along the AC with both ends anchored to it at FAs together with the elements representing MTs and IFs. As like AFs, the ABs were also internally prestressed by introducing the 24 % prestrain (Deguchi et al., 2005), (Barreto et al., 2013). The topological distribution of both MTs and IFs was retained analogous to that of the suspended cell model. Due to the geometric complexity of cell configuration, both cytoplasm and nucleus were meshed with four-node tetrahedral solid elements.

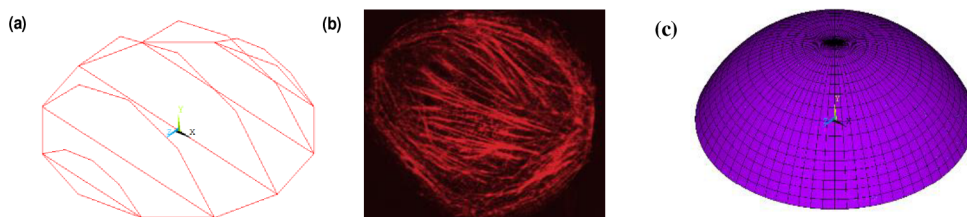


Fig. 3: (a) Computational model of Abs; (b) Microscopic image of Abs (cytoskeleton, Inc); (c) Computational model of adherent cell.

### 3. Conclusion

The presented work aims at realistic computational modelling of mechanical behaviour of cytoskeleton and the endothelial cell as a whole. The FE hybrid model of smooth muscle cell created in (Bansod et al., 2018) and exploiting bendo-tensegrity principle was modified to mimic specific shapes, properties and cytoskeletal arrangement of endothelium cells. It focuses on cytoskeletal mechanics of the endothelial cell in its suspended, flat and adherent shapes to study its passive behaviour. The proposed FE models of the endothelial cell are intended to be used for simulations of mechanical tests of endothelial cells under different loading conditions to validate the model and to enable us to transform different mechanical stimuli into a chosen unique quantity representing the cell mechanical response under different loading conditions. Endothelial cell dysfunction has been linked to atherosclerosis through their response to mechanical loads, especially hemodynamic forces, and these simulations should contribute to understanding this process.

### Acknowledgement

This work was supported by Czech Science Foundation project No. 18-13663S.

### References

- Barreto, S., Clausen, C., Perrault, C., Fletcher, D. and Lacroix, D. (2013) A multi-structural single cell model of force-induced interactions of cytoskeletal components. *Biomaterials*, 34(26), 6119-26.
- Bansod, Y. D., Matsumoto, T., Nagayama, K. and Bursa, J. (2018) A Finite Element Bendo-Tensegrity Model of Eukaryotic Cell, *ASME Journal of Biomechanical Engineering*, vol. 140(10), 101001-9.
- Bursa, J., Holata, J. and Lebis, R. (2012) Tensegrity Finite Element Models of Mechanical Tests of Individual Cells, *Technol. Health Care*, 20(2), 135-150.
- Caille, N., Thoumine, O., Tardy, Y. and Meister, J. (2002) Contribution of the nucleus to the mechanical properties of endothelial cells. *Journal of Biomechanics*, 35, 177-87.
- Cytoskeleton, Inc - The Proteine experts, Denver, USA. Available at: [www.cytoskeleton.com](http://www.cytoskeleton.com).
- Deguchi, S., Ohashi, T. and Sato, M. (2005) Evaluation of tension in actin bundle of endothelial cells based on preexisting strain and tensile properties measurements, *Mole. & Cellular Biomechanics*, 2(3), 125-133.
- Janmey, P., Euteneuer, U., Traub P. and Schliwa, M. (1991) Viscoelastic properties of vimentin compared with other filamentous biopolymer networks. *Journal of Cell Biology*, 113(1), 155-160.
- Jean, R. P., Gray, D. S., Spector A. A. and Chen, C. S. (2004) Characterization of the Nuclear Deformation Caused by Changes in Endothelial Cell Shape, *Journal of Biomechanical Engineering*, 126, 552-558.
- Jean, R. P., Chen, C. S. and Spector A. A. (2005) Finite-element analysis of the adhesion-cytoskeleton-nucleus mechanotransduction pathway during endothelial cell rounding: axisymmetric model, *Journal of Biomechanical Engineering*, 127 (4), 594-600.
- Kojima, H., A. Ishijima and Yanagida, T. (1994) Direct measurement of stiffness of single actin filaments with and without tropomyosin by in vitro nanomanipulation, *Proceedings of the Nati. Acad. of Sci.*, 91(26), 12962-6.
- Konstantinos, K., Sharad, K. and Larry, V. M. (1998) Biomechanics of cell interactions in shear fields, *Advanced Drug Delivery*, 33, 141-164.
- Langille, L. B. and A. S.L (1981) Relationship between blood flow direction and endothelial cell orientation at arterial branch sites in rabbits and mice, *Circulation Research*, 48, 481-488.
- Levesque, M., Liepsch, D., Moravec, S. and Nerem, R. (1986) Correlation of endothelial cell shape and wall shear stress in a stenosed dog aorta, *Arteriosclerosis*, 6, 220-229.
- McGarry, J. G. and Prendergast, P. J. (2004) A three-dimensional finite element model of an adherent eukaryotic cell, *European Cells & Materials*, 7, 27-33.
- Mehrbod, M. and Mofrad, M. (2011) On the Significance of Microtubule Flexural Behavior in Cytoskeletal Mechanics, *PLoS ONE*, 6(10), e25627.
- Rand, R. (1964) Mechanical properties of the red cell membrane: II. Viscoelastic breakdown of the membrane, *Journal of Biophysics*, 4(4), 303-316.
- Sumpio, B. and Timothy, R. J. D. A. (2002) Cells in focus: endothelial cell, *The International Journal of Biochemistry & Cell Biology*, 34(12), 1508-1512.
- Unnikrishnan, G., Unnikrishnan U. and Reddy, J. (2007) Constitutive material modelling of cell: a micromechanics approach, *Journal of Biomechanical Engineering*, vol. 129, no. 3, pp. 315-323.
- Wang, N. and Stamenović, D. (2000) Contribution of intermediate filaments to cell stiffness, stiffening, and growth. *The American Journal of Physiology-Cell Physiology*, 279, C188-194.



## **Appendix E**

**Title:** “Computational Modeling of Mechanical Behavior of Endothelial Cells”

**Authors:** Veera Venkata Satya Varaprasad Jakka, Jiří Burša.

**Conference Name:** 26th Cytoskeletal Club, Vranovská Ves, May 19-21, 2019, Czech Republic.

**Citation:**

Veera Venkata Satya Varaprasad Jakka, Jiří Burša. (2019): “Computational Modeling of Mechanical Behavior of Endothelial Cells”. 26th Cytoskeletal Club, Vranovská Ves, May 19-21

# COMPUTATIONAL MODELING OF MECHANICAL BEHAVIOR OF ENDOTHELIAL CELLS

Veera Venkata Satya Varaprasad JAKKA, Jiří BURŠA

Institute of Solid Mechanics, Mechatronics and Biomechanics, Brno University of  
Technology, Brno, Czech Republic

Recently a hybrid model of smooth muscle cell was created by using the tensegrity concept to complete the continuum parts of the cell with cytoskeleton [1]. The model includes a framework of actin filaments (AFs) as tension supporting cables and microtubules (MTs) as compression-supporting struts. It is created by employing the geometrical shape of icosidodecahedron with its 30 vertices representing focal adhesions (FAs) which results in a nearly isotropic behavior of the model without any preferred orientation. To achieve the synergistic effect of cytoskeletal components, the elements representing AFs, MTs, and Intermediate filaments (IFs) are connected by sharing the same end nodes at the cell membrane (CM) representing FAs. The AFs are prestressed (i.e. stressed without application of external load) which is essential for the cell shape stability, while the IFs are wavy, thus they do not bear any load until straightened. The objective is to modify the existing model for modeling endothelium cells and to validate it with appropriate mechanical responses. The investigation process is going on the mechanical properties of cytoskeletal and continuum components of endothelial cells and also on the cytoskeletal arrangement in endothelial cells. Endothelial cell dysfunction has been linked to atherosclerosis through their response to hemodynamic forces. The modified model is intended to be used for assessment of impact of wall shear stress in arteries on endothelium cells. Endothelial cells are composed in a monolayer, in this manner further advances are needed to investigate the perception of loads by a population of cells.

## **Acknowledgement**

This work was supported by Czech Science Foundation, project No. 18-13663S.

## **References**

Bansod Y.D., Matsumoto T., Nagayama K., Bursa J.: "A Finite Element Bendo-Tensegrity Model of Eukaryotic Cell". ASME J Biomech Engin, vol. 140 (2018)10:101001-9

## **Appendix F**

**Title:** “Computational modelling of cell response to various mechanical stimuli”

**Authors:** Veera Venkata Satya Varaprasad Jakka, Lucie Orlova and Jiří Burša

**Conference Name:** 27th Congress of the European Society of Biomechanics, June 26-29, Porto, Portugal.

**Citation:**

Veera Venkata Satya Varaprasad Jakka, Lucie Orlova and Jiří Burša. (2022). “Computational modelling of cell response to various mechanical stimuli”. 27<sup>th</sup> Congress of the European Society of Biomechanics, June 26-29, Porto, Portugal. (Submitted).

# COMPUTATIONAL MODELLING OF CELL RESPONSE TO VARIOUS MECHANICAL STIMULI

Veera Venkata Satya Varaprasad Jakka, Lucie Orlova and Jiri Bursa

Faculty of Mechanical Engineering, Brno University of Technology, Brno, Czech Republic  
E-mails: 207437@vutbr.cz, 182631@vutbr.cz, bursa@fme.vutbr.cz

## Introduction

Endothelial cells in the arterial wall may play a decisive role in the etiology of atherosclerosis. To improve the understanding of the cell mechanical response, the bendo-tensegrity concept was recently used to describe the characteristic behavior of the cytoskeleton. This helped to overcome the excessive stiffness of microtubules from the previous tensegrity-based cell models. In the presented hybrid model, actin filaments (AFs) serve as tension-supporting cables, while microtubules serve as compression-supporting bended beams. The AFs are prestressed which is essential for the cell shape stability, while the intermediate filaments (IFs) are wavy, thus not bearing any load until straightened.

## Methods

A hybrid FE model was created by combining the cytoskeleton model with continuum parts of the cell (nucleus, cytoplasm and cell membrane) taking into consideration different physiological shapes of endothelial cells. Additionally, four different variants of the model were created (regular flat and domed, elongated flat and domed) being even closer to its physiological shape [1]. To validate the described model with experimental results, the model was transformed (by keeping the same volume) into different shapes observed in vitro which were then used in Finite Element (FE) simulations of tension and compression [2].

## Results

The objective of this work is to investigate the mechanical response of endothelial cells to different loading conditions (compression, uniaxial and biaxial tension, and shear). The cell model was used for assessment of the impact of wall shear stress acting on the endothelium cells in arteries under their biaxial tensional load corresponding to the physiological conditions in the arterial wall (axial pre-stretch and mean arterial blood pressure causing circumferential stresses and strains). Finally, the model is intended to be used in FE simulations of the cell populations and their debonding from the substrate (basal lamina) under cyclic load corresponding to pulsatile blood pressure. Considerations on the role of the mitochondrial network in cell mechanical responses are also scheduled.

## Discussion

The significant contribution of the cytoskeleton and its individual components to overall cell stiffness was assessed and nucleus deformation has been established as a decisive quantity for mechanotransduction.

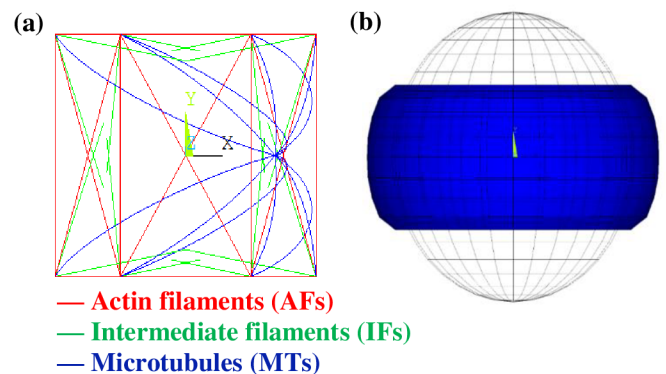


Figure: Suspended cell model for simulation of compression test: (a) unloaded cytoskeleton in front view (b) unloaded model in wireframe and under 50% compression [2].

## References

1. Veera Venkata Satya Varaprasad Jakka, Jiri Bursa, "Impact of physiological loads of arterial wall on nucleus deformation in endothelial cells: A computational study" *Comput. Biol. Med.*, Volume 143, 2022.
2. Jakka VVSV, Bursa J. Finite Element Simulations of Mechanical Behaviour of Endothelial Cells. *Biomed Res. Int.* 2021. Article ID 8847372

## Acknowledgments

This work was supported by Czech Science Foundation project No. 21-21935S.



## CURICULUM VITAE

### Personal Information

---

Name **JAKKA VEERA VENKATA SATYA VARAPRASAD**  
Current Address Cejkova3456/68, 61500, Brno-Zidence, Czech Republic.  
Telephone +420 775898085  
E-mail 207437@vutbr.cz  
jakkaprasad93@gmail.com  
Date of Birth 11 May 1993  
Nationality Indian  
Gender Male

### Educational Qualifications

---

**December 2017-Till Ph.D. in Applied Mechanics (Biomechanics)**  
**date**

Name and Address of organization Brno University of Technology, Brno, Czech Republic  
Thesis topic: Computational Simulation of Mechanical Behaviour of Endothelial Cells

**October 2014-April M.Sc. in Mechanical Engineering**  
**2017**

Name and Address of organization Politecnico di Milano, Milano, Italy  
Principal subjects covered Applied Metallurgy, Advanced Manufacturing Process, Control and Actuating Devices for Mechanical Systems, Mechanical Systems Dynamics, Machine Design, Mechanical Measurements, Design and Management of Production Systems and Energy systems. Unconventional Machining Processes, Industrial Plants, Mechanical Metallurgy and Measuring Techniques and Sensors for Automation.  
Thesis Topic Characterization of Composite Laminates Interlinear Toughness

**October 2010 - May Bachelor of Technology in Mechanical Engineering**  
**2014**

Name and Address of organization Jawaharlal Nehru Technological University, Kakinada, Andhra Pradesh, India  
Grade A-Excellent

### Doctoral internships abroad

---

**Dates (from – to) June 1, 2021 – June 30, 2021**

Name and address of the employer "Cell Adhesion and Mechanics"  
Institut Jacques Monod  
Université de Paris & CNRS, Paris, France  
Academic Position Visiting PhD students

**Dates (from – to) Feb 12, 2022 – March 12, 2022**

Name and address of the employer Swansea University, UK.

Academic Position Visiting PhD student

### **Teaching Experience**

---

**Dates (from – to) February 2018 – Till date**

Name and address of the employer Brno University of Technology, Brno, Czech Republic

Academic Position Researcher at Faculty of Mechanical Engineering

Teaching Activities Strength of Materials 1  
Strength of Materials 2

### **Trainee Experience**

---

**Dates (from – to) January 2017 – June 2017**

Name and address of the employer Intelligent Robot and Autonomous Systems - IRAS  
Institute of Industrial Automation and Technologies - ITIA  
National Research Council - CNR  
Via Bassini, 15, 20133 Milano, Italy

Position held and department **Mechanical Design Engineer.**

Main activities and responsibilities Modeling CAD, FEM modeling, choice of electro-mechanical components available on the market, mechanical design and verification of the stresses

### **Academic Projects & Co-Curricular Activities**

---

- 1 Practical view of Feasibility Study, Politecnico di Milano, Lecco.
- 2 Design and Analysis of thick-walled Pressure vessel.
- 3 Fabrication of Compressed air Automotive, JNTU Kakinada, India.
- 4 Participated in robotics workshop in SAMYAK (2K12) Conducted by KL University, Vijayawada, India.
- 5 Participated in Radio Control Aircraft workshop by Anna University Chennai, India.

### **Publications**

---

- 1 Bansod Y.D., **Jakka Veera V.S.V.P.**, and Burša J. “Bendo-tensegrity model simulates compression test of animal cell”. 24th International Conference on Engineering Mechanics, Svratka, Czech Republic, May 14 –17, 2018, pp. 45–48, doi: 10.21495/91-8-45.
- 2 **Veera Venkata Satya Varaprasad Jakka**, Jiří Burša. Computational Modeling of Mechanical Behaviour of Endothelial Cells”. 26th Cytoskeletal Club, Vranovská Ves, May 19-21, 2019.
- 3 **Veera Venkata Satya Varaprasad Jakka**, Jiří Burša.. Finite element models of mechanical behaviour of endothelial cells. Engineering Mechanics 2020. 2020. p. 222-225. ISBN: 978-80-214-5896-3.
- 4 **Veera Venkata Satya Varaprasad Jakka**, Jiri Bursa, "Finite Element Simulations of Mechanical Behaviour of Endothelial Cells", *BioMed Research International*, vol. 2021, ArticleID 8847372, 17 pages, 2021. <https://doi.org/10.1155/2021/8847372>

- 5 **Veera Venkata Satya Varaprasad Jakka**, Jiri Bursa, “Impact of physiological loads of arterial wall on nucleus deformation in endothelial cells: A computational study”, Computers in Biology and Medicine, Volume 143, 2022, 105266, ISSN 0010-4825, <https://doi.org/10.1016/j.compbiomed.2022.105266>.
- 6 **Veera Venkata Satya Varaprasad Jakka**, Lucie Orlova and Jiří Burša. (2022). “Computational modelling of cell response to various mechanical stimuli”. 27th Congress of the European Society of Biomechanics, June 26-29, Porto, Portugal. (Submitted).

### Technical Skills and Competences

---

<b>Skills</b>	<b>Proficiency</b>
<b>Software's</b>	
• Sound knowledge on <b>Ansys (APDL + workbench)</b>	Excellent
• Sound knowledge on <b>Solid works, AutoCAD, Pro-E, GD&amp;T</b>	Excellent
• Familiar with <b>Catia V5</b>	Excellent
<b>Programming Languages</b>	
MATLAB and C	Good
<b>Tools</b>	
MS Office (Excel, Word, PowerPoint)	Excellent
<b>Operate Systems</b>	
Windows 10/8/7, Mac	Excellent

### Personal Skills and Competences

---

Mother Tongue	<b>Telugu</b>		
Other Languages	<b>English</b>	<b>Czech</b>	<b>Italian</b>
	Excellent	Basic level	Basic level
Social Skills	<ul style="list-style-type: none"> <li>• Months of experience working in multi-cultural environments, often collaborating with a team from different countries and region.</li> </ul>		